HOST SENSITIZED ENERGY TRANSFER IN $CaWO_4:Sm^{3+}$

By

MICHAEL JOSEPH TREADAWAY

Bachelor of Science

Tulane University

New Orleans, Louisiana

1970

Submitted to the Faculty of the Graduate College
of the Oklahoma State University
in partial fulfillment of the requirements
for the Degree of
DOCTOR OF PHILOSOPHY
May, 1974

HOST SENSITIZED ENERGY TRANSFER IN $CaWO_4:Sm^{3+}$

Thesis Approved:

Richard C. Powell
Thesis Adviser

Paul Westhaus

Dean of the Graduate College

ACKNOWLEDGEMENTS

I would like to take this opportunity to express my appreciation to the many people who were responsible for my graduate education. I am grateful to Drs. P. A. Westhaus, E. E. Kohnke and G. J. Mains for serving on my Ph.D. advisory committee. Special thanks to Dr. R. C. Powell for serving as my thesis advisor, for his constant encouragement and for providing hours of stimulating discussion of both theoretical and experimental problems. Financial support made available through the United States Army Research Office, Durham, is also gratefully acknowledged.

I would also like to express my gratitude to my parents for their constant support, to my good friends Richard, Barbara and especially to Cindy whose tolerance and companionship was instrumental in the completion of my graduate education. Finally I would like to thank Davis Cooper for his constant reminder of "Be Here Now".

TABLE OF CONTENTS

LIST OF TABLES

LIST OF FIGURES

LIST OF FIGURES (Continued)

LIST OF FIGURES (Continued)

LIST OF FIGURES (Continued)

CHAPTER I

INTRODUCTION

Purpose of Investigation

Luminescence of solids has been one of the most active areas of basic scientific investigation for over sixty years (1). Inorganic phosphors have been of particular interest due to their commercial use in cathode ray tubes for radar, television and other visual displays and fluorescence lighting systems. Many of these materials have also been found to be usuable as lasers.

Of vital importance to the study of inorganic phosphors is the process of host sensitized energy transfer which can produce both good and bad effects. Energy transfer from the host material to activator ions which have been introduced into the host lattice is an efficient means of producing fluorescence as well as lower thresholds in laser materials. At the same time energy transfer from the host material to sinks or traps where the energy is lost to the lattice is responsible for quenching of the host luminescence.

Trivalent samarium in calcium tungstate has been a commercially important phosphor for years. Surprisingly, however, the basic physics of the energy transfer mechanism has not been thoroughly investigated. The purpose of this investigation is to determine the mechanism by which energy is transferred from the tungstate ions to samarium ions, to determine the energy transfer rates and to study the effect of temperature and samarium

concentration on the energy transfer rates.

Energy Transfer in Solids

Definitions

The movement of a quantum of excitation from one ion (S) to an ion (A) in a crystal is called energy migration if ion S and A are of the same type and energy transfer if S and A are different.

For the case of energy transfer the S ion is called the sensitizer and A is called the activator ion. The activator may be present as an impurity or probe in the lattice of S ions in which case we refer to the energy transfer as host sensitized. Impurity sensitization refers to the case where both the S and A ions are impurities in the host lattice.

Types of Energy Transfer

The process of energy transfer can be broken into five steps (2): (1) an ion S absorbs a quantum of excitation energy E_1 and is raised to an excited state, (2) the lattice surrounding S relaxes, thus reducing the energy that may be released in an electronic transition, the energy available is $E_2 < E_1$, (3) the transfer of energy E_2 to an activator ion A, (4) relaxation of the lattice surrounding A, making the available energy $E_3 < E_2$, (5) the transition of A to the ground state and the emission of a photon of energy E_3.

In general there are four methods by which the third step may take place:

(1) Photoelectric - an ion absorbs a quantum of excitation creating a free electron and hole either of which may travel through the lattice.

(2) Radiative reabsorption - a quantum of excitation is absorbed by an ion which later emits a photon. The photon travels through the lattice until absorbed by another ion.

(3) Long range resonant interaction - an ion which has been excited by absorbing a photon, interacts via a multipole-multipole or exchange interaction with another ion and subsequently transfers the quantum of excitation.

(4) Exciton migration - at the absorbing ion a coupled electron-hole pair, an exciton, is created which then migrates through the lattice carrying excitation but not charge. At some other point in the lattice the pair recombine releasing the excitation energy.

The first two mechanisms have been well studied for years and are not considered in this investigation and in all experimental work steps were taken to insure that these mechanisms were not operating. Further discussion of energy transfer and the derivation of energy transfer rates will pertain only to long range resonant interaction (LRRI, also called Förster-Dexter interaction) and to exciton dynamics.

Methods of Investigation

Three types of experiments were used in this investigation: excitation spectra, fluorescence spectra and time resolved spectroscopy, all of which were performed as a function of sample temperature and activator concentration.

Excitation spectra were obtained by monitoring the fluorescence intensity at a specific wavelength as a function of the wavelength of the light exciting the sample. Excitation spectra give insight into the structure of absorption bands which may otherwise be hidden due to the

large absorption coefficients in certain regions. Excitation spectra are not identical to absorption spectra due to a number of processes such as radiationless quenching and energy transfer. One of the most useful applications of excitation spectra is to indicate which parts of the sensitizer absorption spectra are most efficient in transferring energy to the activator ions. The temperature dependence of the excitation spectra gives insight as to the importance of radiationless transitions between sensitizer excited states to the energy transfer and migration processes.

Fluorescence spectra were obtained by exciting the sample at a specific wavelength and monitoring the intensity of the resulting fluorescence as a function of wavelength. Fluorescence spectra indicate the degree of Stokes shift between the absorbed and emitted radiation as well as the degree of overlap of the sensitizer emission and activator absorption. Comparison of the fluorescence spectra obtained by direct excitation of the activator ions to fluorescence spectra of the activator ions produced when the activator is excited by energy transfer from the sensitizer ions is useful in the determination of an energy transfer model. Finally the ratio of the activator to sensitizer integrated fluorescence intensities as a function of temperature and activator concentration is used to elucidate the characteristics of the energy transfer mechanisms and energy transfer rates.

Time resolved spectroscopy measurements were made using fast electronics and single photon counting techniques. The result of these measurements is to obtain a picture of the fluorescence intensity as a function of time. The spectra are examined to determine if the decay is a single exponential. Non-exponential decay is an indicator that processes

other than a single fluorescence transition from the absorbing level are present.

In the case of exponential decays the lifetime is determined. The lifetime of the sensitizer ions with no activators present is a parameter necessary for determination of the energy transfer rates. Also the ratio of the sensitizer lifetime in the presence of activators to the lifetime of the sensitizer in the absence of activators as a function of temperature and activator concentration helps characterize the energy transfer mechanisms.

Summary of Previous Work

In the late thirties the possibility of using phosphorous materials as a method of artificial lighting sparked renewed interest in inorganic phosphors. Thayer and Barnes (3) and Besse (4) made measurements of the efficiency of production of broad band fluorescence on undoped powdered calcium tungstate for excitation in the vacuum and near ultraviolet regions. At the same time Johnson and Davis (5) made measurements of the trivalent samarium lifetime in powdered samples of calcium tungstate but their apparatus was unable to measure the "very fast" tungstate lifetime.

Most of the currently accepted work on calcium tungstate and calcium tungstate doped with trivalent samarium has been done by Kröger (6) and Botden (7). Kröger's work was mostly to study the effect of different metallic ions on the tungstate fluorescence. Botden investigated the quenching of the tungstate fluorescence as a function of samarium concentration and excitation wavelength in the temperature region $700^{o}K$ to $100^{o}K$.

Although a great deal of experimental work has been reported on this system very little theoretical work has been done. No rigorous molecular orbital calculations have been carried out for calcium tungstate. Butler (8) reported the results of limited molecular orbital calculations for the WO_4^{2-} molecular ion but qualifies the results as being "highly speculative." Molecular orbital calculations on the isoelectronic MnO_4^- molecular ion has been reported by Day (9) and Wolfsburg and Helmholz (10).

Although the spectra of many rare earth ions in calcium tungstate have been studied (11,12) no attempt has been made to explain the Sm^{3+} spectra in calcium tungstate. Several attempts (13,14,15) have been made to explain the free ion spectra of Sm^{3+}. Van Uitert and Johnson (16) studied the quenching of Sm^{3+} fluorescence in calcium tungstate due to samarium ion interaction and again the work was limited to room temperature measurements.

Photoconductivity was observed in calcium tungstate by Randall and Willkins (17) but this work was disputed by Klick and Schulman (18) in 1949. Recent works (19,20,21) indicate that calcium tungstate does exhibit some photoconductivity.

Summary of Investigation

In this investigation we characterized the host sensitized energy transfer in samarium doped calcium tungstate. The investigation consisted of three parts the first of which was to formulate a model for the undoped calcium tungstate. By studying the temperature dependence of the fluorescent intensities, lifetimes and excitation spectra of the undoped calcium tungstate a model of the undoped sample was formulated.

This model is a configurational coordinate model of the ground state and first few excited states of the WO_4^{2-} center which convincingly explains the observed intensity data and a model of the energy migration mechanism which explains the observed temperature dependence of the WO_4^{2-} lifetime data.

The second part of the investigation was to explain the spectra of the Sm^{3+} ions in $CaWO_4$. From the spectra of the intrinsic Sm^{3+} fluorescence an empirical energy level diagram of trivalent samarium in calcium tungstate was constructed.

The third part of the investigation was to study the quenching of the WO_4^{2-} lifetime and integrated fluorescence intensity as a function of temperature and samarium concentration. From this data and the results of the first two parts of the investigation the important energy transfer mechanisms were identified and the energy transfer rates determined.

Measurements were made at numerous temperatures between room temperature and $10^{o}K$. Good single crystal samples were used, one undoped $CaWO_4$ sample and three Sm^{3+} doped $CaWO_4$ samples with Sm^{3+} concentrations of .01, .1 and 1.0 atomic percent. Our investigation has several significant advantages over previous work on this system. No previous work was done using good single crystals but was all performed on powdered samples. No previous work extended to temperatures below $100^{o}K$. Extension of the measurements to $10^{o}K$ was vitally important in establishing a realistic configurational coordinate model for the WO_4^{2-} site and in establishing the energy migration model for the undoped sample, as well as for the empirical determination of the energy levels of Sm^{3+} in $CaWO_4$. No previous work obtained the excitation spectrum of Sm^{3+} in $CaWO_4$.

Finally no previous work has been done using the powerful technique of time resolved spectroscopy. The unusual results of the T.R.S. measurements led us to propose an energy transfer mechanism which could not be arrived at by only steady state fluorescence measurements.

CHAPTER II

THEORETICAL

Förster-Dexter Interaction

Much of the pioneer work on the formalism of energy transfer via a resonant interaction was done by Theodore Förster (22,23) and D. L. Dexter (24) and consequently long range resonant interaction is often referred to as Förester-Dexter interaction. The following derivation of the dipole-dipole energy transfer rate follows closely the development of Dexter.

Energy transfer from a sensitizer to an activator can be described by a semi classical model of the interaction. The initial state of the system is taken to be a product of the states of the two ions with the sensitizer in an excited state and the activator in the ground state. Mathematically this can be written as

$$|\psi_I\rangle = \hat{A}|\psi_s'(\bar{r}_s,w_s')\rangle|\psi_A(\bar{r}_A,w_A)\rangle$$

where the primes indicate excited states, $\hat{A}$ is the antisymmeterizer operator, $\bar{r}$ is the electrons position vector and w is the energy. Similarly the final state is taken to be the sensitizer in the ground state and the activator in an excited state,

$$|\psi_F\rangle = \hat{A}|\psi_s(\bar{r}_s,w_s)\rangle|\psi_A(\bar{r}_A,w_A')\rangle .$$

The transition rate between the initial and final states is given by Fermi's golden rule,

$$P_{sA} = \frac{2\pi}{\hbar} |\langle\psi_F|\hat{H}|\psi_I\rangle|^2 \qquad [1]$$

where $\hat{H}$ is the interaction which couples the initial and final states. We can consider the interaction to be the coulombic interaction between all of the electrons of the sensitizer ion and all the electrons of the activator ion. Assuming only one electron on each ion makes a transition, classically we can write the interaction as

$$H = \frac{e^2}{K}\left[\frac{1}{|\bar{R} + \bar{r}_A - \bar{r}_s|}\right]$$

where $\bar{r}_s$ and $\bar{r}_A$ are the position vectors of the electron on the sensitizer and activator respectively. A more complete development of the Hamiltonian is given in the Appendix. $\bar{R}$ is the vector position of the A ion with respect to the S ion.

If only one electron on each ion makes a transition due to the interaction, then the initial and final states can be written as

$$|\psi_I\rangle = \frac{1}{\sqrt{2}}\left(|\psi_s'(\bar{r}_1,w_s')\rangle|\psi_A(\bar{r}_2,w_A)\rangle|\chi_s'(1)\rangle|\chi_A(2)\rangle\right.$$

$$\left. - |\psi_s'(\bar{r}_2,w_s')\rangle|\psi_A(\bar{r}_1,w_A)\rangle|\chi_s'(2)\rangle|\chi_A(1)\rangle\right)$$

and

$$|\psi_F\rangle = \frac{1}{\sqrt{2}}\left(|\psi_s(\bar{r}_1,w_s)\rangle|\psi_A'(\bar{r}_2,w_A')\rangle|\chi_s(1)\rangle|\chi_A'(2)\rangle\right.$$

$$\left. - |\psi_s(\bar{r}_2,w_s)\rangle|\psi_A'(\bar{r}_1,w_A')\rangle|\chi_s(2)\rangle|\chi_A'(1)\rangle\right) \qquad [2]$$

and $\langle\psi_F|\hat{H}|\psi_I\rangle$ becomes

$$= \langle\psi_s(\bar{r}_1,\omega_s)|\langle\psi'_A(\bar{r}_2,\omega'_A)|\hat{H}|\psi'_s(\bar{r}_1,\omega'_s)\rangle|\psi_A(\bar{r}_2,\bar{\omega}_A)\rangle$$

$$\langle\chi_s(1)|\chi'_s(1)\rangle\langle\chi'_A(2)|\chi_A(2)\rangle$$

$$- \langle\psi_s(\bar{r}_1,\omega_s)|\langle\psi'_A(\bar{r}_2,\omega'_A)|\hat{H}|\psi'_s(\bar{r}_2,\omega'_s)\rangle|\psi_A(\bar{r}_1,\omega_A)\rangle$$

$$\langle\chi_s(1)|\chi_A(1)\rangle\langle\chi'_A(2)|\chi'_s(2)\rangle \qquad [3]$$

The second term of Equation [3] represents the exchange interaction of the sensitizer and activator ions and allows for transitions in which spin flips occur. Exchange terms will be considered later in this development, consideration will be given now exclusively to the first term which has the selection rules, $\chi'_s = \chi_s$ and $\chi'_A = \chi_A$. In light of these selection rules the spin functions will no longer be written explicitly.

Equation [1] gives the probability per unit time of a transition occurring from a specific initial state ψ_I to a specific final state ψ_F. The probability must be summed over all possible combinations of sensitizer and activator states which fulfill the energy conservation condition, $E_F = E_I = \omega'_s - \omega_s = \omega'_A - \omega_A$. This can be accomplished by including the distribution function $\rho'_s(\omega'_s)$ which describes the probability of the s ion being initially in an excited state of energy ω'_s and by introducing an analogous function for the A ion, $\rho_A(\omega_A)$. The energy eigenvalues will be considered to be closely spaced and ω'_s and ω_A will be considered then as continuous variables. Consideration must also be given to the probability that the excited state $\psi'_s(\bar{r}_1,\omega'_s)$ of the sensitizer and the ground state of the activator may be degenerate by factors of g'_s and g_A respectively. With these considerations the sum of all

transition rates over all possible transitions can be represented as an integral over energy and a sum over all other quantum numbers. The transition rate can be written as

$$P_{SA} = \frac{2\pi}{\hbar} \sum_I \sum_F (g_s' g_A)^{-1} \int d\omega_A' \int d\omega_s \int d\omega_A \rho_A(\omega_A) \int d\omega_s' \rho_s'(\omega_s') \langle \psi_F | \hat{H} | \psi_I \rangle |^2 \delta((\omega_s' - \omega_s) - (\omega_a' - \omega_A)) \quad [4]$$

where conservation of energy for the transition has been included explicitly by the delta function. Making use of the delta function integration over ω_a' is easily accomplished and substituting for $\omega_s = E - \omega_s'$ Equation [4] becomes

$$P_{SA} = \frac{2\pi}{\hbar} \sum_I \sum_F (g_s' g_A)^{-1} \int dE \int d\omega_A \rho_A(\omega_A) \int d\omega_s' \rho_s'(\omega_s') | \langle \psi_F | \hat{H} | \psi_I \rangle |^2 \quad [5]$$

This form of the transition rate may be more easily handled if the Hamiltonian is expanded in a Taylor series about $\bar{R}$, the internuclear separation of the sensitizer and activator. The Hamiltonian becomes

$$\begin{aligned} H(\bar{R}) = {} & \frac{e^2}{KR^3} \{ \bar{r}_s \cdot r_A - 3(\bar{r}_s \cdot \bar{R})(\bar{r}_A \cdot \bar{R}/R^2 \} \\ & + 3 \frac{e^2}{2KR^4} \{ \sum_{i=1}^{3} (\frac{R_i}{R}) r_{Ai}^2 r_{si} (-3 + 5 (\frac{R_i}{R})^2) \\ & + 10(XYZ)\bar{R}^3 (X_A Y_A Z_S + X_A Z_A Y_S + Y_A Z_A X_S) \\ & + \sum_{\substack{i=1 \\ i \neq j}}^{3} \sum_{j=1}^{3} [\frac{R_j}{R} - 5 \frac{R_i^2 R_j}{R^3}][-r_{Ai}^2 r_{Sj} - 2 r_{Ai} r_{Aj} r_{Si}] \} \\ & + \ldots \end{aligned} \quad [6]$$

where the first term in brackets can be identified with the interaction between S and A if both were dipoles; the second term in brackets describes S as a dipole and A as a quadrupole and there are an infinite number of higher order terms. This is the very familiar multipole expansion and as usual is carried out with the expectation that one or two terms will predominate and all others may be ignored.

Dipole-Dipole Interaction

If the sensitizer and activator both have allowed electric dipole transitions then the interaction between the ions can be approximated by the dipole-dipole term of the Hamiltonian, H_{dd} and we can write

$$|\langle\psi_F|H_{dd}|\psi_I\rangle|^2 = \frac{e^4}{K^2R^6}|\langle\bar{r}_s\rangle\cdot\langle\bar{r}_A\rangle - \frac{3}{R^2}(\langle\bar{r}_s\rangle\cdot\bar{R})(\langle\bar{r}_A\rangle\cdot\bar{R})^2$$

which when averaged over all possible orientations of $\bar{R}$ becomes

$$|\langle\psi_F|H_{dd}|\psi_I\rangle|^2 = \frac{2}{3}\frac{e^4}{K^2R^6}|\langle\bar{r}_s\rangle|^2\,|\langle\bar{r}_A\rangle|^2 \qquad [7]$$

substituting this expression in Equation [5] yields

$$P_{SA}(dd) = \frac{4\pi e^4}{3\hbar K^2R^6}(g'_s g_A)^{-1}\sum_I\sum_F\int dE\int d\omega'_s\rho'_s(\omega'_s)|\langle\bar{r}_s\rangle|^2\int d\omega_A\rho_A(\omega_A)|\langle\bar{r}_A\rangle|^2 \qquad [8]$$

At this point it is helpful to try and identify some of the terms in the Equation for $P_{SA}(dd)$ with quantities that may be determined experimentally such as fluorescence and absorption spectra.

The rate of spontaneous transitions from a state i to a state f of an ion in a crystal with index of refraction n is given by the Einstein

A coefficient. Taking a thermodynamic statistical average over all initial states yields

$$A(E) = \sum_i \sum_f \frac{4e^2E^3}{3\hbar^4C^3g_i'} \left(\frac{\varepsilon_c}{\varepsilon}\right)^2 n^3 \int |\langle \bar{r}_{if} \rangle|^2 \rho'(\omega')d\omega' \qquad [9]$$

where $\left(\frac{\varepsilon_c}{\varepsilon}\right)$ is the ratio of the electric field as seen by the ion in the crystal to the electric field in a vacuum. Since $\int A(E)dE = \frac{1}{\tau}$ where τ is the radiative lifetime, a normalized function f(E) can be defined such that

$$f(E) = \tau A(E)$$

which is related to the integrated emission intensity of the ion. Similarly the integral over ω_s' in Equation [8] is related to the integrated fluorescence intensity of the sensitizer.

The rate of absorption by an ion in a crystal can be written as the Einstein B coefficient

$$B(E) = \sum_i \sum_f \frac{2\pi e^3}{2\hbar g_i} \left(\frac{\varepsilon_c}{\varepsilon}\right)^2 \int \rho(\omega)d\omega \; |\langle r_{if} \rangle|^2 \qquad [10]$$

The B coefficient is related to the absorption cross section by $\sigma(E) = \frac{B(E)}{\frac{c}{n}}$. Introducing another normalized function F(E) such that

$$F(E) = \frac{\sigma(E)}{Q} \quad \text{where } Q = \int \sigma(E)dE$$

then

$$\sum_i \sum_f \int d\omega_A' \rho_A(\omega_A') |\langle \bar{r}_A \rangle|^2 = \frac{3\hbar c \, g_A}{4\pi^2 e^2 nE} \left(\frac{\varepsilon}{\varepsilon_c}\right)^2 Q_A F_A(E). \qquad [11]$$

Making substitutions of F(E) and f(E) into Equation [8]

$$P_{SA}(dd) = \frac{3}{4\pi}\frac{\hbar^4 c^4}{n^4}\left(\frac{\varepsilon}{\varepsilon_c}\right)^4 \frac{1}{K^2}\frac{1}{R^6}\frac{1}{\tau_s} Q_A \int dE \frac{f(E)F(E)}{E^4} \qquad [12]$$

which can be simplified as

$$P_{SA}(dd) = \frac{1}{\tau_s^o}\left(\frac{R_o}{R}\right)^6 \qquad [13]$$

where

$$R_o^6 = \phi_s \frac{3}{4\pi}\left(\frac{\hbar c}{n}\right)^4 \left(\frac{\varepsilon}{\varepsilon_c}\right)^4 \frac{1}{K^2} Q_A \int dE \frac{f(E)F(E)}{E^4},$$

τ_s^o is the lifetime of the sensitizers in the absence of activators and ϕ_s is the quantum efficiency of the sensitizers with activators present.

The concentration dependence of the energy transfer rate is contained in the sensitizer-activator separation, R. The temperature dependence is contained in the spectra overlap integral $\int dE \frac{f(E)\ F(E)}{E}$.

Consideration now must be given to the fact that in a crystal there are many sensitizer and activator ions, and therefore a sensitizer can interact with more than one activator (25). The sensitizers can then be divided into classes where each sensitizer in a given class sees the same activator environment. For any class γ' the transfer probability is

$$k_{\gamma'} = \frac{1}{\tau_s}\sum_{i=1}^{N_A}\left(\frac{R_o}{R_i}\right)^6 \qquad [14]$$

where R_i is the distance from the sensitizer to the ith activator and the sum is over all N_A activator ions, compare this to Equation [13]. The rate equation describing the time rate of change of the population of the γth class of excited sensitizers is

$$\frac{d\, n^*_{s\gamma'}(t)}{dt} = -\left(k_{\gamma'} + \frac{1}{\tau^o_s}\right) n^*_{s\gamma'}(t) \qquad [15]$$

assuming negligible sensitizer-sensitizer transfer, and a delta function excitation at time zero. Equation [15] can be easily integrated to give the time evolution of the population of excited sensitizer

$$n^*_{s\gamma'}(t) = n^*_{s\gamma'}(o)\, e^{-\left(k_{\gamma'} + \frac{1}{\tau^o_s}\right)t} \qquad [16]$$

substituting for k_{γ} from Equation [14]

$$n^*_{s\gamma'}(t) = n^*_{s\gamma'}(o)\, e^{-\frac{\tau}{\tau^o_s}} e^{-\frac{\tau}{\tau^o_s}\sum_{i=1}^{N_A}\left(\frac{R_o}{R_i}\right)^6}$$

$$= n^*_{s\gamma'}(o)\, e^{-\frac{\tau}{\tau^o_s}} \prod_{i=1}^{N_A} e^{-\frac{\tau}{\tau^o_s}\left(\frac{R_o}{R_i}\right)^6} \qquad [17]$$

Assuming a random distribution of activators then the number of sensitizers belonging to class γ' is given by

$$n_{s\gamma'} = N_s\, P_{\gamma'}(d\gamma') = N_s \prod_{i=1}^{N_A} \frac{4\pi R_i^2\, dR_i}{V} \qquad [18]$$

where V is the volume of the crystal. Averaging $n^*_{s\gamma'}(t)$ over all classes γ we obtain $n^*_s(t)$ such that

$$n^*_s(t) = n^*_s(o) \exp\left\{-\frac{\tau}{\tau^o_s} - \gamma\left(\frac{\pi t}{\tau^o_s}\right)^{1/2}\right\} \qquad [19]$$

where $\gamma = \frac{N_A}{C_o}$ and $C_o = \frac{1}{4\pi (R_o)^3}$ here N_A is the activator concentration. If the rate equation describing the excited sensitizer population is written, similar to Equation [15], and Equation [19] is differentiated with respect to time we find that the energy transfer rate becomes

$$k = \frac{1}{2}\left(\frac{\gamma\, \pi}{\tau^o_s t}\right)^{1/2} . \qquad [20]$$

Note that the energy transfer rate is proportional to $t^{-\frac{1}{2}}$.

Similarly the time evolution of the excited activator population can be obtained from the rate equation

$$dn_A^*(t) = k_s n_s^*(t) - \frac{1}{\tau_A} n_A^*(t) \qquad [21]$$

integrating yields

$$n_A^*(t) = \gamma \tau_s^{-\frac{1}{2}} \exp\left(-\frac{t}{\tau_s^o}\right) \int_o^t e^{\varepsilon/\tau_A} n_s^*(\xi)\, \xi^{-\frac{1}{2}} d\xi \qquad [22]$$

Connection With Experiments

Experimentally the fluorescence intensity of the sensitizer I_s and activator I_A of a doped sample can be measured. Also the lifetime of the sensitizers and activators can be measured. Although Equation [20] predicts a non-exponential decay of the excited sensitizer population a lifetime can still be defined for the fluorescence as τ_s^e such that $n_s^*(\tau_s^e) = \frac{1}{e} n_s^*(o)$. Substituting this definition into Equation [20], the ratio $\frac{\tau_s^e}{\tau_s^o}$ is found to be

$$\frac{\tau_s^e}{\tau_s^o} = 1 + \left(\pi^{\frac{1}{2}} \frac{\gamma}{2}\right)\left[\pi^{\frac{1}{2}} \gamma - (\pi \gamma^2 + 4)^{\frac{1}{2}}\right] \qquad [23]$$

Alternatively Equation [20] can be solved for the case of steady state excitation to give I_s, the intensity of the sensitizer in the presence of activators and this can be compared to I_s^o, the intensity in the absence of activators, which yields

$$\frac{I_s}{I_s^o} = 1 - \frac{\pi}{2}\gamma \exp\left(\frac{\pi\gamma^2}{4}\right)\left[1 - \operatorname{erf}\left(\sqrt{\pi}\ \frac{\gamma}{2}\right)\right] \qquad [24]$$

where $\operatorname{erf}(x) = \frac{2}{\sqrt{\pi}} \int_o^x \exp(-Y^2)dY$. To obtain this ratio requires making a measurement of the sensitizer fluorescent intensity on two samples, a doped and undoped sample. In practice this entails a great deal of tedious and difficult work which may be avoided by considering the ratio $\frac{I_A}{I_S}$. I_A is the activator intensity and I_S is the sensitizer intensity where both are measured in the same sample. This ratio can be related to Equation [24] by the introduction of the activator and sensitizer quantum efficiencies. Defining the quantum efficiency as the ratio of the rate of spontaneous transition to the rate of all possible decay mechanisms, i.e., radiative decay, radiationless decay and energy transfer denoted by $\frac{1}{\tau^s_{rad}}$, L and k respectively.

$\frac{1}{\tau^s_{rad}} + k + L = \frac{1}{\tau_s}$ where τ_s is the observed fluorescent lifetime of the sensitizer. The quantum efficiency is also defined as the ratio of the number of photons emitted to the number of incident photons. Equation [22] can be related to $\frac{I_s}{I_A}$ by

$$\frac{I_s}{I_A} = \frac{\phi_A}{\phi_s^o}\left(\frac{I_s^o}{I_s} - 1\right) \qquad [25]$$

where ϕ_A is the quantum efficiency of the activator upon direct excitation and ϕ_s^o is the quantum efficiency of the sensitizer with no activators present.

As mentioned before the temperature dependence of the energy trans-

fer rate is contained in the spectral overlap integral. For the case of transfer involving only a single excited level in the sensitizer and activator which are out of resonance by an amount ε_o, Miyakawa and Dexter (26) have shown that the energy transfer rate varies as $\exp(-\frac{\varepsilon_o}{KT})$. For systems in which transfer takes place from more than one sensitizer level or in which intersystem crossing is of importance the temperature dependence cannot be determined in a general form but is dependent upon the individual system.

Exchange Interaction

The second term in Equation [3] is the exchange integral, which arises due to the indistinguishability of the electrons and would not be present in a purely classical description. This term takes into account the degree of overlap of the sensitizer and activator wavefunctions. If there is no overlap the exchange term is zero. Spin selection rules can be deduced and require that

$$\chi_S' = \chi_A' \quad \text{and} \quad \chi_S = \chi_A$$

otherwise the exchange term is again identically zero.

Derivation of the energy transfer rate is not straightforward because it requires knowledge about the shape of the wavefunctions. By means of some very broad assumptions Dexter (24) showed the energy transfer rate due to exchange interaction to be

$$P_{SA}(EX) = \frac{1}{\tau_s^o} \exp\left(\gamma\left[1 - \frac{R}{R_o}\right]\right) \qquad [26]$$

where

$$\gamma = \frac{2R_o}{L}$$

and

$$\frac{e^{\gamma}}{\tau_s^o} = \frac{2\pi}{\hbar} K^2 \int f_s(E)\, F_A(E) dE \,. \qquad [27]$$

L is an effective Bohr radius, R_o is the critical transfer distance and K is a constant with dimensions of energy. In order to get the simple form of Equation [26] a number of approximations must be made concerning the nature of the sensitizer and activator wavefunctions. One assumption is that the wavefunctions can be represented as hydrogenlike and another assumption is that the sensitizer wavefunction does not vary greatly over the volume of the activator ion.

Inokuti and Hirayama (27) carried Dexter's work further to include the case of more than one activator. This was done analagously to the extension of Dexter's dipole-dipole transfer rate as outlined in section 1 of this chapter. The results that they obtain, however, for the intensity and lifetime ratios are not as simple as for the case of dipole-dipole interaction and must be evaluated numerically.

From Equation [26] it can be seen that the exchange energy transfer rate will vary as the exponential of the sensitizer-activator separation as compared to the R^{-6} dependence of the dipole-dipole rate. In general it has been found that the energy transfer rates obtained by making use of Dexter's equation are a lower limit to the actual energy transfer rate by exchange. This has been attributed to the very simple model needed to obtain Dexter's equation.

Excitons

General Considerations

The previous developments described the rate of energy transfer from a sensitizer to an activator and is based on the assumption that sensitizer to sensitizer transfer does not take place or is negligible compared to other processes. This assumption is valid when considering the sensitizers and activators as impurities in an inert host lattice if the concentration of sensitizers is small.

For the interesting case of host sensitization in which the sensitizer is an ion of the host lattice the rate of energy transfer between sensitizer ions cannot be ignored. Even for cases in which the lattice surrounding an excited sensitizer relaxes faster than energy transfer takes place, the sensitizer to sensitizer transfer cannot be ignored due to the small ion-ion separation and the large number of sensitizers comprising the environment of an excited sensitizer. In the case of host sensitization the energy transfer rate to activators can no longer be expressed as the sum of a number of independent rates because the process from initial excitation of a sensitizer to the transfer of the excitation to an activator is not a single step process because the excitation has a probability of wandering randomly through the lattice before transferring to an activator ion. In this case the development of the energy transfer rate to activators can be more easily envisioned in terms of an exciton model which takes into account the random movement of the excitation through the lattice.

An exciton is a coupled electron-hole pair. Two models of the exciton have been proposed which differ only in the degree of the coupling

between the electron and hole. The Wannier (28) or Mott (29) exciton is the weak coupling case where the electron-hole separation is large compared to a lattice spacing and consequently the exciton is spread out over a number of ions. The tight binding or Frenkel (30) exciton model pictures the exciton as being localized on only one ion. In both cases the exciton motion can be described by a hopping model if the scattering mechanisms limit the mean free path to the order of a lattice spacing. In this case each step takes place via a Förster-Dexter interaction. After each jump the exciton can 1) jump to another lattice site, 2) decay spontaneously with a decay rate B_S and thus be eliminated from consideration, 3) be eliminated because it has landed on a trap from which it cannot hop, or 4) be eliminated because it has landed on an activator ion.

Derivation of Energy Transfer Rate

Random walk and diffusion mathematics are formalisms readily adaptable to this problem. Consider the exciton as being a particle that undergoes a number of well defined but randomly oriented displacements on the three dimensional lattice of the host. The probability per unit time of the displacements is determined by the energy transfer rate between sensitizers as determined by consideration of the appropriate Förester-Dexter interaction. Also consider a randomly distributed number of spherical perfectly absorbing traps (activator ions) as being present on certain lattice sites in place of sensitizer ions. Whenever an exciton comes with the sphere of influence of the trap it is removed from consideration. This problem was considered by S. Chandrasekar (31) in his work on the problem of random flights. The transition to diffus-

ion mathematics can be made by allowing the number of displacements to become large which was also solved by Chandrasekar in the same paper in his consideration of the theory of coagulation in colloids. Using his results in the limit of many steps the differential equation describing the time rate of change of the exciton population is

$$\frac{dN(\bar{r},t)}{dt} = G(t) - B_S N(\bar{r},t) + DV^2 N(\bar{r},t) \qquad [28]$$

with the boundary conditions

$N = N_o$ = unit concentration at $t = o$, $|\bar{r}| > R$ and

$N = o$ at $t = o$, $|\bar{r}| \leq R$ where R is the radius of the trap, B_S is the intrinsic decay rate of the exciton, G(t) is the rate of production of "new" excitons and D is the diffusion coefficient. Equation [28] is a simple diffusion equation which describes the flow of particles into a perfectly absorbing sphere of radius R but with the additional consideration that the particles are being eliminated from consideration at a constant rate B_S outside of the trap. The boundary conditions imply that at $t = o$ there are created N_o excitons outside of the trap. Equation [28] was derived for the case of a single trap but may be easily extended to a large number of traps if the assumption is made that the number of excitons falling into any one trap is not decreased by the presence of the other traps. The rate of energy transfer between sensitizers is contained in D, the diffusion coefficient.

Equation [28] can be integrated to yield the time rate of change of the exciton population as

$$N(\bar{r},t) = e^{-B_S t} N_o\left[1 - \frac{R}{r} + \frac{2R}{r\sqrt{\pi}} \int_o^{\frac{r-R}{2(Dt)^{1/2}}} e^{-x^2} dx\right] \qquad [29]$$

where delta function excitation has been assumed. The rate of trapping of excitons by activators can be obtained by writing the total flux of excitons into traps.

$$\text{Total Flux} = N_A(D \text{ grad } N(\bar{r},t)\Big|_{r=R})_{ave} \qquad [30]$$

where N_A is the activator concentration and the average is over all orientations. Making use of Equation [29] and Equation [30] the total flux becomes

$$4\pi DR\left[1 + \frac{R}{\sqrt{\pi Dt}}\right] N_o N_A e^{-B_S t} \qquad [31]$$

which is just the flux into one trap times the number of traps. The flux of excitons into traps, however is the same as the rate of energy transfer to activators times the number of excitons, therefore, the energy transfer rate can be written as

$$k = 4\pi D R N_A \left[1 + \frac{R}{\sqrt{\pi Dt}}\right] \qquad [32]$$

which for typical values of R and D can be approximated as

$$k = 4\pi D R N_A \qquad [33]$$

for times of interest greater than a nanosecond.

Connection With Experiment

To make the development of the previous section experimentally meaningful we must be able to relate it to the concentration and temperature dependencies of the lifetime and intensity ratios.

The rate equations for the time rate of change of the excited sensitizers in the presence and absence of activators can be written as

$$\frac{d\, n_s^o(t)}{dt} = G(t) - B_S\, n_s^o(t)$$

and

$$\frac{d\, n_s(t)}{dt} = G(t) - B_S\, n_s(t) - k\, n_s(t) \qquad [34]$$

respectively where the superscript o indicates the excited sensitizer population with no activators present. These may be easily solved to yield excited sensitizer populations as a function of time in the undoped and doped samples assuming delta function excitation as

$$n_s^o(t) = n_s^o(o)\, e^{-B_S t}$$

and

$$n_s(t) = n_s(o)\, e^{-(B_S + k)t} . \qquad [35]$$

The lifetimes of the undoped and doped samples become $\tau_s^o = B_S^{-1}$ and $\tau_s = (B_S + k)^{-1}$ respectively. The lifetime ratio then becomes

$$\frac{\tau_s^o}{\tau_s} = 1 + \tau_s^o k . \qquad [36]$$

Exciton theory predicts that by plotting $(\frac{\tau_s^o}{\tau_s} - 1)\frac{1}{\tau_s^o}$ versus concentration the concentration independent energy transfer rate can be determined by the slope of the resulting line.

Similarly the concentration independent energy transfer rate can be determined from the ratio of the host fluorescence intensity in the undoped sample to the host fluorescence intensity in doped sample by solving Equation [34] for the case of steady state excitation. Equation

[34] become

$$0 = WN_S - B_S n_s^o$$

and

$$0 = WN_S - B_S n_s - k\, n_s \qquad [37]$$

which yield

$$n_s^o = \frac{WN_S}{B_S} \quad \text{and} \quad n_s = \frac{WN_S}{(B_S + k)} \qquad [38]$$

respectively, where W is the rate of creating excited sensitizers and it has been assumed that N_S the number of unexcited sensitizers is much greater than the number of excited sensitizer. The excited state populations are related to the intensities by the radiative lifetime of the excited sensitizers B_S'. The intensity ratio becomes then

$$\frac{I_s^o}{I_s} = \frac{B_S' n_s^o}{B_S' n_s} = 1 + \tau_s^o k \qquad [39]$$

where it has been assumed that the radiative lifetime of the host is not affected by the presence of the activators and that both samples are being equally excited. As for the lifetime ratio the intensity ratio can be used to obtain k.

As mentioned in the Förster-Dexter development it is experimentally easier to measure the ratio of the activator to host fluorescence in the same sample than it is to measure $\frac{I_s^o}{I_s}$.

From Equation [33] it can be seen that the energy transfer rate varies directly with the activator concentration. The temperature de-

pendence of the energy transfer rate is contained in the diffusion coefficient and except for very simple cases is not easily determined. One such simple case is where the time which the exciton spends on each lattice site is long enough for the lattice surrounding the excited site to relax. In this case the excitation will be out of resonance with the surrounding lattice by an energy ΔE and is usually referred to as self-trapped. Thermal detrapping may occur by the absorption of a phonon which will make up the energy difference and the energy transfer rate will exhibit a temperature dependence analogous to the temperature dependence of the probability for absorption of a phonon.

CHAPTER III

EXPERIMENTAL

Samples and Temperature Control System

Four single crystal boules were obtained for this investigation from Airtron, Inc., an undoped $CaWO_4$ boule and three doped with Sm^{3+} in concentrations of .01, .1 and 1. atomic percent. The doped samples were charge compensated with Na^+ in concentrations equivalent to the samarium concentration. All boules were grown along the crystallographic a axis. Samples were cut perpendicular to the a axis and polished at the Crystal Growth Laboratory facilities at Oklahoma State University. Sample thicknesses were 3 mm undoped; 2.7 mm for the 1% Sm^{3+}, 2.7 mm for the .1% Sm^{3+} and 3.2 mm for the .01% Sm^{3+}.

Cooling of the samples was achieved by mounting them on the cold finger of an Air Products and Chemicals, Inc. Displex Cryogenic Refrigerator model CS202. This is a closed cycle helium refrigerator with the capability of continuously varying the sample temperature from room temperature to $7^{\circ}K$ by means of a heater mounted on the copper sample holder. Optical access to the samples was achieved by means of two quartz windows mounted on the Displex outer vacuum jacket. Thermal contact between the cold finger and the samples was achieved by mechanical clamps since all thermal contact greases tested showed significant fluorescence in the wavelength region of interest to this investigation.

Steady State Apparatus

All absorption measurements were made on a Cary 14 spectrophotometer, using the tungsten-halogen visible light source. No far ultraviolet absorption measurements were possible due to the large absorption coefficient of $CaWO_4$ in this region.

All steady state fluorescence and excitation spectra were made using the arrangement shown in Figure 1. An AH 6 1000 watt mercury lamp was the light source for all fluorescence spectra. The lamp was operated at approximately 1000V and 1 amp, and was simultaneously water and air cooled. The Hg lamp was encased in a fused quartz jacket. The excitation spectra of the doped samples were also made using the Hg light source. The undoped excitation spectra were made using a 150 watt Xenon light source, model X150 obtained from PEK, Inc. Convection was the only means of cooling for the Xenon source. The light from either source was focused onto the entrance slits of a Spex model 1670 minimate monochrometer by means of a condensing lens system. The minimate has a dispersion of 40 Å/mm and the grating was blazed at 3000Å with 1200 grooves/mm, grating model 1653A. For fluorescence spectra 5 mm slits were used while 2.5 mm slits were used for excitation spectra. The output of the monochrometer was focused by means of a short focal length lens (lens 2) onto the sample. The exciting light was incident on the broad face of the sample.

The fluorescence signal was monitored at 90° to the exciting light path. The signal was chopped by a PAR model 125 mechanical chopper at a rate of 2000 cps and was focused by means of lenses 3 and 4 onto the entrance slit of a Spex 1 meter Czerny-Turner spectrometer. The spectrometer, Spex model 1704, has 4 Å/mm dispersion with ultimate resolution of

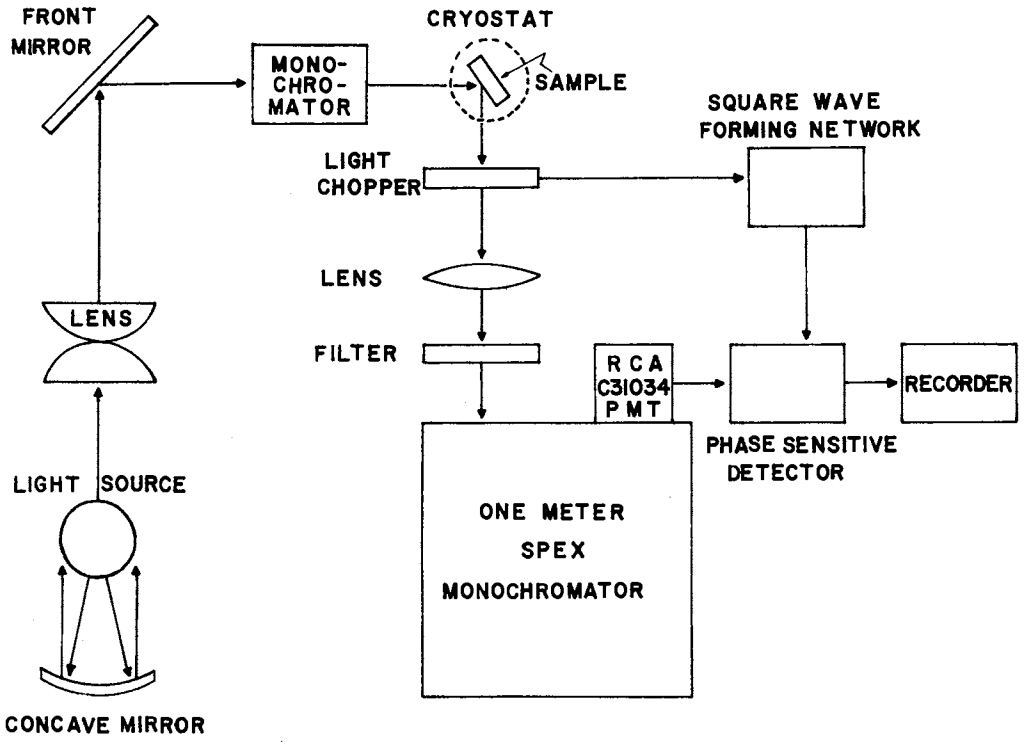

Figure 1. Block Diagram of the Continuous Fluorescence Measurement Apparatus

better than .1 Å. The grating, a Bausch and Lomb number 35-53-15-280 with 1200 grooves/mm was blazed at 5000 Å. The slit width was varied dependent upon the particular circumstances of the spectra. At the spectrometer output was mounted an R.C.A. C31034 phototube which was operated at +1900 VDC. The phototube was cooled by means of a Products for Research Thermoelectric Refrigerated chamber model TE-104 for maximum reduction of dark current. A special optical window was used with the chamber to focus the light onto the photocathode. Chamber specifications indicate cooling of the tube to be at least to -20°C.

The output of the phototube was connected to the A input of a PAR model 128 Lock-In Amplifier, the output of which was monitored on a Heath model EU-205-11 strip chart recorder. The reference signal for the Lock-In Amplifier was taken directly from the light chopper.

A minimum of 24 hours was allowed to achieve cooling of the phototube. All other electronics were allowed a 2 hour warm up period before measurements were made.

Coarse optical alignment of the fluorescence system was achieved by maximizing the 4400Å fluorescence signal with the minimate set on 0 Å and using no slits. Finer alignment was obtained by maximizing the 4400Å fluorescence signal with the minimate selectively exciting the sample at 2800Å with 5 mm slits.

Fluorescence spectra were obtained by fixing the wavelength reading of the minimate and then scanning the Czerny-Turner observing monochrometer from 3300Å to the long wavelength limit of the fluorescence while simultaneously monitoring the Lock-In Amplifier output via the strip chart recorder.

Excitation spectra were obtained by fixing the wavelength monitored

by the Czerny-Turner monochrometer and then scanning the minimate over the wavelength region of interest, while monitoring the output of the Lock-in amplifier via the strip chart recorder.

No attempt was made to correct the spectra for the spectral response of the system. Using published data on the spectral response of the phototube, monochrometers and light sources it was ascertained that the only case in which any significant adjustment to the spectra should be made was in the short wavelength region of the excitation spectra.

Lifetime Apparatus

All lifetime measurements were made using single photon counting time resolved spectroscopy. Two techniques were used: for fluorescence with lifetimes of less than 150 μsec (WO_4^{2-} lifetimes) a coincident pulse height analysis system was used and for lifetimes of greater than .5 msec (Sm^{3+} lifetimes) multichannel scaling was used.

The optical system used for pulse height analysis is shown in Figure 2. The light source was an air filled free running spark gap oscillator Ortec model 9352. Using a 200 megohm resistor and voltages in the range of 5 to 10 KVDC and by utilizing the adjustable gap distance the frequency of the oscillator could be adjusted over a wide range while keeping the duration of each light pulse less than 15 nsec. Selective excitation of the sample was achieved by placing a Schoeffel model GM100 grating monochrometer between the oscillator and the sample. The Schoeffel has a dispersion of 85 Å/mm and grating blazed at 3000Å, 1.4 mm slits were used at all times. The oscillator window was placed at the entrance aperture of the Schoeffel and the distance between the sample and exit aperature of the Schoeffel was 2.5 in. The fluorescence

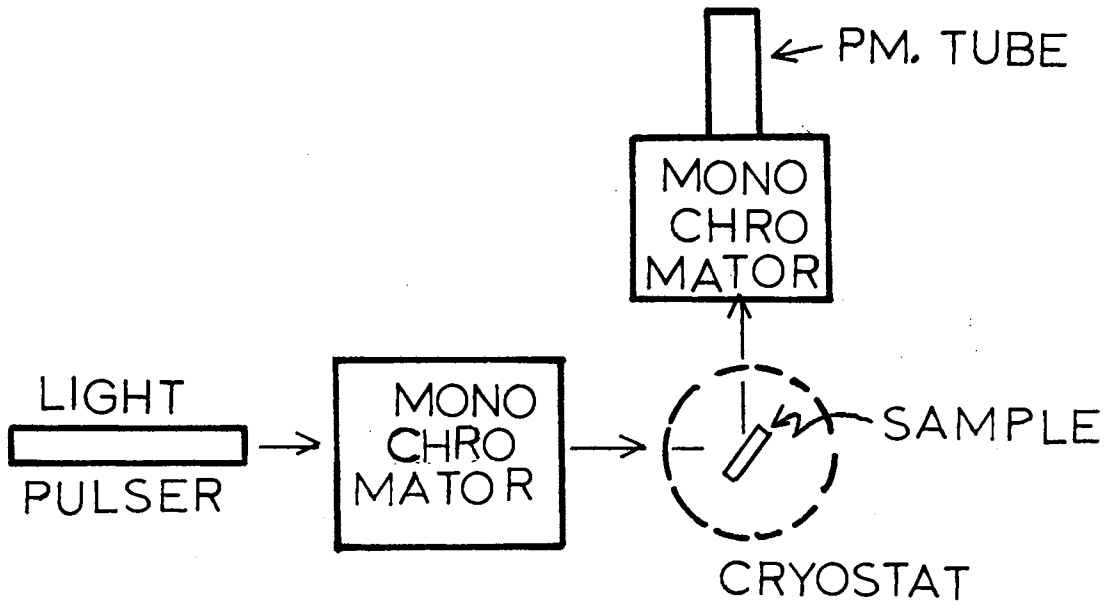

Figure 2. Optical Apparatus for PHA and MCS Measurements

signal was monitored at 90^{o} to the excitation light path with the sample at an angle of approximately 45^{o} to the excitation path as shown in Figure 2. As stated earlier pulse height analysis was used to obtain WO_4^{2-} lifetimes. An R.C.A. 8850 phototube was used to detect the fluorescence. The response of the 8850 is negligible in the spectral region of the Sm^{3+} fluorescence. However, to insure that no Sm^{3+} fluorescence arrived at the phototube a Corning color filter c.s. number 5-60 was placed between the sample and the phototube. Also a second glass filter c.s. number 0-52 was used to insure that no reflected light from the oscillator reached the phototube. Both filters were checked for fluorescence.

The electronic apparatus used for pulse height analysis is shown in block form in Figure 3. Each time the oscillator produced a light pulse an electrical signal was sent to an Ortec 436 100 mHz Discriminator which provided pulse shaping. The negative output of the 436 was then delayed by means of an Ortec 425 Nanosecond Delay, which is capable of introducing 1.7 to 32.7 nsec delay in steps of 1 nsec. The output of the 425 provided a start signal to an Ortec 457 Biased Time to Pulse Height Converter.

The fluorescence signal produced as a result of the light from the pulser striking the sample was detected by an R.C.A. 8850 phototube which was operated at +1900 VDC. The hot anode configuration was used for all lifetime work due to its favorable single photon counting characteristics. The signal produced at the anode of the phototube when light was incident on the cathode provided a signal to an Ortec 454 Timing Filter Amplifier. The 454 was used for pulse shaping and amplification. The output was then presented to an Ortec 463 Constant Fraction Discrimina-

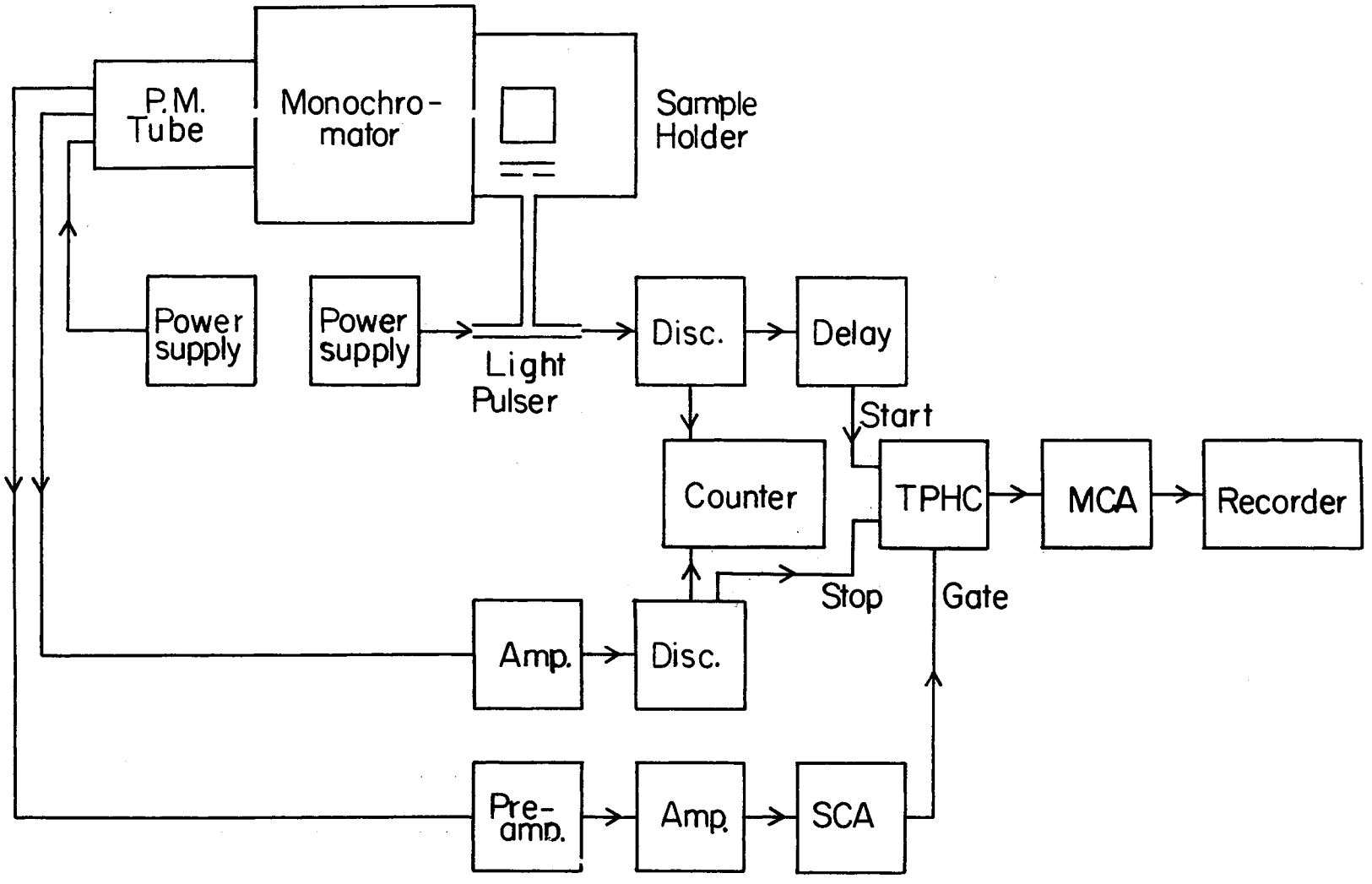

Figure 3. PHA Electronics

tor. The 463 uses a specific point on the leading edge of the input pulse as a trigger to produce a standard output pulse. The standardized negative output of the 463 provided the stop signal to the Ortec 457 Biased Time to Pulse Height Converter. The 457 converts the time between the arrival of the start and stop signals into a proportional voltage in the range of 0 to 10V.

In addition to the start and stop channels a linear or single photon channel was also used. Signals for the linear channel were taken from the last dynode stage of the phototube. The signal was then amplified by an Ortec 113 Scintillation Preamplifier. The output of the 113 was then shaped by an Ortec 451 Spectroscopy Amplifier, the bipolar output of which was used as the input for an Ortec 420A Timing Single Channel Analyzer. The 420A provided a positive going square wave to the strobe input of the 457 Biased Time to Pulse Height Converter if the following conditions were met 1) the input signal to the 420A was above a certain level E' and 2) was within a range $\Delta E'$ above E', where both $\Delta E'$ and E' were preset by the operator. If the 457 did not receive a strobe signal within 100 μsec of the stop signal then the start and stop channels of the 457 were internally cleared and the process was started again.

If the 420A received a signal fulfilling the two conditions of the last paragraph then a positive going square wave was sent to the strobe input of the 457 Biased Time to Pulse Height converter. Upon receiving the strobe signal the 457 sent a positive pulse to a Nuclear Data Analogue to Digital Converter with the height of the pulse proportional to the time between the start and stop signals received by the 457. The A.D.C. Nuclear Data model 1024 was used in combination with a Nuclear Data memory unit and multichannel analyzer. This combination was adjust-

ed so that the output range of the Biased Time to Pulse Height analyzer was divided into 256 regions corresponding to the 256 channels of the memory unit. Each pulse input received by the ADC caused the count in one of the memories' 256 channels to be incremented by +1, the channel being determined by the height of the input pulse to the ADC only.

The process described above was repeated thousands of times to produce a single time resolve spectra. Data was gathered until a smooth curve was obtained. The data was then plotted on a strip chart recorder, the time axis of which was calibrated with reference to the time per channel of the M.C.A. by means of a Tennelac Precision Time Calibrator model TC 850. The outputs of the calibrator were connected to the start and stop channel of the Biased Time to Pulse Height Converter and the strobe switched to interval then the M.C.A. was placed on acquire and data gathered for a period of time. The results were plotted on the strip chart recorder resulting in a straight line representing channels having zero counts and a series of spikes corresponding to channels separated by a time period as determined by the settings of the Tennelac calibrator. Knowing the time separation of the spikes allowed calibration of the time per channel display of the M.C.A.

When using the method described above serious consideration had to be given to the validity of the statistics involved. Two factors were found to greatly effect the statistics, the frequency of the pulser and the ratio of stop to start pulses received by the Biased Time to Pulse Height Converter. A constant monitor on these factors was accomplished by the use of an Ortec Model 715 Dual Counter/Timer. The output of the Constant Fraction Discriminator (stop signals) was used as the input to channel A of the counter and the output of the 100 MHz discriminator

start signals, also the frequency of pulsing) was used as the input to channel B.

In this manner the frequency of pulsing was monitored making use of the timing features of the Ortec 715. By adjusting the gap length and the voltage applied to the spark gap oscillator the frequency of pulsing was limited to at most 1 pulse per 4 lifetimes. This would insure that the sample fluorescence due to one pulse was sufficiently low in intensity to not contribute significantly to the fluorescence signal produced by the next pulse.

In addition to the frequency of pulsing the ratio of stop to start signals could also affect the statistics. If the Biased Time to Pulse Height Converter received more stop signals than start signals the resulting spectra was confused. However, if the ratio of stop to start counts was approximately .9 or 1 the spectra produced was not so obviously distorted but was indeed biased toward shorter lifetimes. This problem was dealt with in two ways. An aperature inserted between the sample and the phototube was used to reduce the fluorescence signal received by the phototube and thereby lowering the number of stop counts. The second and most advantageous method was the use of the linear channel. By properly adjusting the E' and ΔE' levels of the Timing Single Channel Analyzer the linear channel could be used to discard all events which did not correspond to the event of a single photon being incident on the phototube. With the linear channel operating ratio's of stop to start signals as large as .8 could be used safely. Without the linear channel ratio's of less than .1 stop to start are recommended. The E' and ΔE' levels used were dependent upon the phototube used and proper adjustment of these levels are outlined in detail in a technical note published by

Ortec, "The Single Photon Technique for Measuring Light Intensity and Decay Characteristics." (32)

Multichannel scaling was used to determine the Sm^{3+} lifetimes. A Xenon Corporation model 437A Nanopulser and Nanolamp which produced a 19 nsec light pulse was used as an excitation source. The rest of the optical arrangement was identical to that used for pulse height analysis except for the phototube which was a cooled R.C.A. C31034. Specification of the cooling system is given in the previous section of this chapter. The electronics configuration used is shown in Figure 4.

The nanolamp pulsed each time a positive going signal of 3 to 7 volts arrived at the Remote Auto Trigger input of the nanopulser. This signal was provided by a Tektronics type 163 pulse generator which was triggered by a Tektronics type 162 waveform generator. A second type 163 pulse generator provided a start signal of positive 6V to the start input of the M.C.A.

Upon receipt of a start signal the M.C.A. would step to channel 1 and add to the memory of that channel the number of counts received at the M.C.A. Counts input during the preset dwell time. At the end of the dwell time the M.C.A. was internally stepped to the next channel where the process was repeated. When the dwell time in the last, 256 th, channel ended the M.C.A. was internally stepped to a stop and wait sequence. This stop and wait sequence was broken when 1) the mode switch was manually changed to display or 2) another start signal was received.

The counts channel input was obtained from the fluorescence signal incident on the phototube. The electronics between the last dynode stage of the phototube and the M.C.A. counts input were identical to the linear channel as described for the pulse height analysis measure-

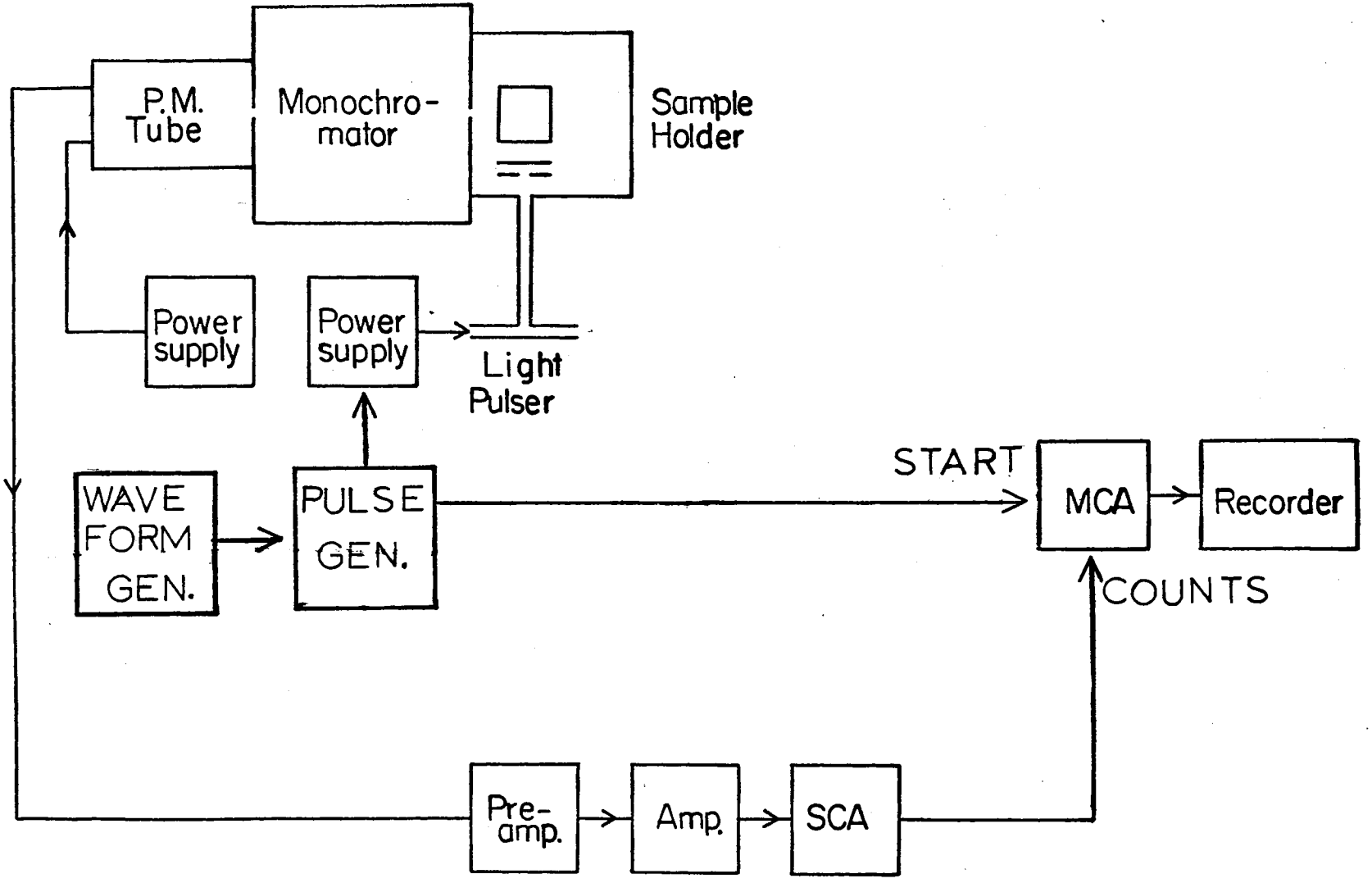

Figure 4. MCA Electronics

ments. The E' and ΔE' levels of the Timing Single Channel Analyzer were adjusted to discard all but single photon events occurring at the photo-tube.

A time resolved spectrum of the fluorescence was obtained by allowing the pulser to excite the sample a large number of times until a smooth display was obtained. Again care had to be taken to avoid pulsing the sample faster than it could decay. The frequency of pulsing was determined by the period of the waveform generated by the Tektronics 162 waveform generator. Calibrator of the M.C.A. time per channel was not necessary because each channel corresponded to the preset dwell time.

CHAPTER IV

EXPERIMENTAL RESULTS

$CaWO_4$ Undoped

Absorption Spectra

The absorption spectra of a 3 mm thick undoped $CaWO_4$ sample is shown in Figure 5. The spectrum exhibits a strong absorption below 3100Å and a small tail that extends past 5000Å. The spectrum is smooth except for a small broad shoulder at approximately 3900Å.

Excitation Spectra Vs. Temperature

The excitation spectra exhibit structure in the region of high WO_4^{2-} absorption. Figure 6 shows the excitation spectrum obtained for the undoped $CaWO_4$ sample at 10°K and room temperature while monitoring the fluorescence at 3800Å. At room temperature there is an intense band which peaks at about 2690Å and has several shoulders at lower wavelengths. At wavelengths longer than 2900Å structure appears at low temperatures as broad weak bands peaking at 2990Å, 3090Å and 3560Å.

Figure 7 shows the excitation spectrum obtained at 10°K and room temperature while monitoring the fluorescence at 6000Å. At room temperature there is a broad band which peaks at 2830Å with a shoulder at 2780Å. As the tempeature is lowered the intensity of the band decreases and the peak shifts to lower wavelengths peaking near 2750Å at 10°K. No

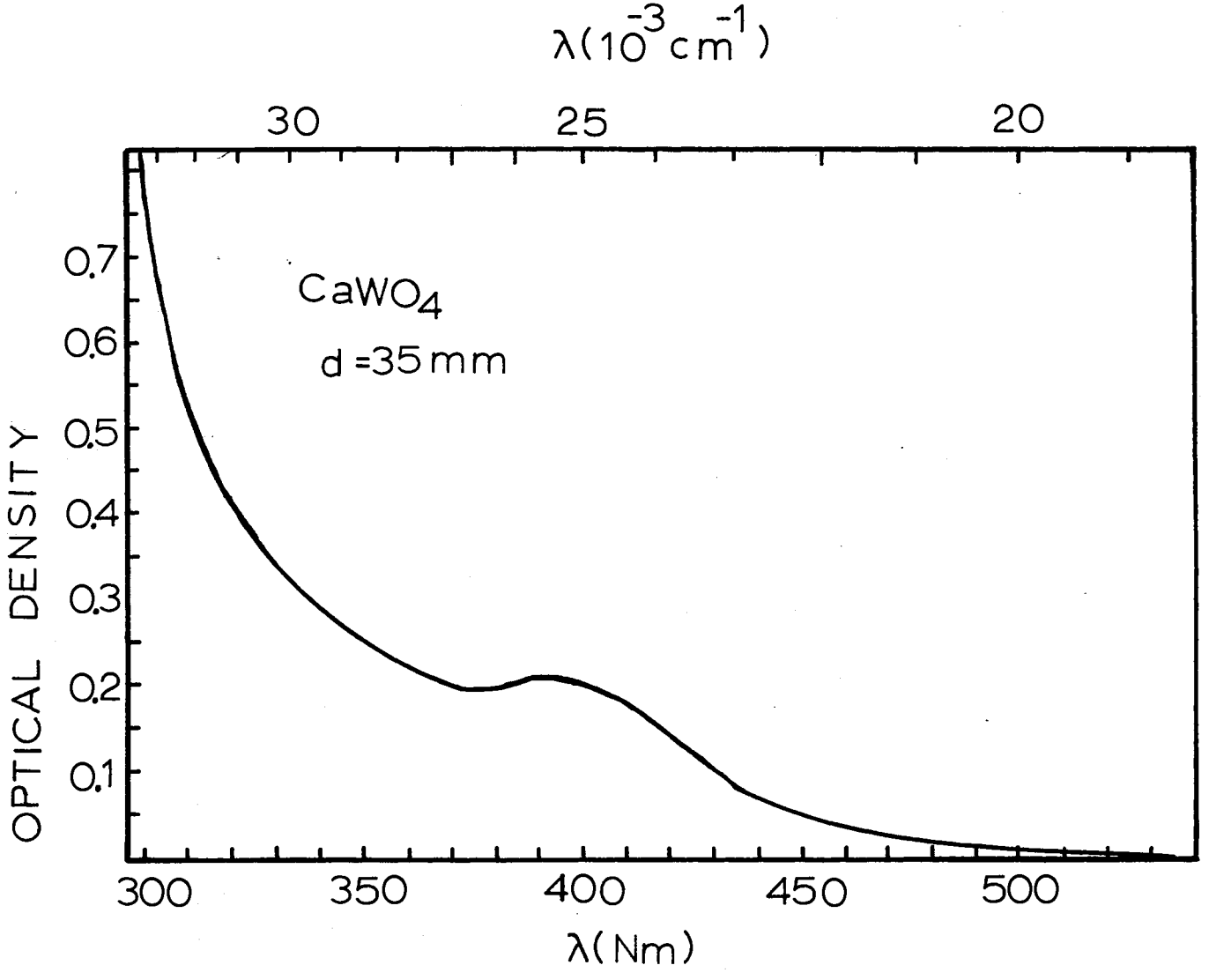

Figure 5. Absorption Spectra of Undoped Calcium Tungstate

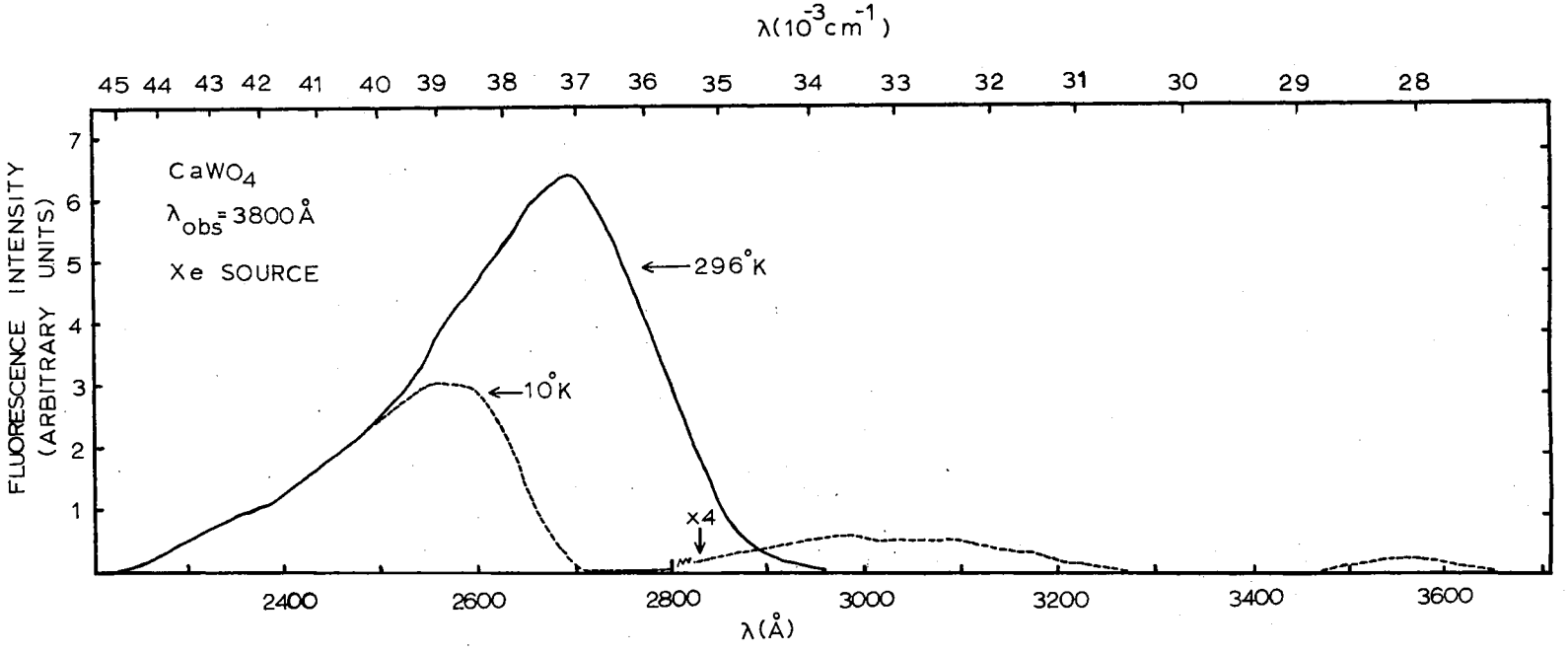

Figure 6. Excitation Spectra of Undoped $CaWO_4$ for Observation at 3800Å at 10°K and 296°K

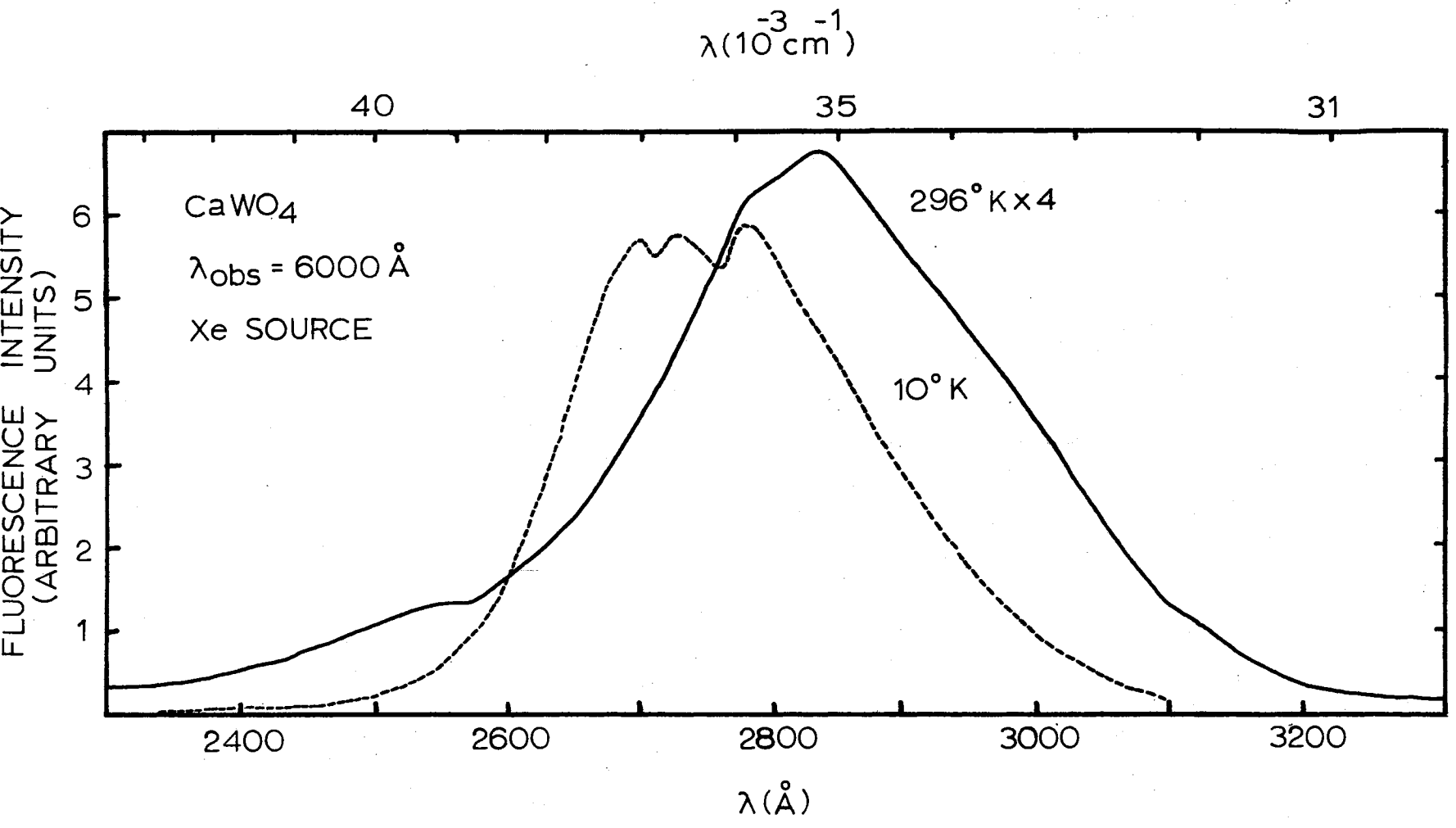

Figure 7. Excitation Spectra of Undoped $CaWO_4$ for Observation at 6000Å at 10°K and 296°K

structure was observed past 3200Å for observation at 6000Å.

Fluorescence Spectra Vs. Temperature

For excitation at 2400Å a broad characteristic fluorescence band peaking near 4400Å was obtained at all temperatures and is shown at 10°K and room temperature in Figure 8. The integrated fluorescence intensity of this band exhibited virtually no temperature dependence as shown in Figure 9. Excitation at 3150Å, however produced an unusual, heretofore, unreported fluorescence band which peaked near 5200Å at all temperatures and is shown at 10°K and 121°K in Figure 10. Below 150°K two zero phonon lines appear at 3680Å and 3750Å. The intensity of the high energy zero phonon line increased with decreasing temperature while simultaneously the intensity of the low energy line decreased. The integrated fluorescence intensity remained relatively constant up to 150°K and then increases to a maximum at about 220°K and then decreases as the temperature is raised further.

The fluorescence bands produced upon excitation with 2650Å light at 10°K and room temperature are shown in Figure 11. At room temperature a broad band peaking near 4400Å is produced. As the temperature is lowered, however, the band shifted to longer wavelengths peaking near 5300Å at 10°K. The integrated fluorescence intensity as shown in Figure 9 indicates a temperature dependence similar to that for excitation at 3150Å with the maximum occurring at a slightly lower temperature approximately 180°K.

Lifetime Vs. Temperature

The lifetimes of the broad band fluorescence for selective excita-

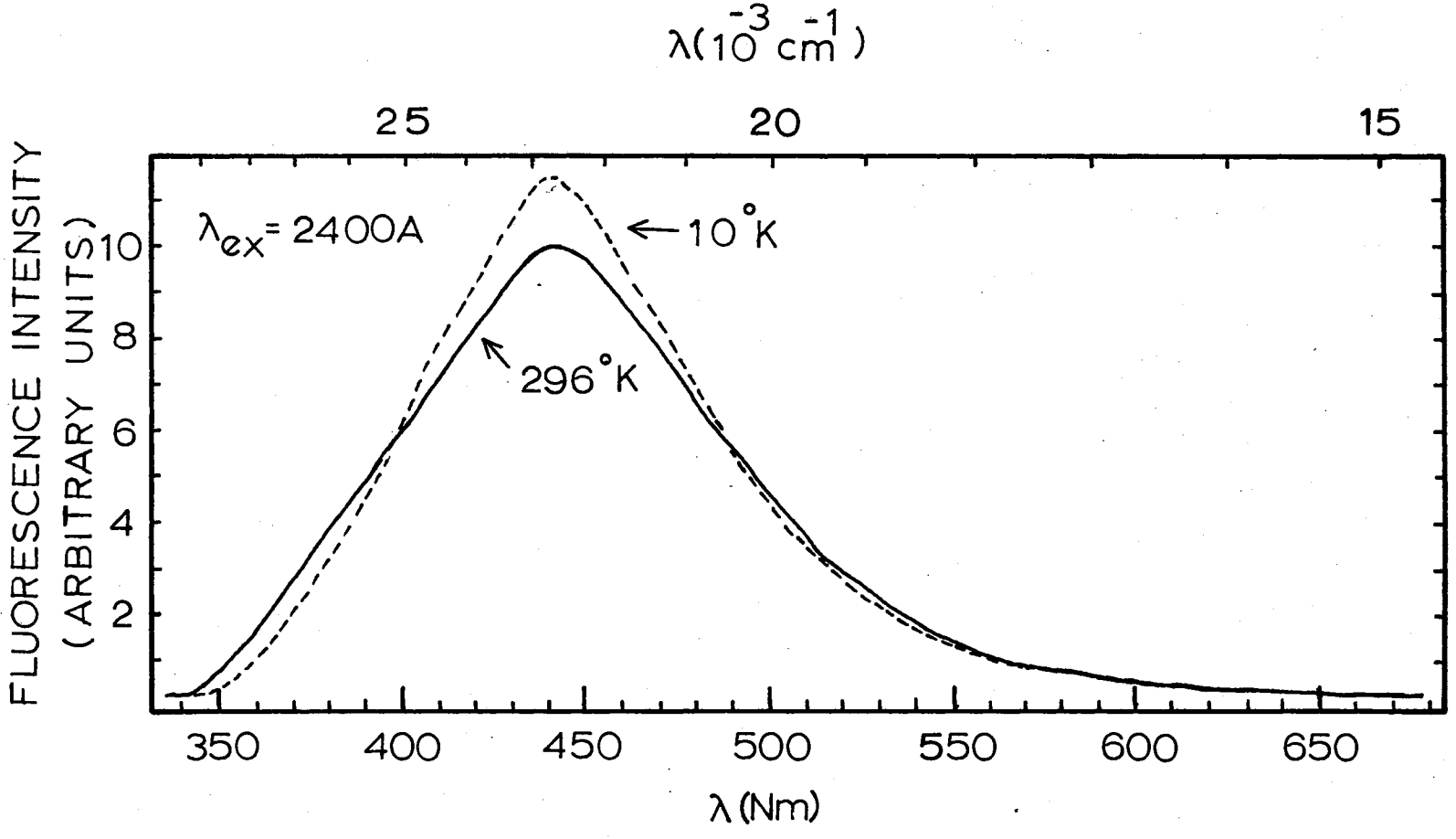

Figure 8. Fluorescence Spectra of Undoped $CaWO_4$ for 2400Å Excitation at 10°K and 296°K

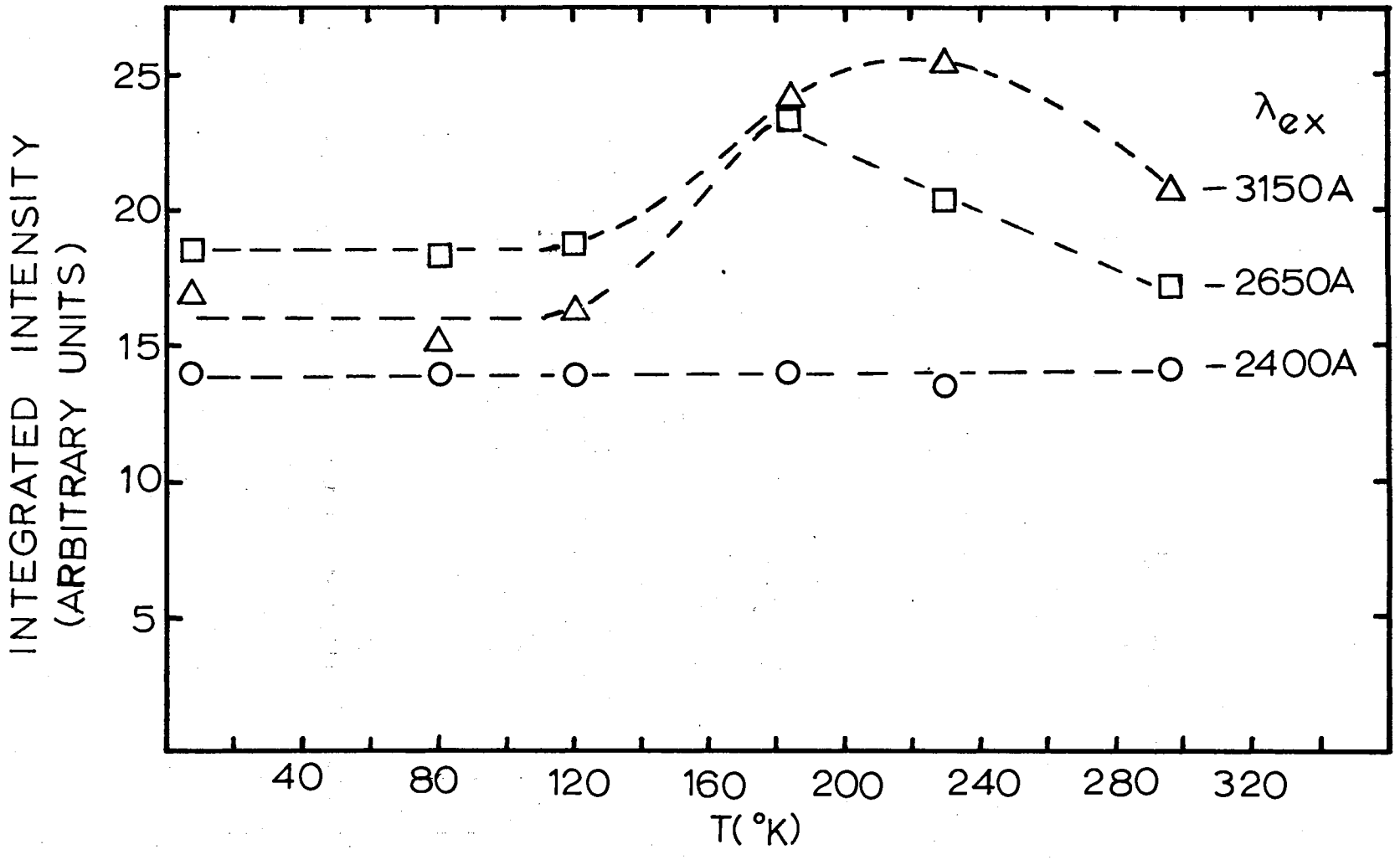

Figure 9. Integrated Fluorescence Intensity of Undoped $CaWO_4$ as a Function of Temperature and Excitation Wavelength

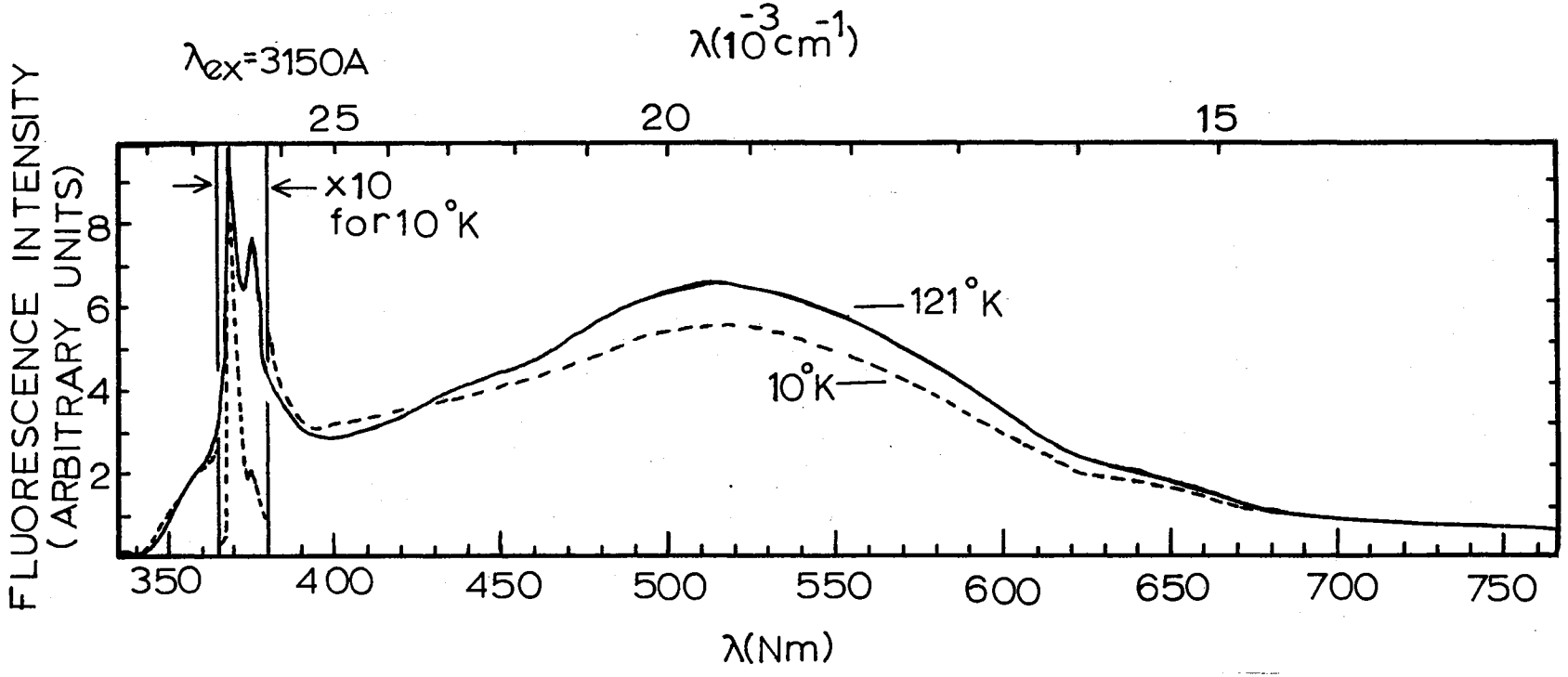

Figure 10. Fluorescence Spectra of Undoped $CaWO_4$ for 3150Å Excitation at 10°K and 121°K

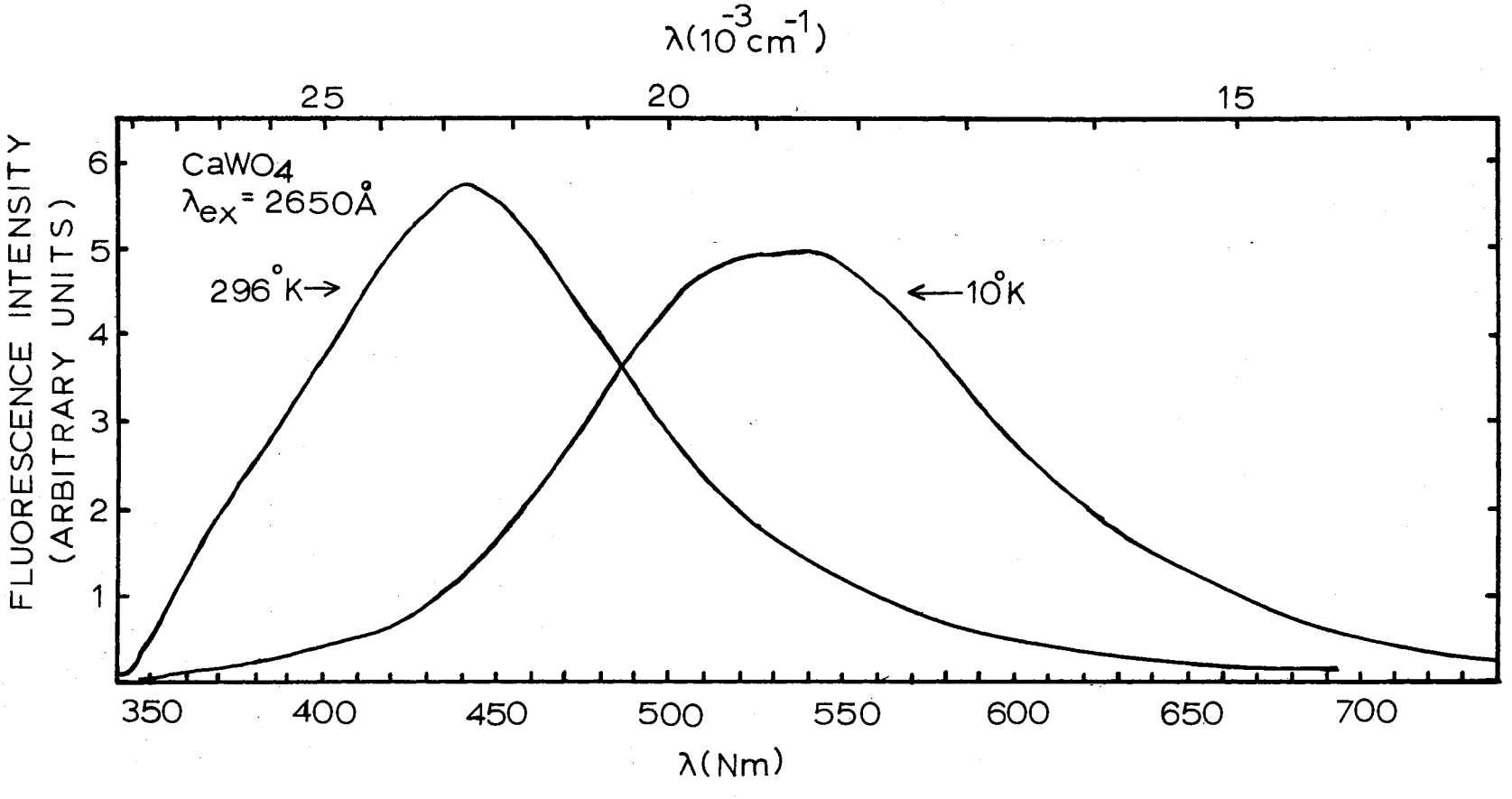

Figure 11. Fluorescence Spectra of Undoped $CaWO_4$ for 2650Å Excitation at 10°K and 296°K

tion at 2400Å, 2650Å and 3150Å are shown in Figure 12 as a function of temperature and are tabulated in Table I. Below 220°K the lifetimes for 3150Å excitation became too long to be measured by the pulse height analysis method and yet too short to be determined by multichannel scaling. However, the two points obtained indicate a sharp temperature dependence of the lifetime.

The lifetimes for 2400Å and 2650Å excitation decrease rapidly as temperature is raised from 10°K to 120°K and then level off. This flat region extends to approximately 220°K where again the lifetimes begin decreasing but not as rapidly as at low temperatures. At room temperature all three lifetimes are approximately the same, as shown in Figure 12.

$CaWO_4:Sm^{3+}$

Absorption Spectra

Figure 13 shows the absorption spectra of a 23 mm thick sample of calcium tungstate containing 1% Sm^{3+} at room temperature. The spectra was obtained using unpolarized light and with the light path along the crystallographic a axis. The spectra appears to be the superposition of the smoothly decreasing $CaWO_4$ absorption as shown in Figure 5 and the relatively sharp absorption lines of the Sm^{3+} centers. Table II lists the position of the 58 lines observed in the absorption spectrum. Their intensities are designated as strong (S), Medium (M), weak (W) and very weak (VW) while their widths are listed as narrow (N) or broad (B). A peak not resolved from a major line is designated as a shoulder. Polarization measurements showed little effect on the relative intensities of

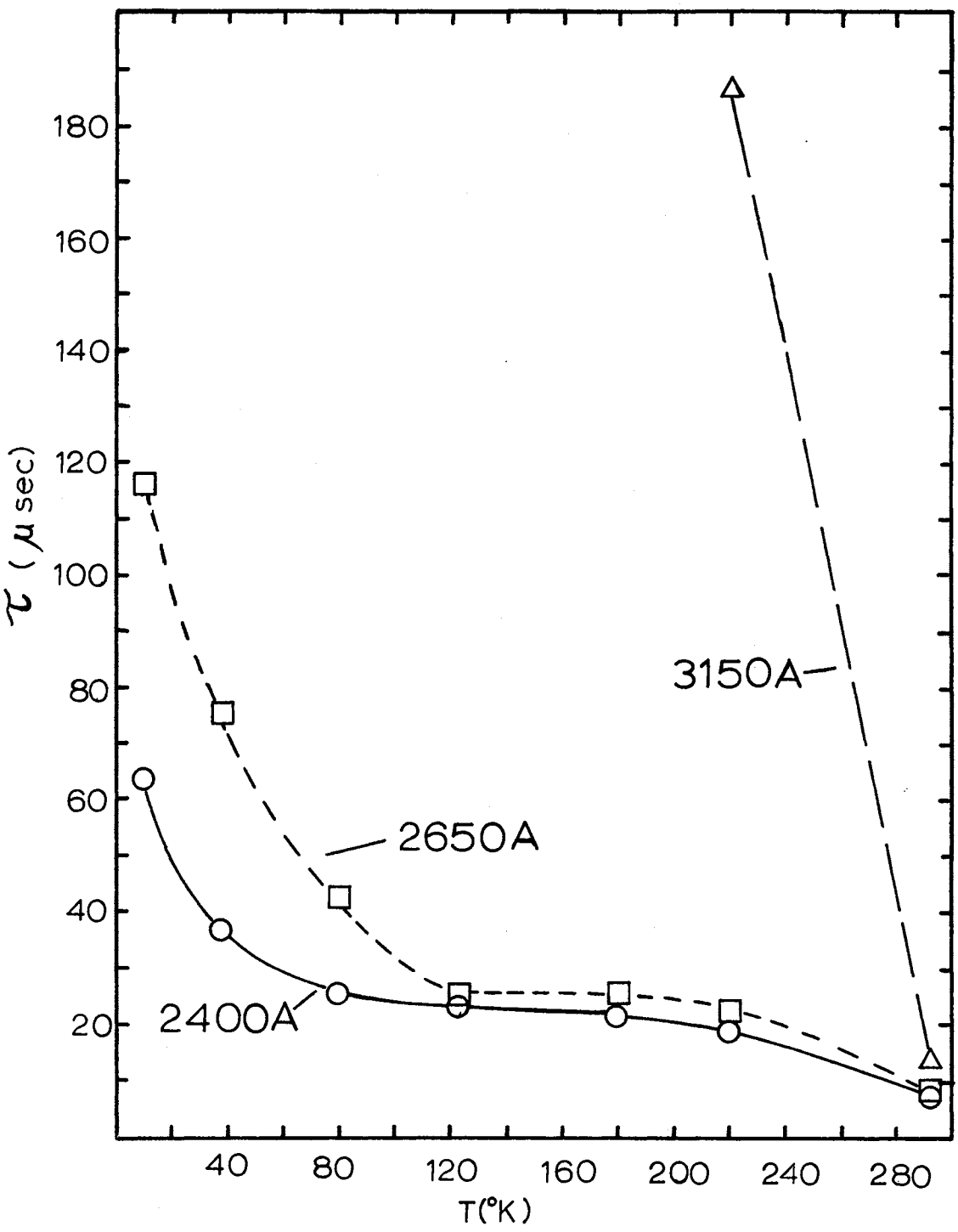

Figure 12. Measured Tungstate Fluorescence Lifetimes as a Function of Temperature and Excitation Wavelength

TABLE I

UNDOPED $CaWO_4$ TUNGSTATE LIFETIMES

Temperature °K	Excitation Wavelength 2400Å	2650Å	3150Å
296	7.62	7.77	13.93
220	18.39	22.73	186.
180	21.27	25.34	
123	23.56	25.06	
80	25.64	42.2	
38	36.2	75.4	
11.5	63.	117.	

All lifetimes in μsec.

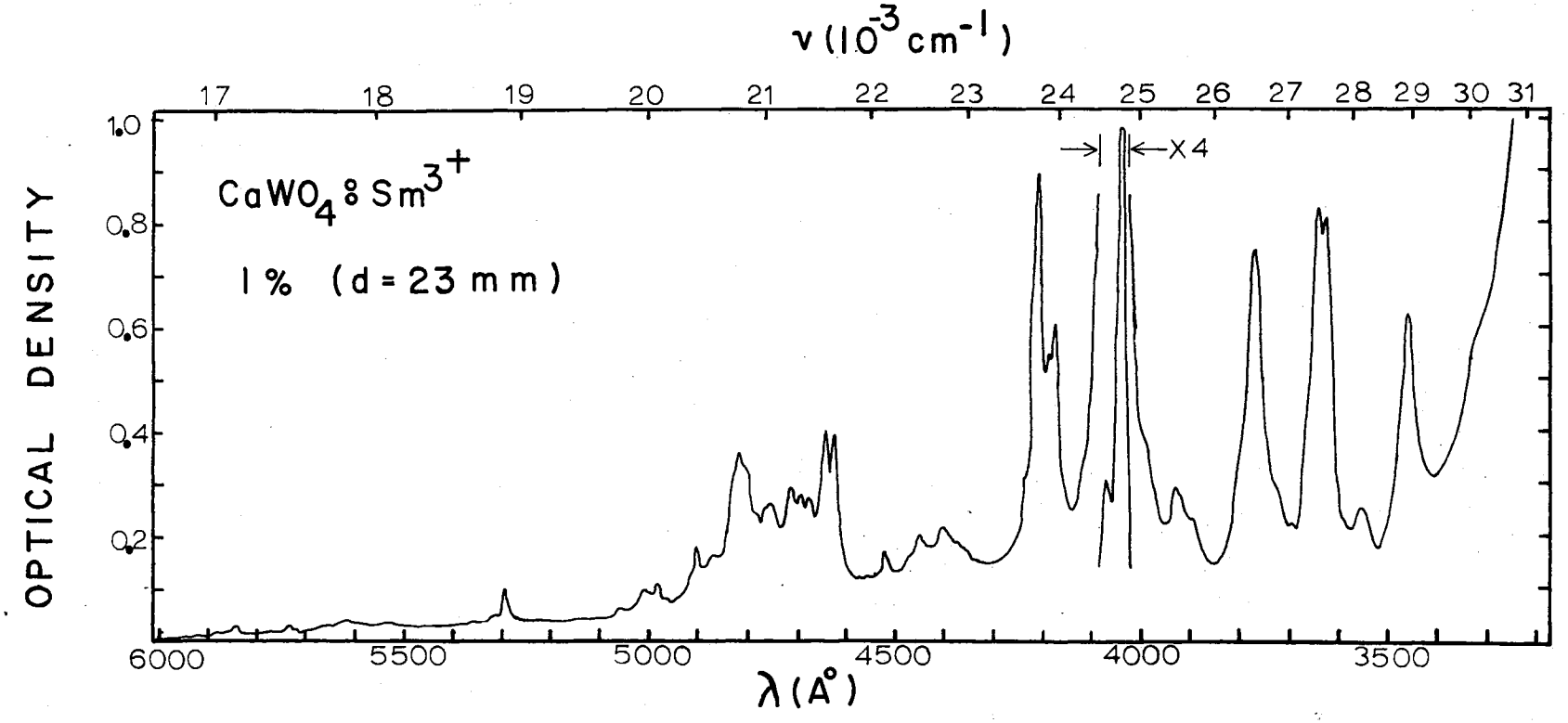

Figure 13. Absorption Spectra of $CaWO_4:Sm^{3+}$ 1.0%

TABLE II

SPECTRAL LINES OF Sm^{3+} IN $CaWO_4$

A. ABSORPTION

λ(A)	$\tilde{\nu}(cm^{-1})$	Comments	λ(A)	$\tilde{\nu}(cm^{-1})$	Comments
3322	30,102	shoulder	4623	21,631	W,N
3431	29,146	shoulder	4639	21,556	W,N
3458	28,918	M,N	4672	21,404	W,N
3482	28,719	shoulder	4690	21,322	W,N
3540	28,249	shoulder	4710	21,231	W,N
3554	28,137	W,N	4750	21,053	W,N
3575	27,972	shoulder	4760	21,008	shoulder
3620	27,624	M,N	4780	20,921	shoulder
3630	27,548	M,N	4805	20,812	shoulder
3642	27,457	M,N	4815	20,768	W,N
3660	27,322	shoulder	4825	20,725	shoulder
3695	27,064	W,N	4865	20,555	shoulder
3725	26,846	shoulder	4900	20,408	W,N
3762	26,582	M,N	4912	20,358	shoulder
3800	26,316	shoulder	4940	20,243	shoulder
3891	25,700	shoulder	4980	20,080	W,N
3919	25,517	shoulder	5008	19,968	W,B
3928	25,458	W,N	5055	19,782	W,B
3988	25,075	shoulder	5291	18,900	W,N
4026	24,839	shoulder	5312	18,825	shoulder
4045	24,722	S,N	5360	18,657	VW,B
4072	24,558	shoulder	5525	18,100	VW,B
4169	23,987	M,N	5622	17,787	VW,B
4180	23,923	shoulder	5660	17,668	VW,B
4200	23,810	M,N	5734	17,440	VW,N
			5846	17,106	VW,N
			5882	17,001	VW,B
			5920	16,892	VW,B

B. FLUORESCENCE

λ(A)	$\tilde{\nu}(cm^{-1})$	Comments	λ(A)	$\tilde{\nu}(cm^{-1})$	Comments
5467.0	18,291.6	VW,VB	6467.6	15,461.7	shoulder
5619.3	17,795.8	W,N	6468.8	15,458.8	shoulder
5631.2	17,758.2	W,N	6475.2	15,443.5	shoulder
5633.8	17,750.0	shoulder	6480.0	15,432.1	W,B
5635.1	17,745.9	S,N	6483.5	15,423.8	W,B
5636.0	17,743.1	shoulder	6512.0	15,356.3	S,B
5654.2	17,686.0	W,B	6516.0	15,346.8	S,B
5656.5	17,678.8	W,B	6517.6	15,343.1	VS,N
5659.0	17,671.0	W,B	6519.2	15,339.3	shoulder
5661.2	17,664.1	W,B	6521.2	15,334.6	W,N
5690.0	17,574.7	VW,B	6523.2	15,329.9	W,N

TABLE II (Continued)

λ(A)	$\tilde{\nu}(cm^{-1})$	Comments	λ(A)	$\tilde{\nu}(cm^{-1})$	Comments
5706.5	17,523.9	W,B	6556.5	15,252.0	W,VB
5782.3	17,294.2	VW,VB	6618.5	15,109.2	VW,B
5845.5	17,107.2	VW,VB	6645.0	15,048.9	VW,VB
5888.5	16,982.2	VW,N	6702.0	14,920.9	VW,VB
5894.0	16,966.4	VW,N	6810.0	14,684.3	VW,VB
5912.0	16,914.7	VW,N	6818.5	14,666.0	VW,VB
5917.5	16,899.0	VW,N	6850.0	14,598.5	VW,VB
5945.5	16,819.4	VW,N	6856.0	14,585.8	VW,VB
5967.5	16,757.4	VW,N	6875.0	14,545.4	VW,VB
5972.5	16,743.4	VW,N	6877.0	14,541.2	VW,VB
5991.2	16,691.1	shoulder	6922.0	14,446.7	VW,VB
5993.3	16,685.3	S,N	6935.0	14,419.6	VW,VB
6004.4	16,654.4	S,N	6980.0	14,326.6	VW,VB
6046.6	16,538.2	shoulder	7035.5	14,213.6	VW,N
6050.8	16,526.7	S,N	7056.5	14,171.3	W,N
6054.0	16,518.0	shoulder	7060.8	14,162.7	shoulder
6076.0	16,458.2	S,B	7063.8	14,156.7	VS,N
6121.0	16,337.2	VW,B	7066.5	14,151.3	shoulder
6136.0	16,297.3	VW,B	7069.0	14,146.3	shoulder
6147.0	16,268.1	VW,B	7075.0	14,134.3	VW,N
6159.5	16,235.1	VW,B	7081.5	14,121.3	VW,N
6280.5	15,922.3	VW,B	7085.5	14,113.3	VW,N
6293.0	15,890.7	VW,B	7092.0	14,100.4	shoulder
6298.5	15,876.8	VW,B	7098.5	14,087.5	shoulder
6343.0	15,765.4	VW,B	7110.0	14,064.7	VS,B
6373.0	15,691.2	VW,VB	7118.0	14,048.9	VS,B
			7123.0	14,039.0	shoulder
			7149.0	13,988.0	S,N
			7178.0	13,931.5	S,B
			7250.0	13,793.1	W,VB

the peaks; however, the optical densities appeared to be lower for polarization parallel to the c axis than for perpendicular polarization. The largest polarization effect is exhibited by the 3762Å and 4623Å peaks which are slightly larger for perpendicular polarization relative to the other peaks.

The absorption spectra of calcium tungstate containing 0.1% samarium is shown in Figure 14 for a 20 mm thick sample. The absorption lines correspond to those observed for the 1% samarium sample as shown in Figure 13 but much of the fine structure is unresolved.

Excitation Spectra

The excitation spectra obtained by observing the tungstate fluorescence at 4400Å at room temperature and 10°K from calcium tungstate samples containing 1.0%, .1% and .01% samarium are shown in Figures 15, 16 and 17 respectively. For the 1% samarium sample Figure 15 shows at room temperature two broad bands peaking near 2500Å and 2700Å. The 2700Å band is more intense and has a shoulder near 2750Å. At 10°K the 2500Å band has increased by more than a factor of 2 compared to its room temperature intensity and the 2700Å band is totally quenched. Figures 16 and 17 show that the quenching of the 2700Å band decreases with decreasing samarium concentration. Also the 2500Å band at 10°K shifts slightly to longer wavelengths with decreasing samarium concentration as does the 2700Å peak at room temperature. At room temperature the 2700Å band becomes increasingly efficient in producing host fluorescence with decreasing samarium concentration relative to the 2500Å band.

The excitation spectra obtained by observing the 6463Å samarium fluorescence line at room temperature and 10°K from calcium tungstate

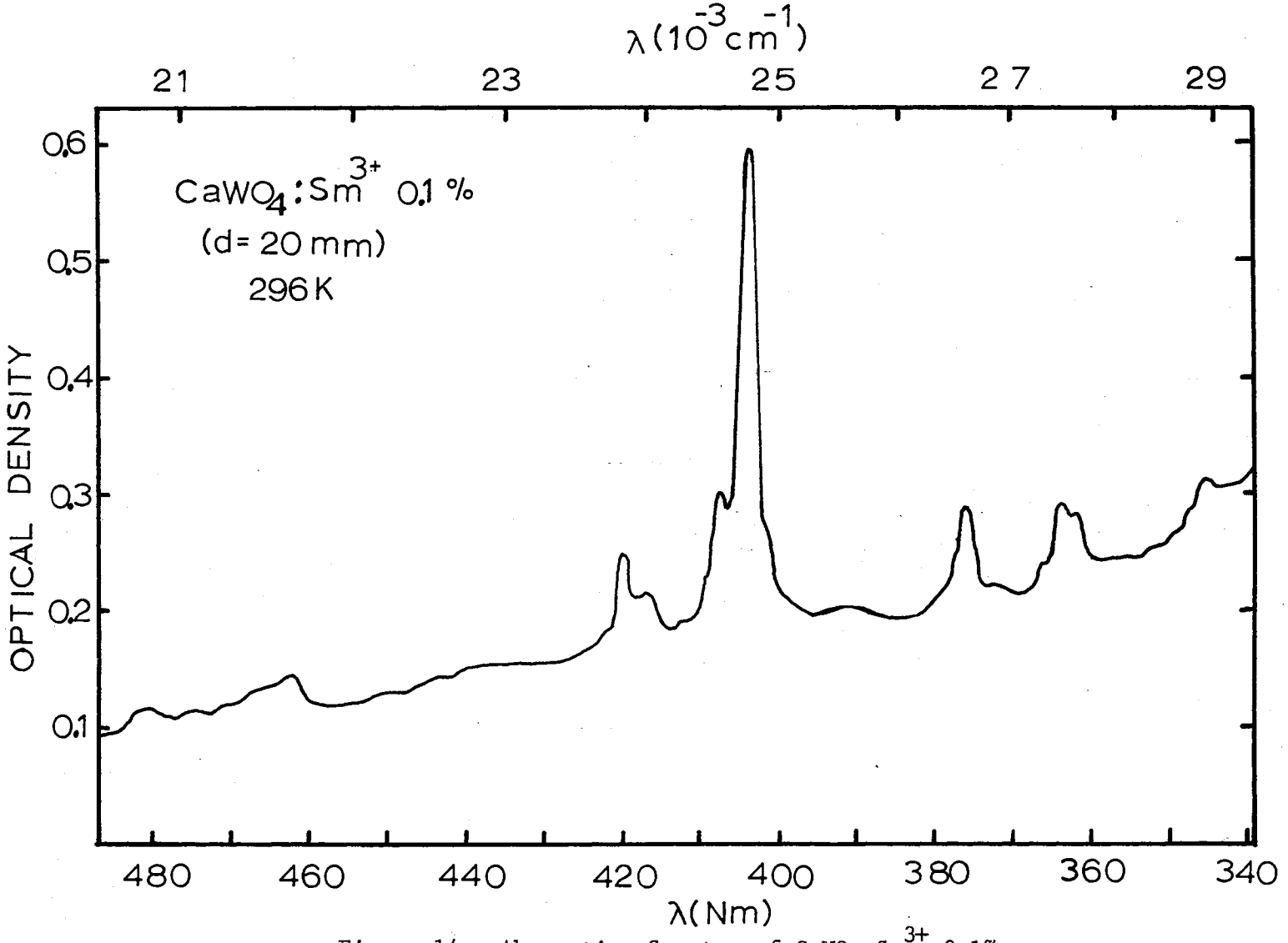

Figure 14. Absorption Spectra of $CaWO_4:Sm^{3+}$ 0.1%

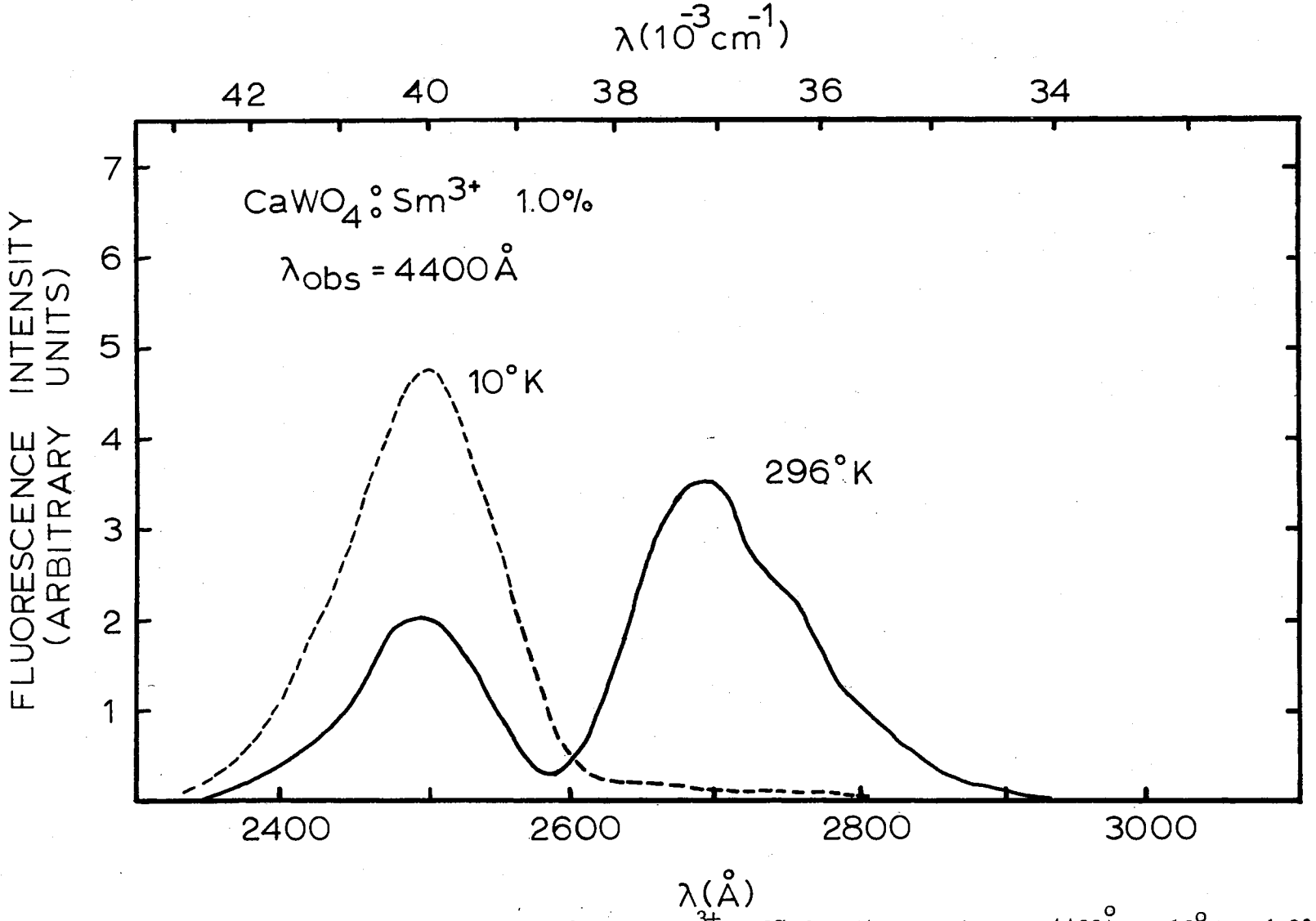

Figure 15. Excitation Spectra of $CaWO_4:Sm^{3+}$ 1.0% for Observation at 4400Å at 10°K and 296°K

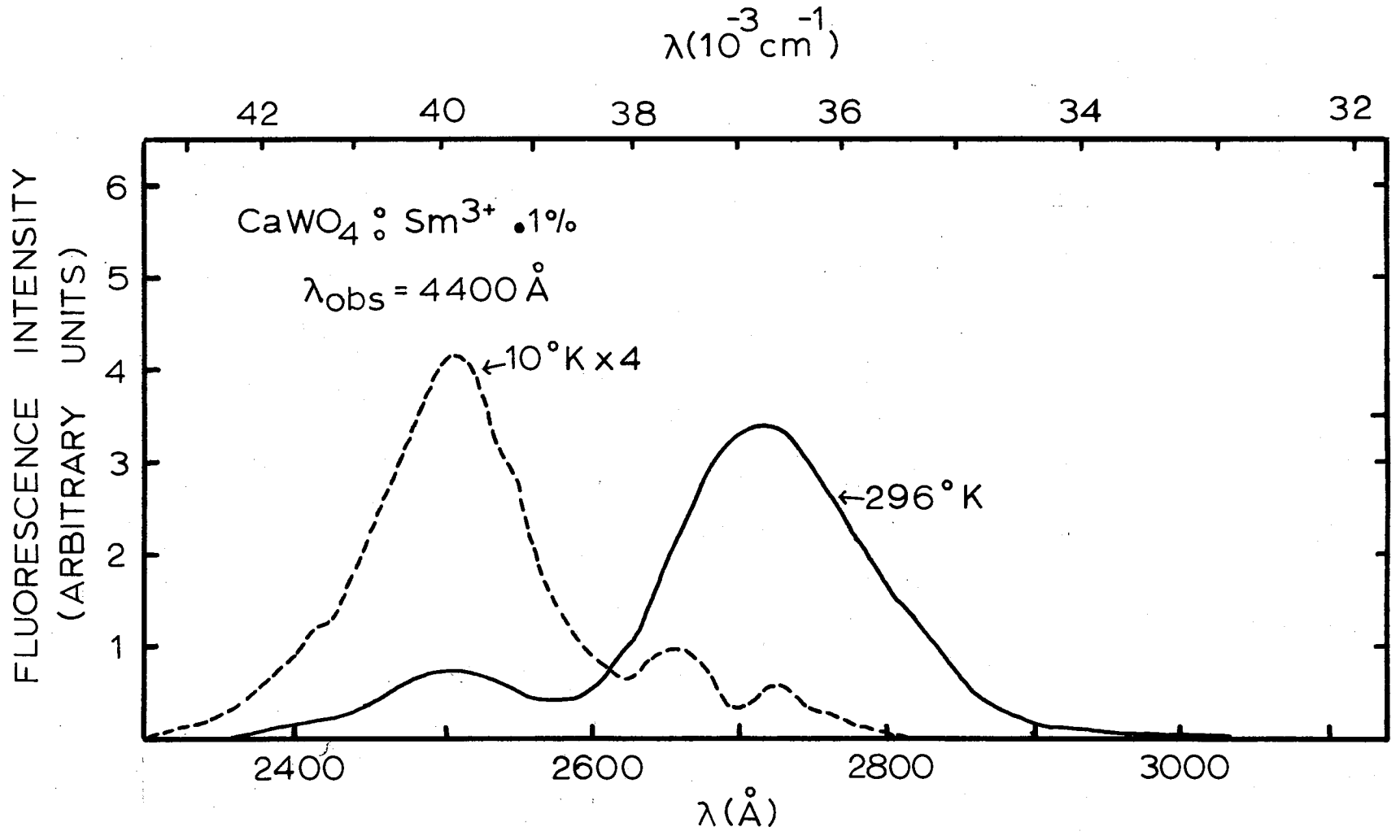

Figure 16. Excitation Spectra of $CaWO_4:Sm^{3+}$ .1% for Observation at 4400Å at 10°K and 296°K

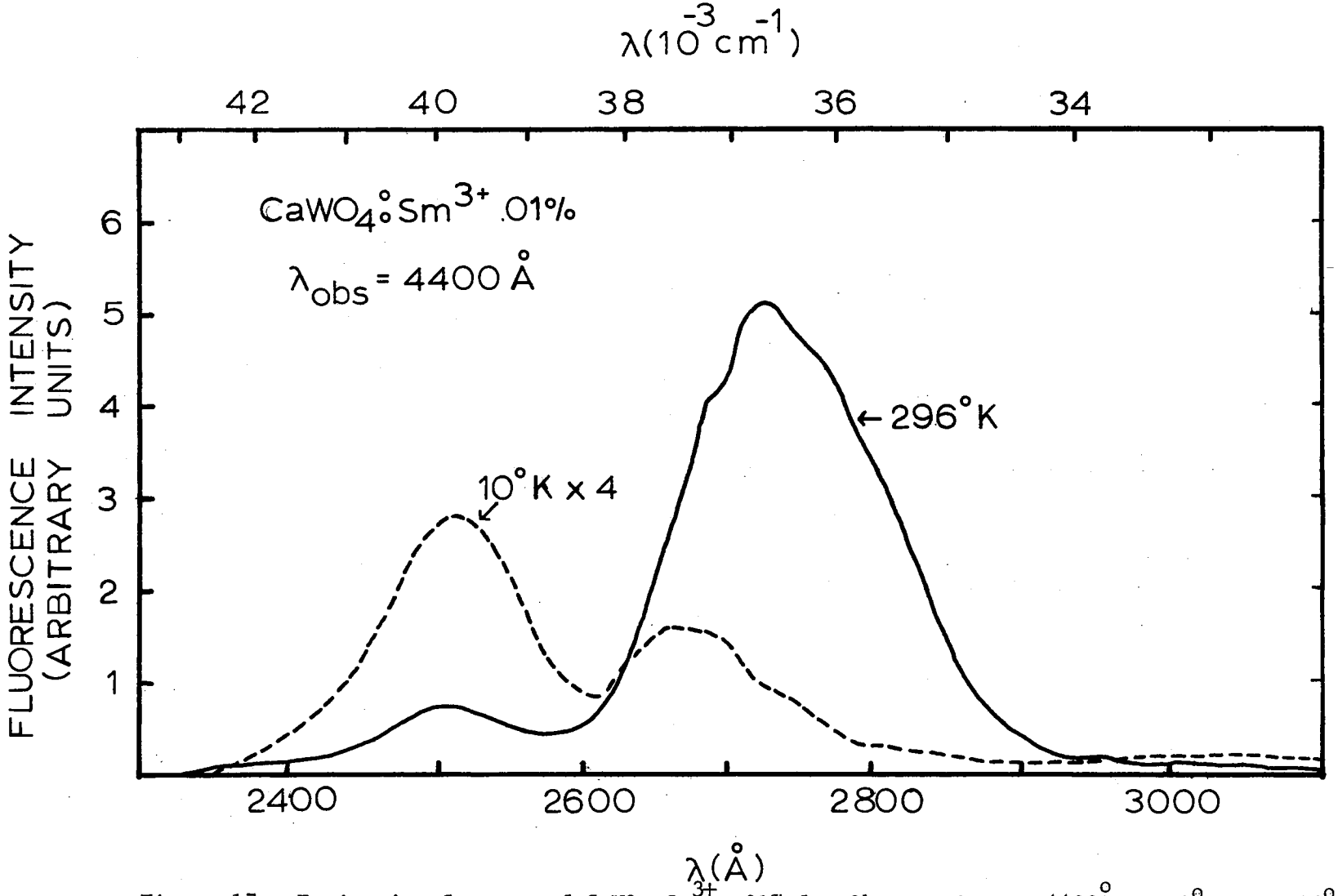

Figure 17. Excitation Spectra of $CaWO_4:Sm^{3+}$ .01% for Observation at 4400Å at 10°K and 296°K

containing 1.0%, .1% and .01% samarium are shown in Figures 18, 19 and 20 respectively. Comparison with the absorption spectra for calcium tungstate with 1.0% samarium as shown in Figure 13 indicates that most of excitation bands at wavelengths longer than 3400Å are the result of direct excitation of the samarium. All excitation bands at wavelengths shorter than 3400Å are the result of excitation of the samarium via energy transfer from the calcium tungstate. These bands increase in intensity with increasing samarium concentration and decrease in intensity with decreasing temperature relative to the intrinsic samarium excitation bands.

The intrinsic samarium bands exhibit little temperature dependence. At lower temperatures the overall intensity increases and the broad band which peaks near 3700Å at room temperature is split at 10°K into two peaks at 3640Å and 3760Å.

The bands at 2500Å and 2700Å exhibit a temperature and concentration dependence similar to the 2500Å and 2700Å excitation bands of the calcium tungstate fluorescence in samples containing samarium as described previously. The excitation bands at 3050Å and 3150Å decrease in intensity with decreasing temperature relative to the 3450 intrinsic samarium excitation band and this effect increases with increasing samarium concentration. An excitation band is shown at 3350Å in the 1% samarium sample but is present only at low temperatures in the .1% samarium sample and not observed at all in the .01% samarium sample.

Fluorescence Spectra Vs. Temperature

Intrinsic Sm^{3+}

Direct excitation of samarium in calcium tungstate was achieved by

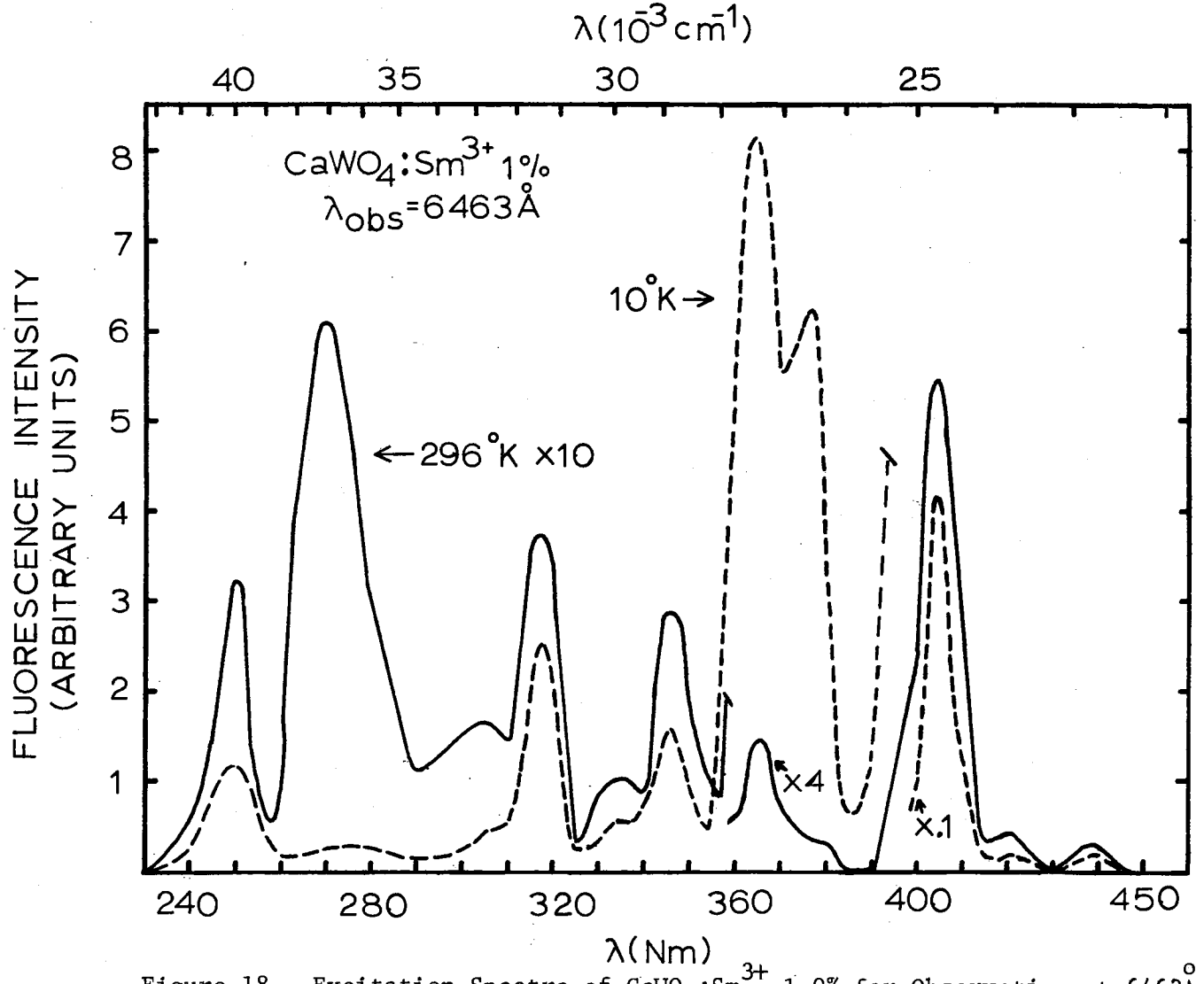

Figure 18. Excitation Spectra of $CaWO_4:Sm^{3+}$ 1.0% for Observation at 6463Å at 10°K and 296°K

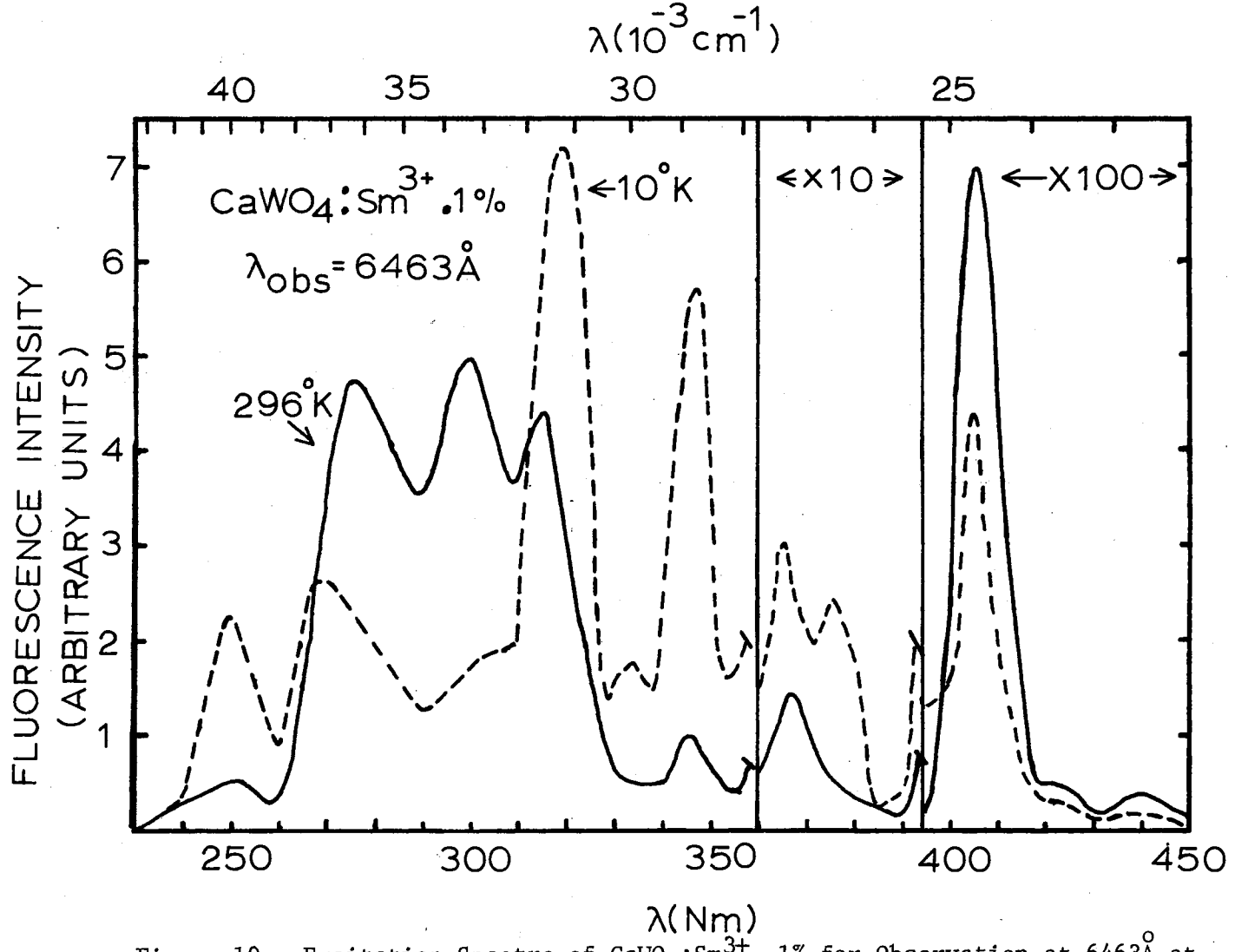

Figure 19. Excitation Spectra of $CaWO_4:Sm^{3+}$ .1% for Observation at 6463Å at 10°K and 296°K

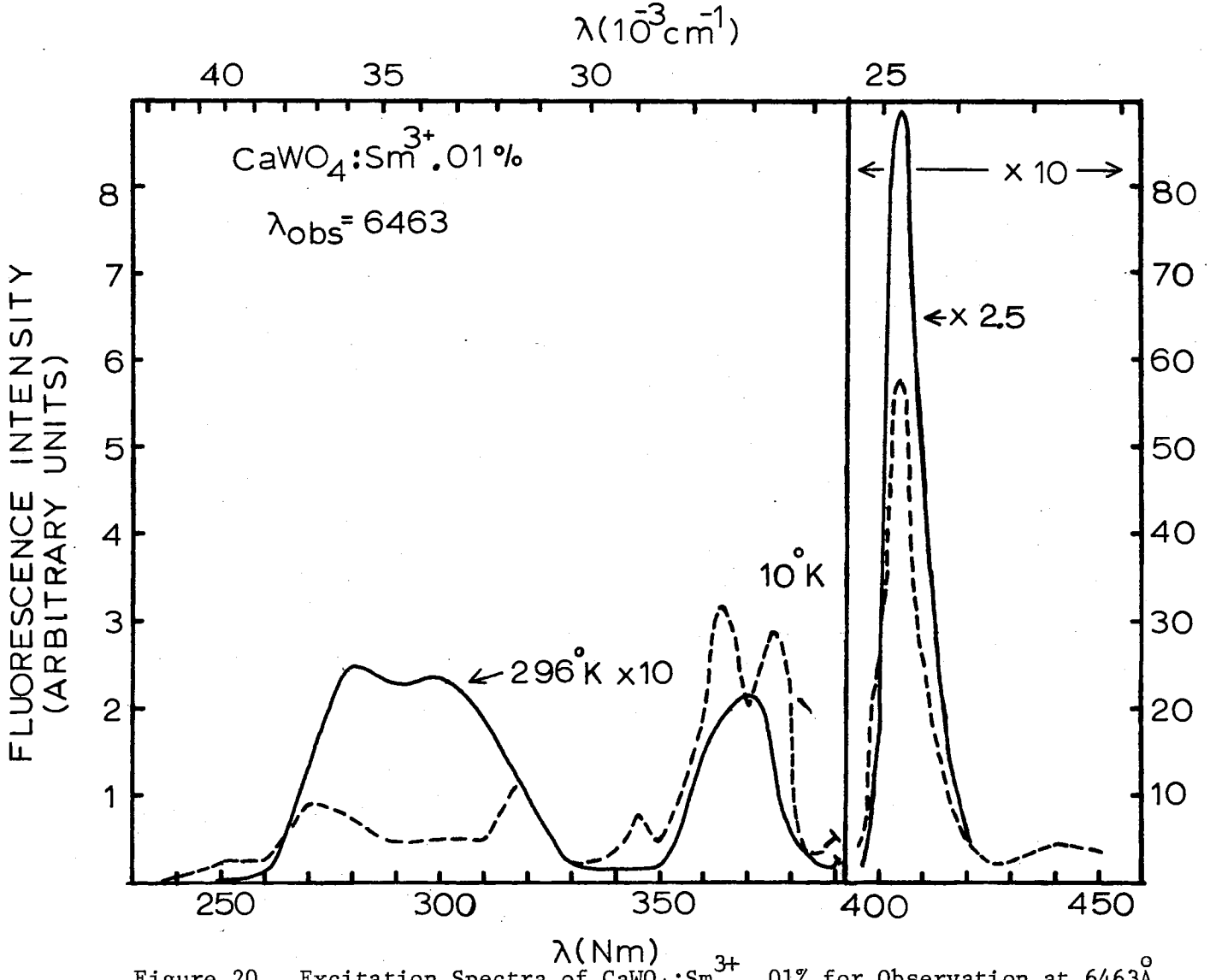

Figure 20. Excitation Spectra of $CaWO_4:Sm^{3+}$ .01% for Observation at 6463Å at 10°K and 296°K

excitation of the samples at 4150Å. The four regions exhibiting the most intense fluorescence are shown in Figure 21 for calcium tungstate with 1.0% Sm^{3+} at 8°K. Many smaller peaks are observed between these regions and a total of 83 fluorescence lines are listed in Table II. Similar spectra were obtained for calcium tungstate samples containing .1% and .01% samarium and the latter is shown in Figure 22 at 10°K, the only difference being the absence of many of the weak lines. No relative intensity changes occur for different polarizations. As temperature is increased the lines broaden and the spectra for calcium tungstate with 1% samarium at room temperature is shown in Figure 23. Although the lines broaden with temperature the total integrated fluorescence intensity remains constant in the temperature range from 8°K to 296°K.

For excitation at 4150Å the fluorescent lifetime was measured as .85 msec at room temperature and decreased slightly with decreasing temperature. The samarium lifetimes are tabulated in Table III.

Host Excitation

Excitation at 2400Å of calcium tungstate samples containing samarium resulted in both tungstate and samarium fluorescence for the samples containing 1.0% and .1% samarium and only host fluorescence for the .01% samarium sample. The shape of the tungstate fluorescence band was identical to that produced in undoped calcium tungstate. The samarium fluorescence for the 1.0% and .1% samarium samples is shown in Figures 24 and 25 respectively at 10°K and 296°K. The relative intensities of some lines change with temperature as shown in Figure 24. Comparison of Figures 24 and 25 obviates the low intensity structure on both sides of

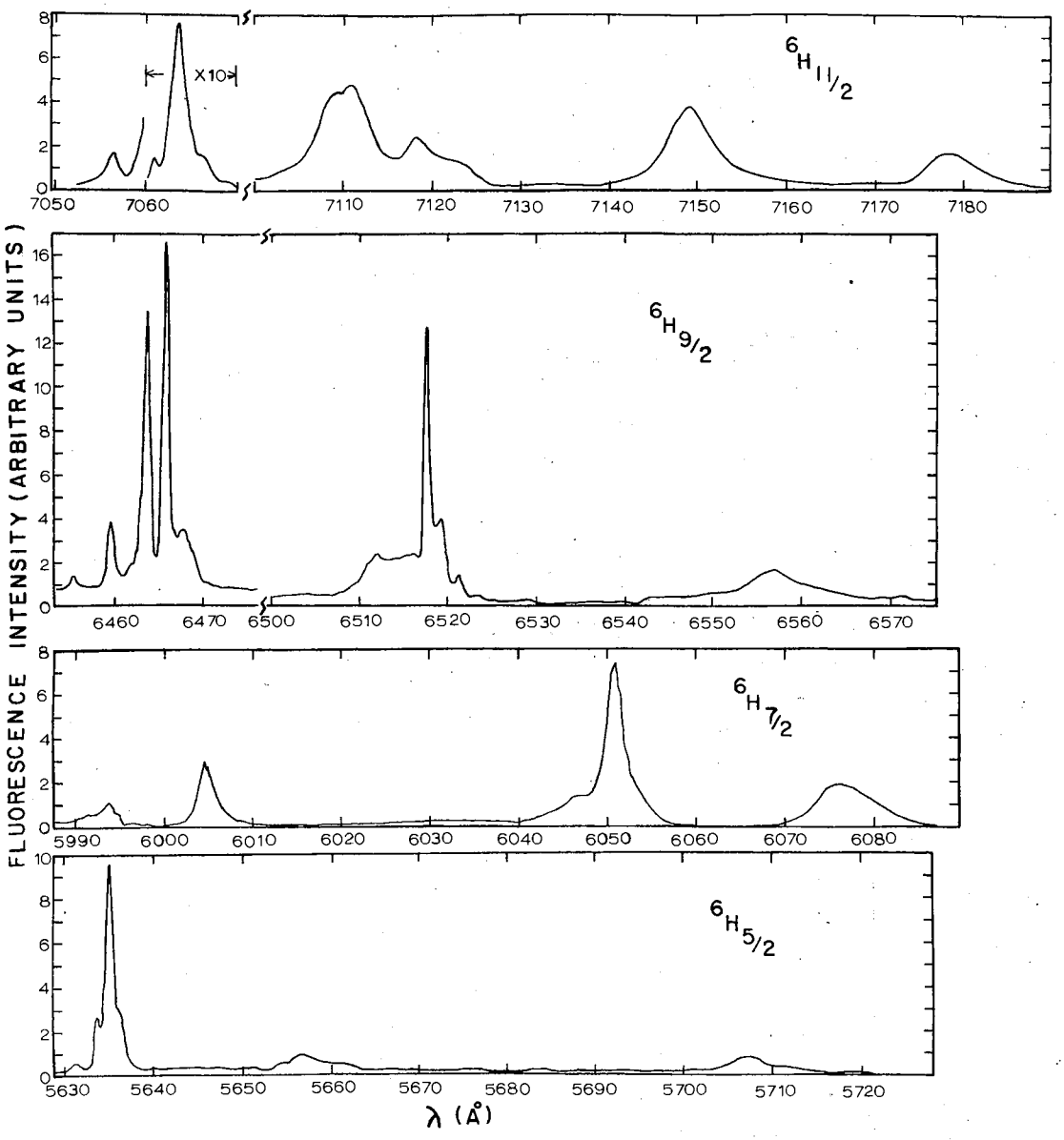

Figure 21. Fluorescence Spectra of $CaWO_4:Sm^{3+}$ 1.0% for 4150Å Excitation at 8°K

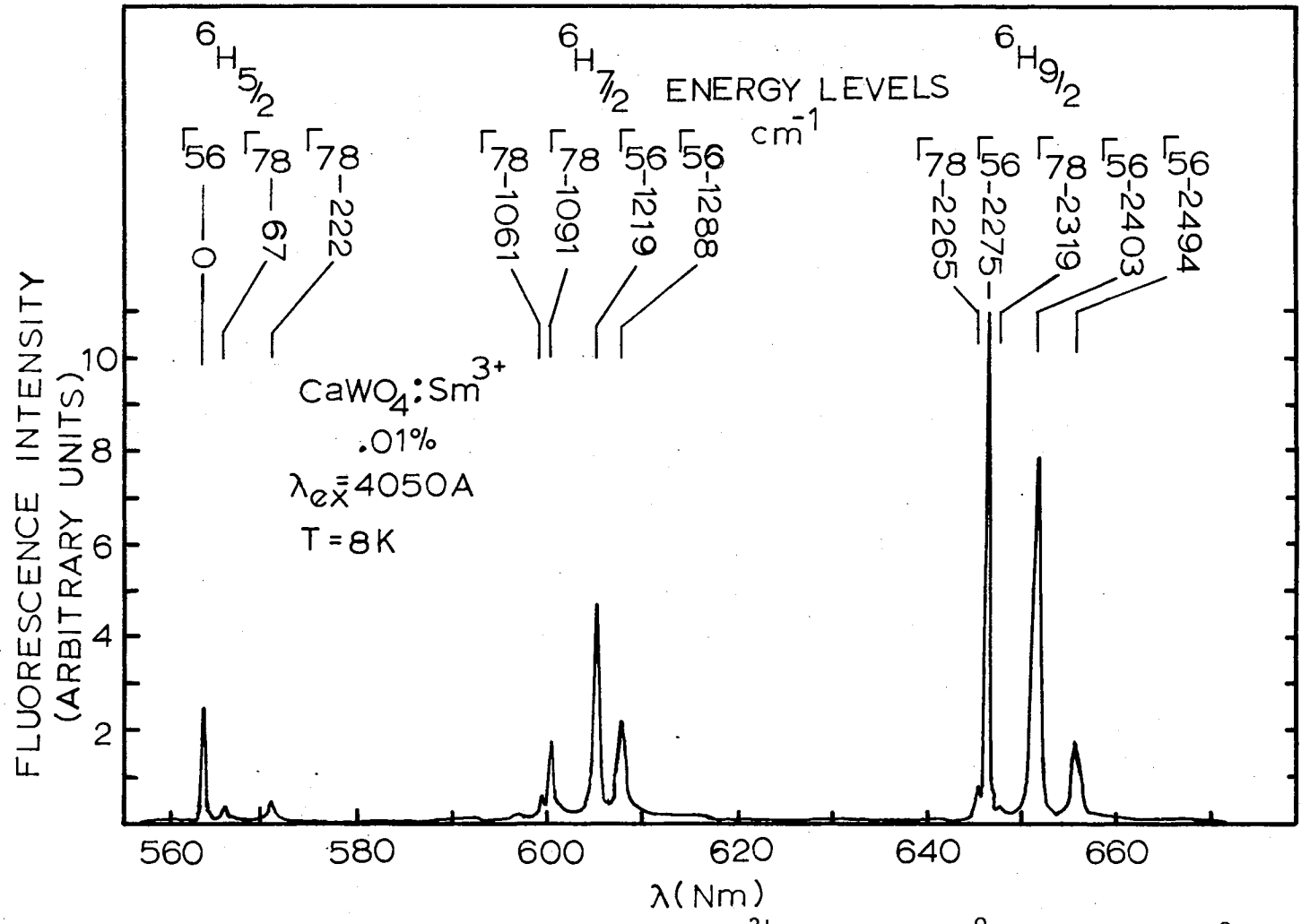

Figure 22. Fluorescence Spectra of $CaWO_4:Sm^{3+}$ .01% for 4050Å Excitation at 8°K

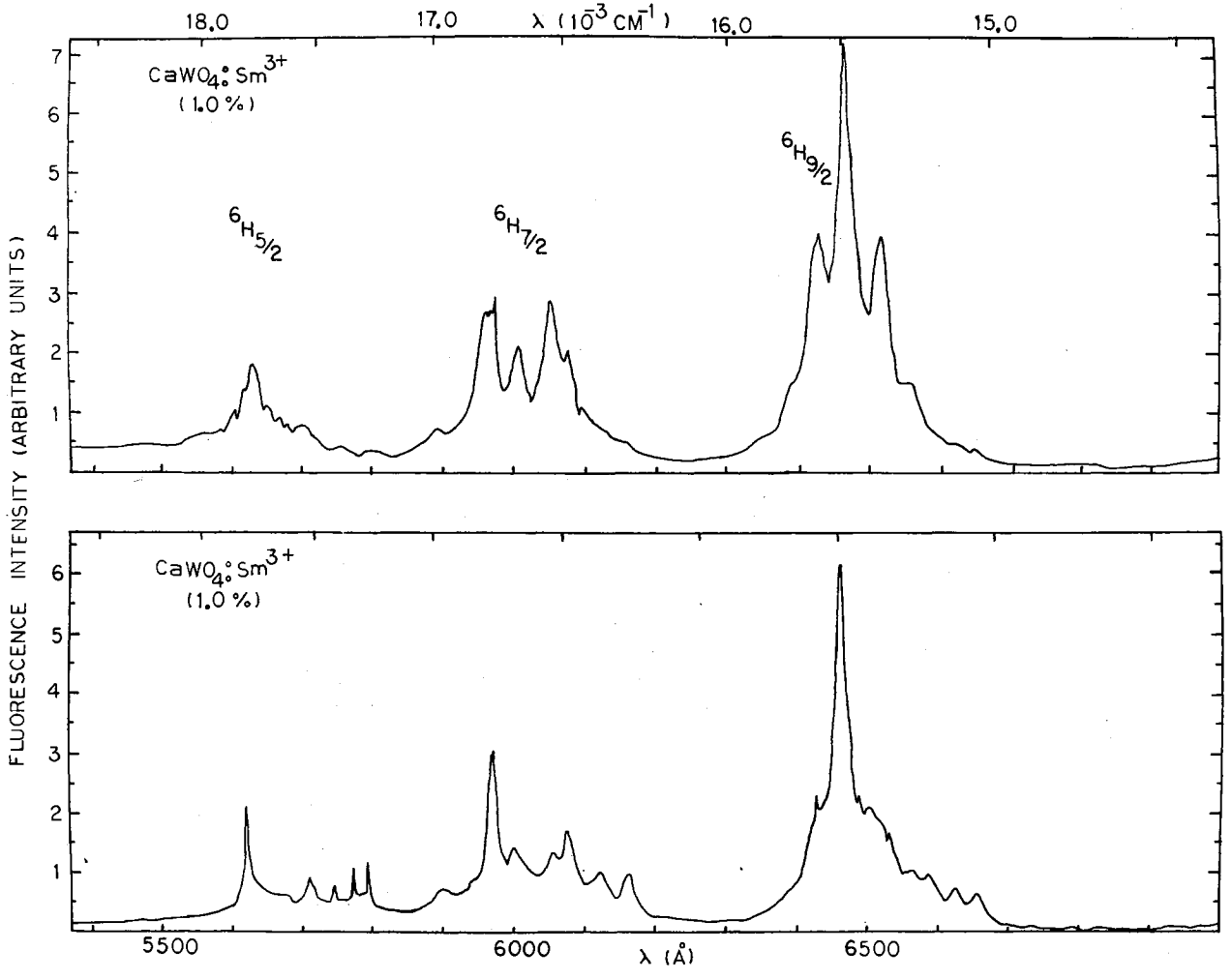

Figure 23. Fluorescence Spectra of $CaWO_4:Sm^{3+}$ 1.0% for 3050Å and 4150Å Excitation at 296°K

TABLE III

INTRINSIC SAMARIUM LIFETIMES

Temperature °K	Sm^{3+} Concentration		
	.01%	.1%	1.0%
296	.88	.85	.83
227	.86		
180			.88
126	.72	.86	.78
8	.77	.72	.65

All lifetimes in msec.

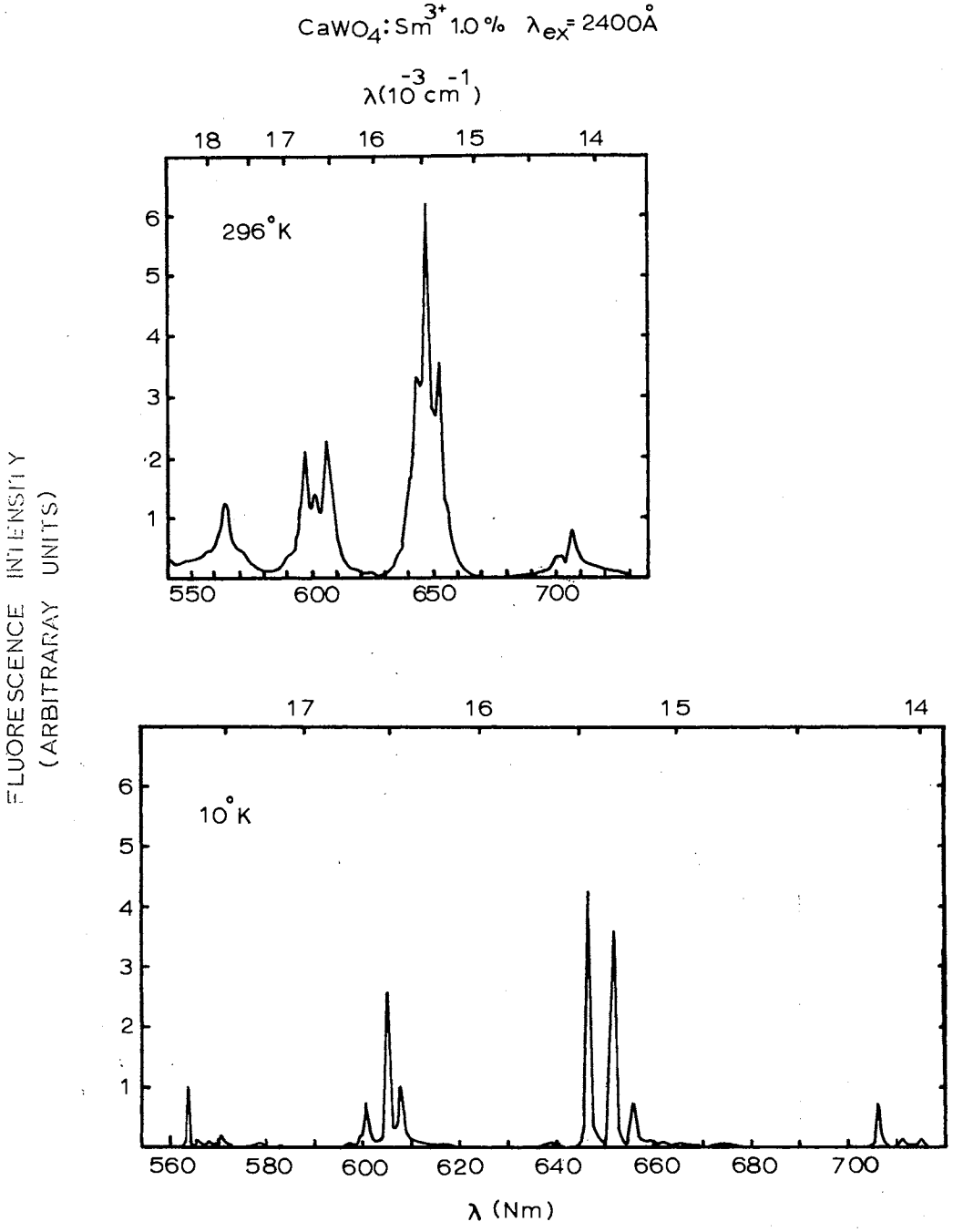

Figure 24. Fluorescence Spectra of $CaWO_4:Sm^{3+}$ 1.0% for 2400Å Excitation at 10°K and 296°K

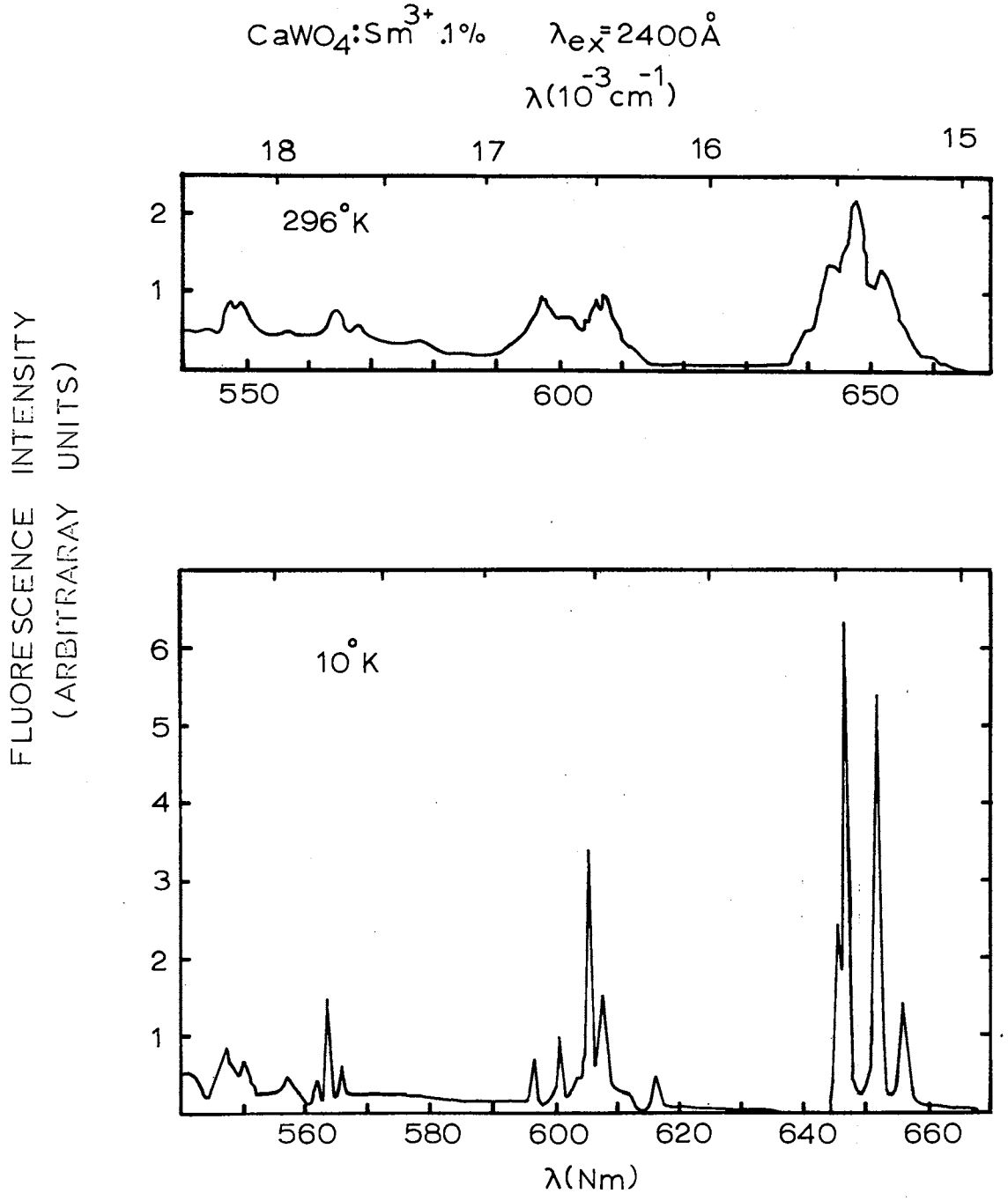

Figure 25. Fluorescence Spectra of $CaWO_4:Sm^{3+}$ .1% for 2400Å Excitation at 10°K and 296°K

the main fluorescence lines which becomes observable in the .1% samarium sample. Both the tungstate and samarium integrated fluorescence intensities exhibit an irregular temperature dependence as shown in Figure 26 for both 1.0% and .1% samarium samples and are tabulated in Table IV. The ratio of the samarium to tungstate integrated fluorescence intensities remains almost constant with temperature in both samples as shown in Figure 27 and the values are tabulated in Table IV.

The tungstate and samarium fluorescence spectra for excitation at 2650Å of the .1% samarium sample at room temperature is shown in Figure 28a. The shape of the tungstate fluorescence is the same as that produced for this wavelength of excitation in the undoped calcium tungstate sample. The dips near 4050Å and 4190Å correspond to regions of high samarium absorption and are due to reabsorption. Figure 28b shows the spectra obtained for 2650Å excitation of the .1% sample at 10°K. The shape of the host fluorescence is markedly different from that obtained in the undoped sample as shown in Figure 11. Similar tungstate fluorescence spectra were obtained for the 1.0% and .01% samarium samples, however, the samarium spectra were different for each samarium concentration as shown by comparing Figures 28, 29 and 30. Figures 29 and 30 show the samarium fluorescence spectra for 2650Å at 10°K and room temperature in the 1.0% and .01% samarium samples respectively.

For excitation at 2650Å the tungstate integrated fluorescence intensity decreases markedly with decreasing temperature. This is true for all samarium concentrations and is not accompanied by a marked increase in the samarium fluorescence as shown in Figure 31. The ratio of the samarium to tungstate integrated fluorescence intensity as a function of temperature is shown in Figure 32 and the values of the samarium and

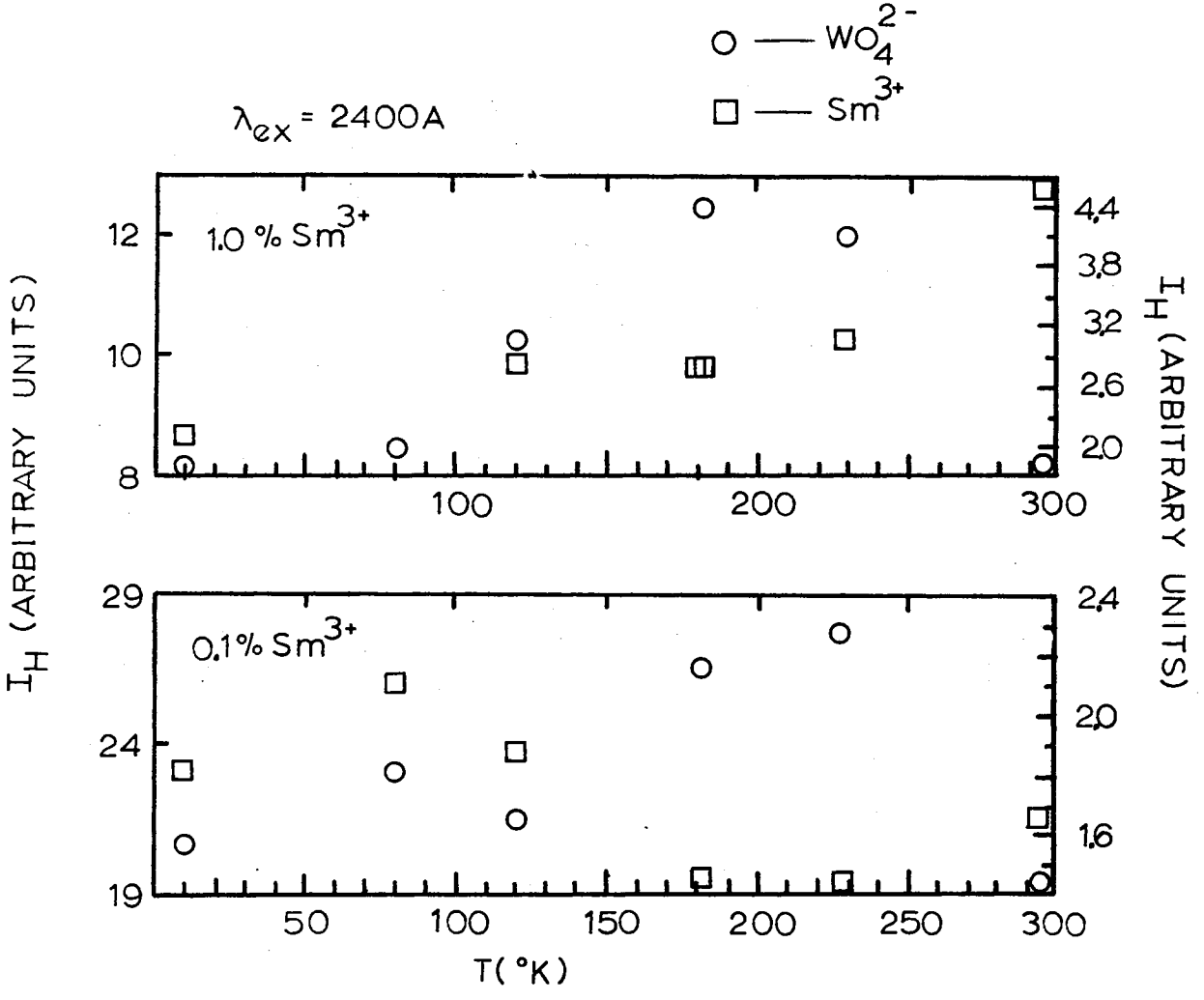

Figure 26. Integrated Samarium and Tungstate Fluorescence Intensities Versus Temperature for 2400Å Excitation

TABLE IV

INTEGRATED SAMARIUM AND TUNGSTATE FLUORESCENCE INTENSITIES AND THEIR RATIOS FOR 2400Å EXCITATION

Temperature in °K	.1% Sm^{3+}			1.0% Sm^{3+}		
	I_G	I_H	$\frac{I_G}{I_H}$	I_G	I_H	$\frac{I_G}{I_H}$
10	1.830	20.778	.088	2.15	8.056	.267
81	2.119	23.216	.091	1.775	8.436	.211
121	1.888	21.543	.088	2.838	10.275	.276
183	1.416	26.629	.053	2.817	12.413	.227
229	1.432	27.858	.051	3.003	12.062	.249
296	1.581	19.131	.088	4.694	8.134	.578

I_G and I_H in arbitrary units.

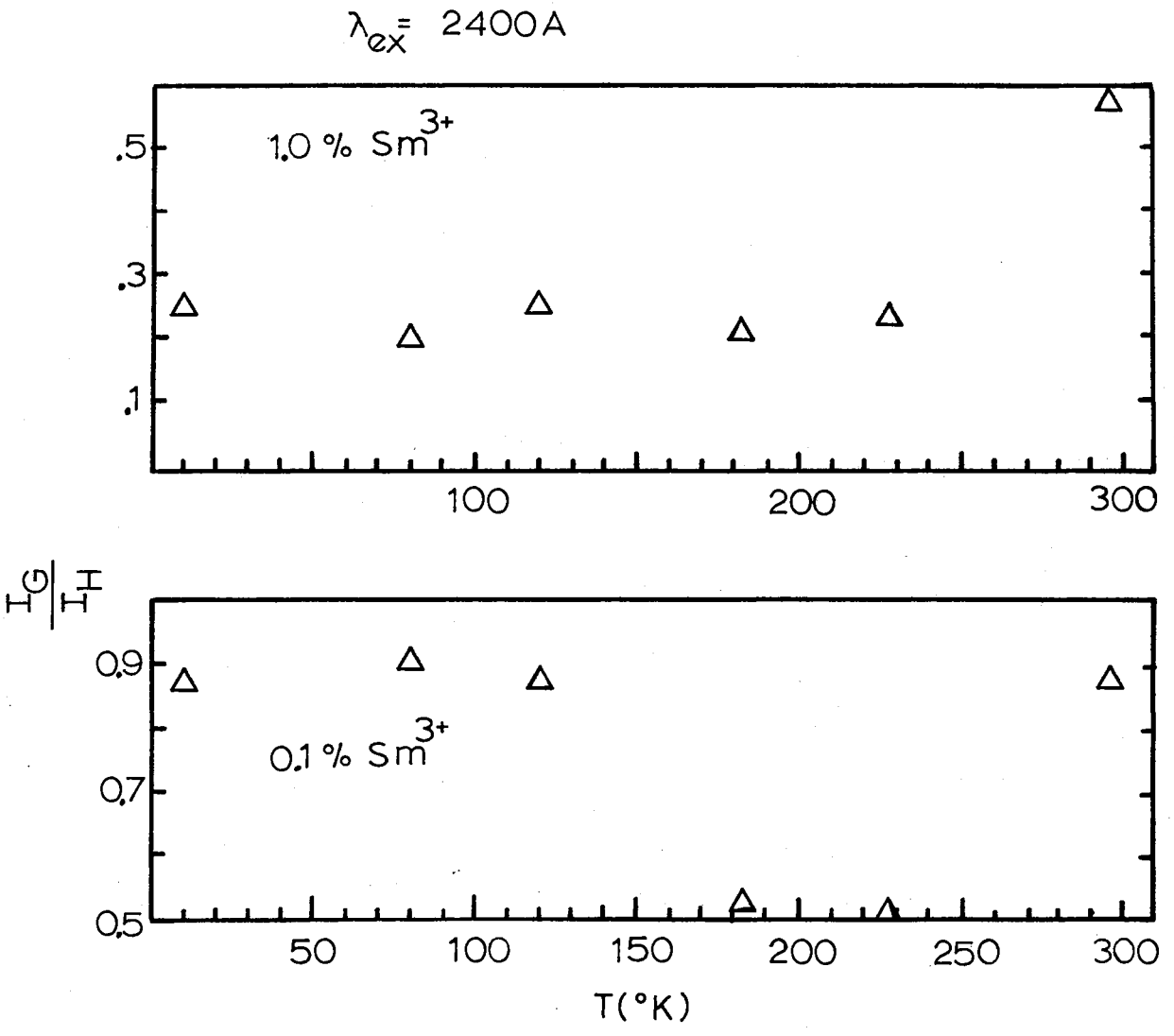

Figure 27. Integrated Fluorescence Intensity Ratio Versus Temperature for 2400Å Excitation

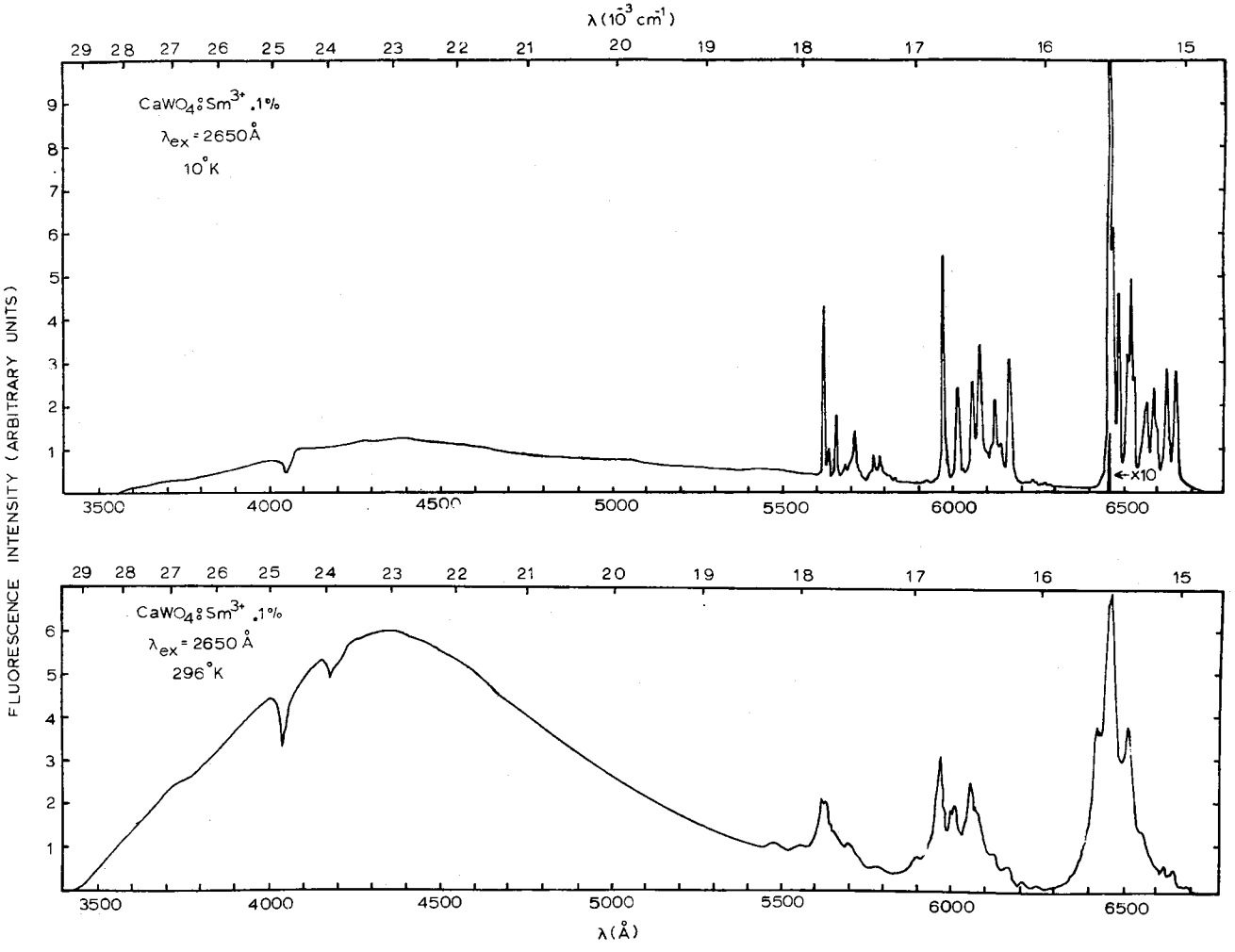

Figure 28. Fluorescence Spectra of $CaWO_4:Sm^{3+}$ .1% for 2650Å Excitation at $10^{\circ}K$ and $296^{\circ}K$

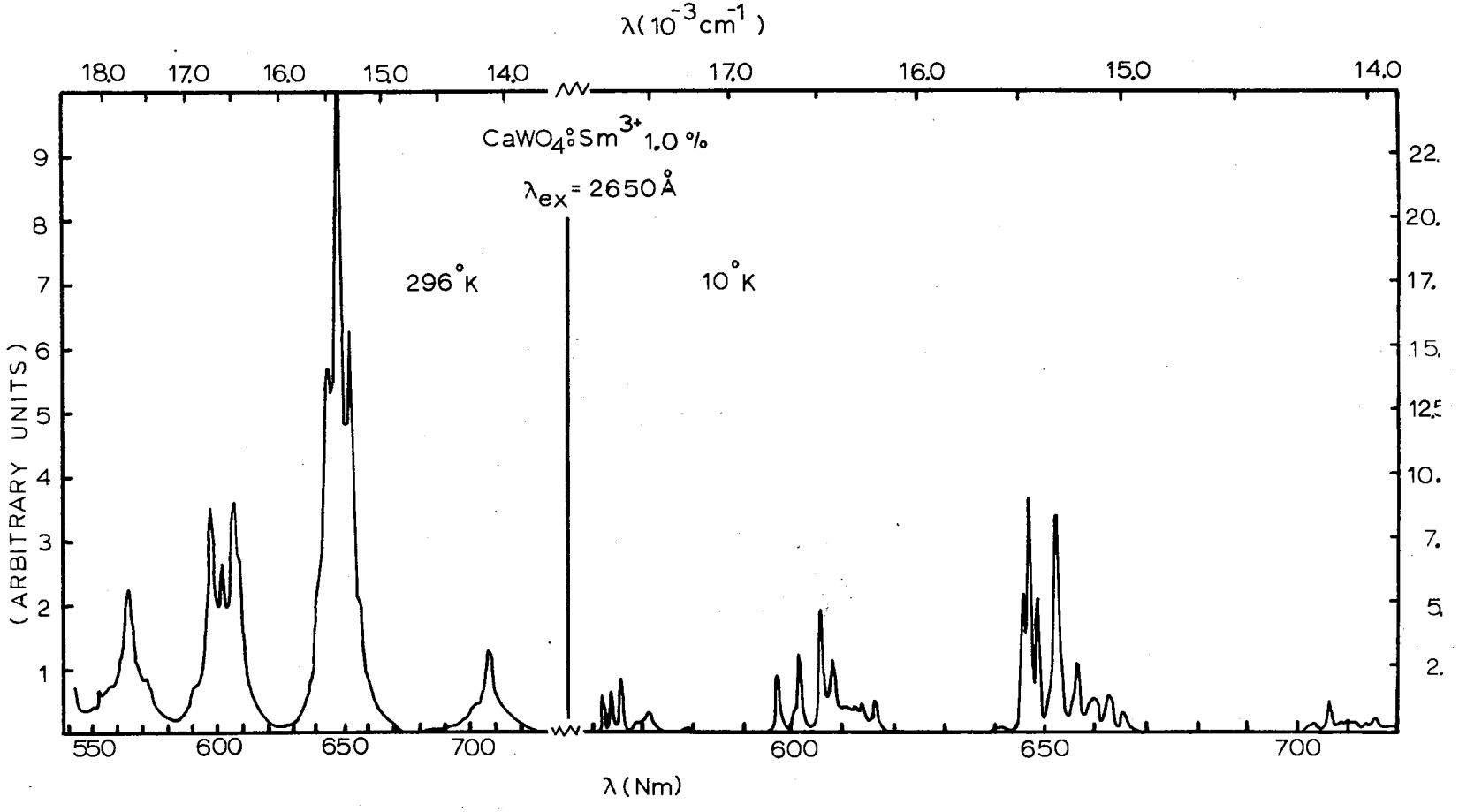

Figure 29. Fluorescence Spectra of $CaWO_4:Sm^{3+}$ 1.0% for 2650Å Excitation at 10°K and 296°K

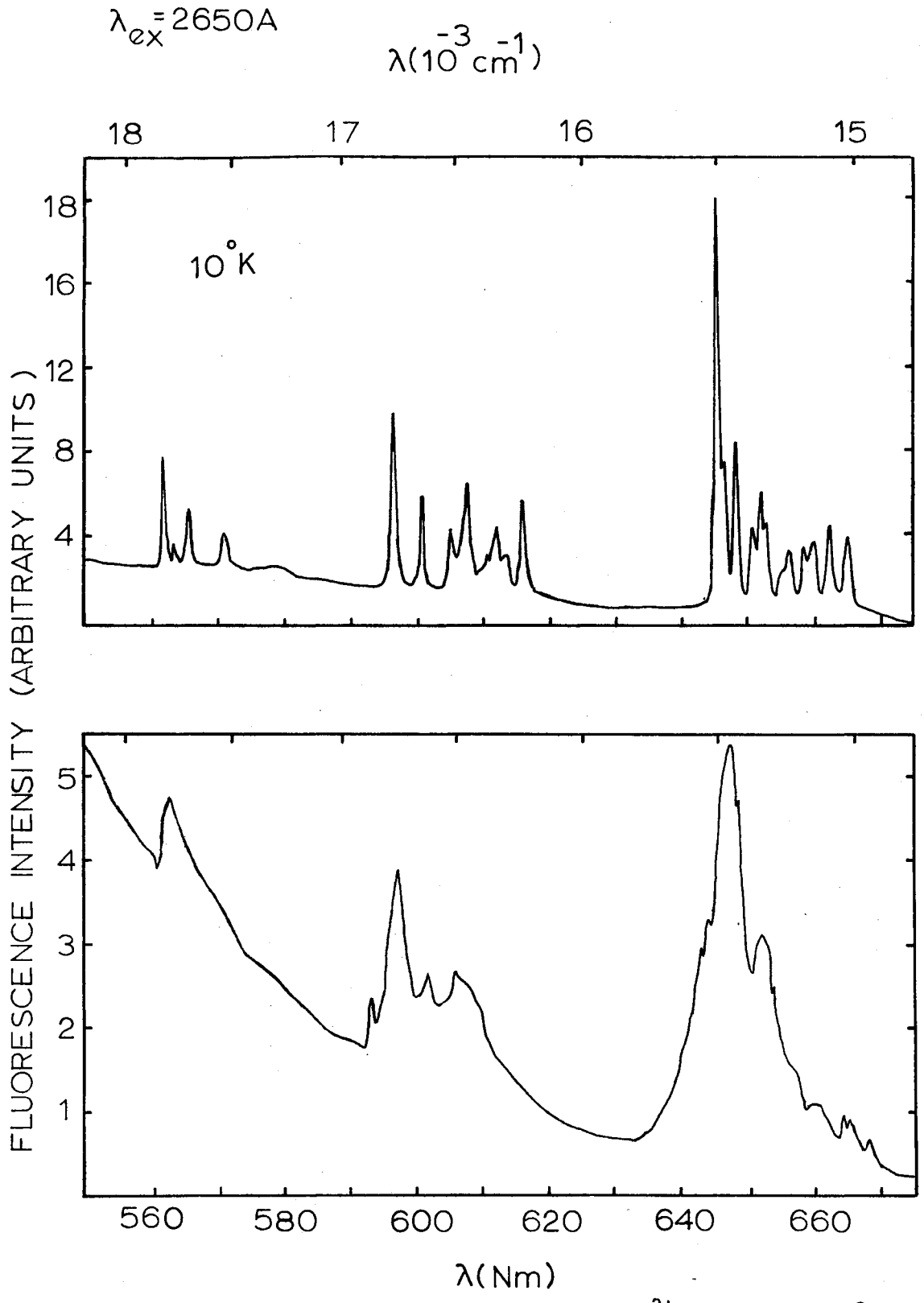

Figure 30. Fluorescence Spectra of $CaWO_4:Sm^{3+}$ .01% for 2650Å Excitation at 10°K and 296°K

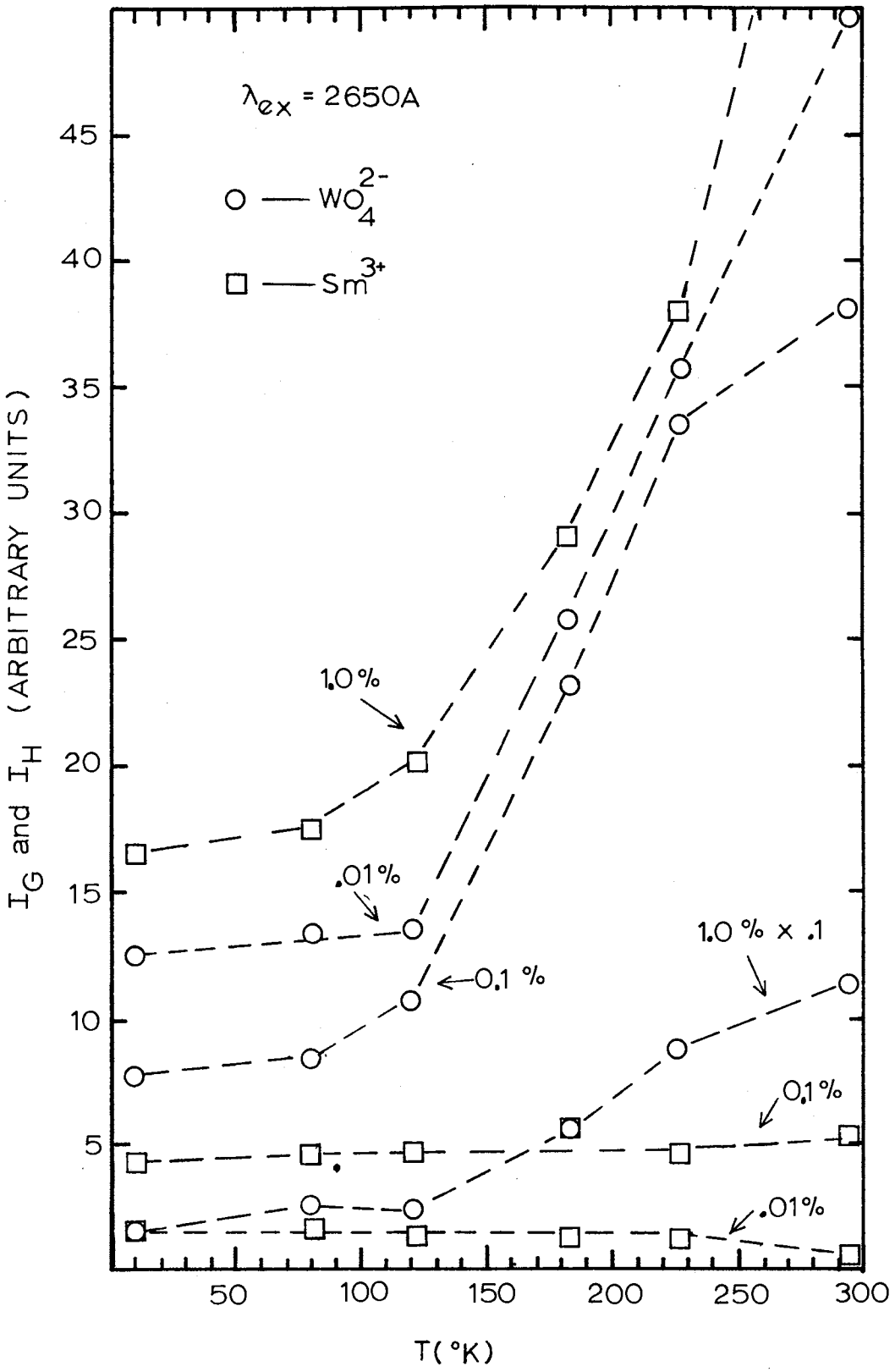

Figure 31. Integrated Samarium and Tungstate Fluorescence Intensities Versus Temperature for 2650Å Excitation

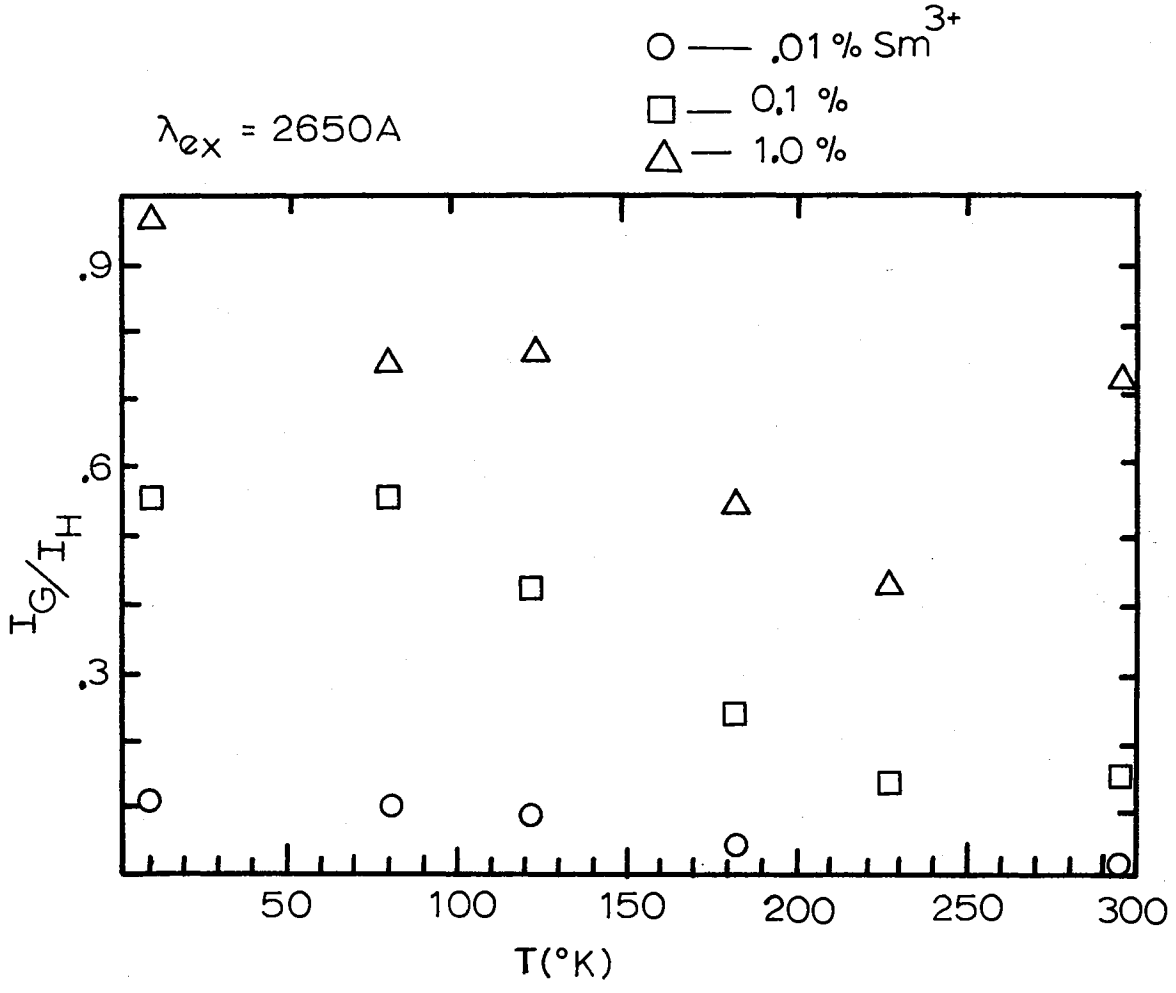

Figure 32. Integrated Fluorescence Intensity Ratio Versus Temperature for 2650Å Excitation

tungstate integrated fluorescence intensities and their ratios are tabulated in Table V.

For excitation at 3150Å tungstate fluorescence could be observed only in the .01% samarium sample at low temperatures. The shape of the tungstate fluorescence was the same as that produced for 2650Å excitation of the doped samples at low temperature. The samarium fluorescence spectra for 3150Å at 10°K and 296°K are shown in Figures 33, 34 and 35 for the 1.0%, .1% and .01% samarium samples respectively. Again each samarium concentration produces fluorescence spectra with different degrees of structure. At low temperatures the spectra are sharp lines and broaden as temperature is increased. Figure 36 shows the temperature dependence of the samarium integrated fluorescence intensity for the 1.0% sample for excitation at 3150Å. Also shown in Figure 36 are the integrated samarium and tungstate fluorescence intensity in the .01% sample at the two temperatures at which tungstate fluorescence was observed and their ratio. These values are tabulated in Table VI.

Pulsed fluorescence measurements were made as a function of temperature and concentration to determine the tungstate and samarium fluorescence lifetimes. The samples were excited with 2400Å, 2650Å and 3150Å light but the absence of tungstate fluorescence for 3150Å made it impossible to measure a tungstate lifetime for this wavelength of excitation in the doped samples. Figures 37 and 38 show the measured tungstate fluorescence lifetime as a function of temperature in samples containing 1.0%, .1% and .01% samarium for excitation at 2400Å and 2650Å respectively. Both figures indicate at low temperatures that the measured tungstate lifetime depends upon the samarium concentration. The lifetimes decrease with increasing temperature and above 100°K remaining fairly

TABLE V

INTEGRATED SAMARIUM AND TUNGSTATE FLUORESCENCE INTENSITIES AND THEIR RATIO FOR 2650Å EXCITATION

Temperature °K	.01% Sm^{3+}			.1% Sm^{3+}			1.0% Sm^{3+}		
	I_G	I_H	$\frac{I_G}{I_H}$	I_G	I_H	$\frac{I_G}{I_H}$	I_G	I_H	$\frac{I_G}{I_H}$
10	1.537	12.517	.123	4.315	7.825	.551	16.53	16.987	.973
81	1.661	13.442	.124	4.680	8.354	.560	17.034	22.736	.752
121	1.346	13.726	.098	4.703	10.962	.429	20.052	25.983	.774
183	1.284	26.986	.048	5.606	23.322	.240	29.17	53.78	.542
229	1.160	35.900	.030	4.505	33.566	.134	38.07	87.42	.435
296	.901	49.783	.018	5.332	38.093	.140	82.74	113.50	.729

I_G and I_H in arbitrary units.

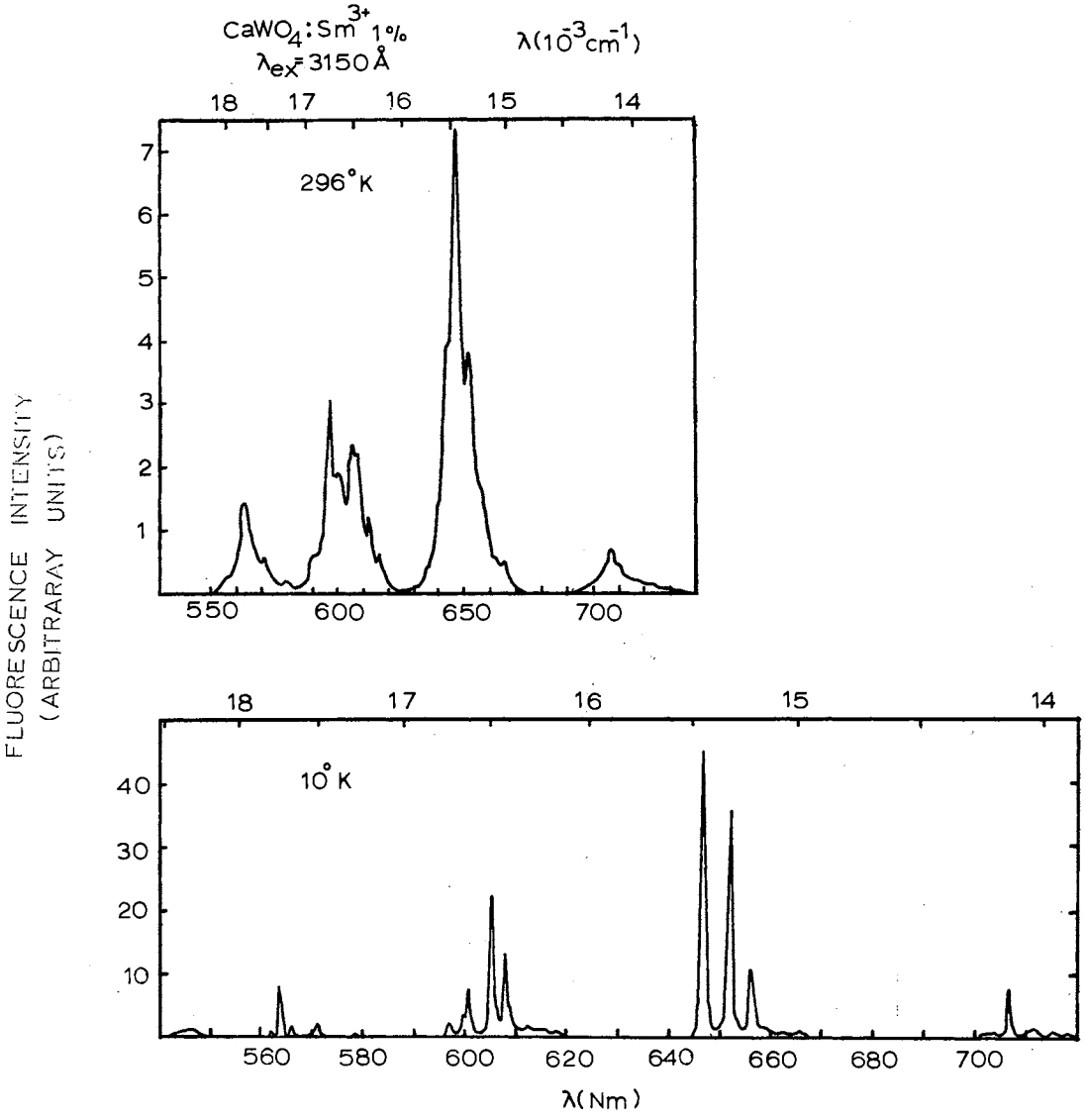

Figure 33. Fluorescence Spectra of $CaWO_4$ Sm^{3+} 1% for 3150Å Excitation at 10°K and 296°K

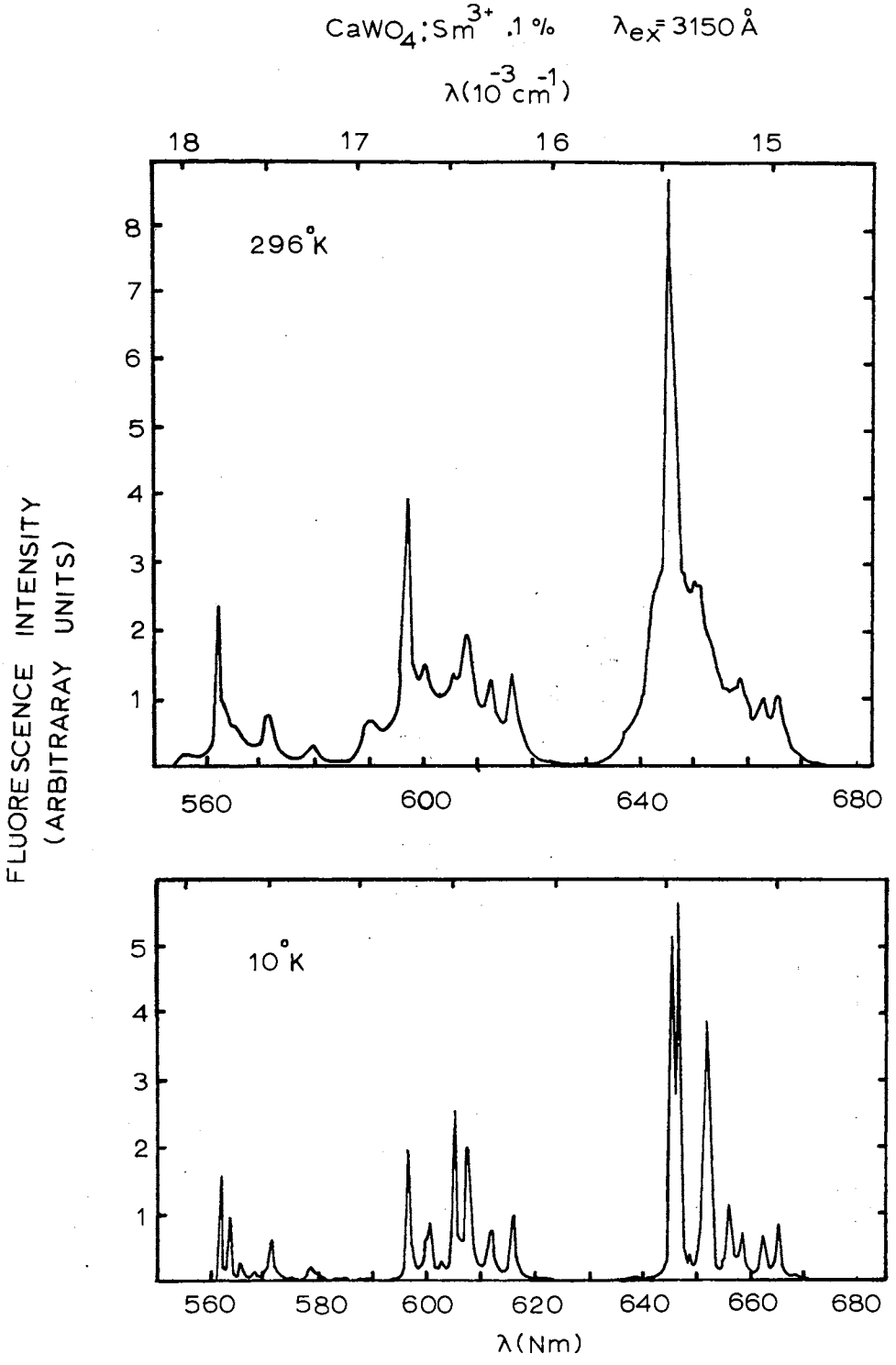

Figure 34. Fluorescence Spectra of $CaWO_4:Sm^{3+}$ .1% for 3150Å Excitation at 10°K and 296°K

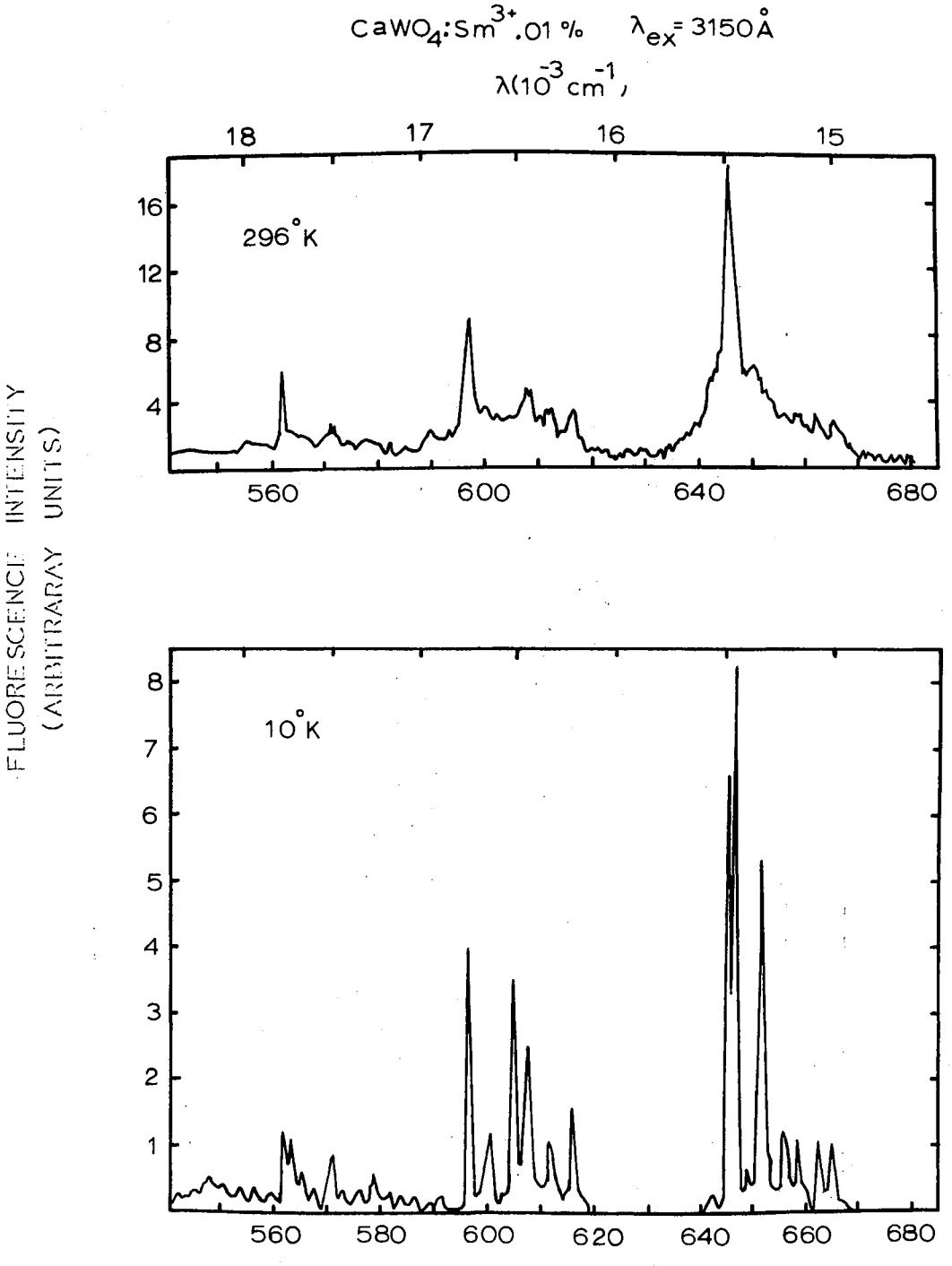

Figure 35. Fluorescence Spectra of $CaWO_4:Sm^{3+}$ .01% for 3150Å Excitation at 10°K and 296°K

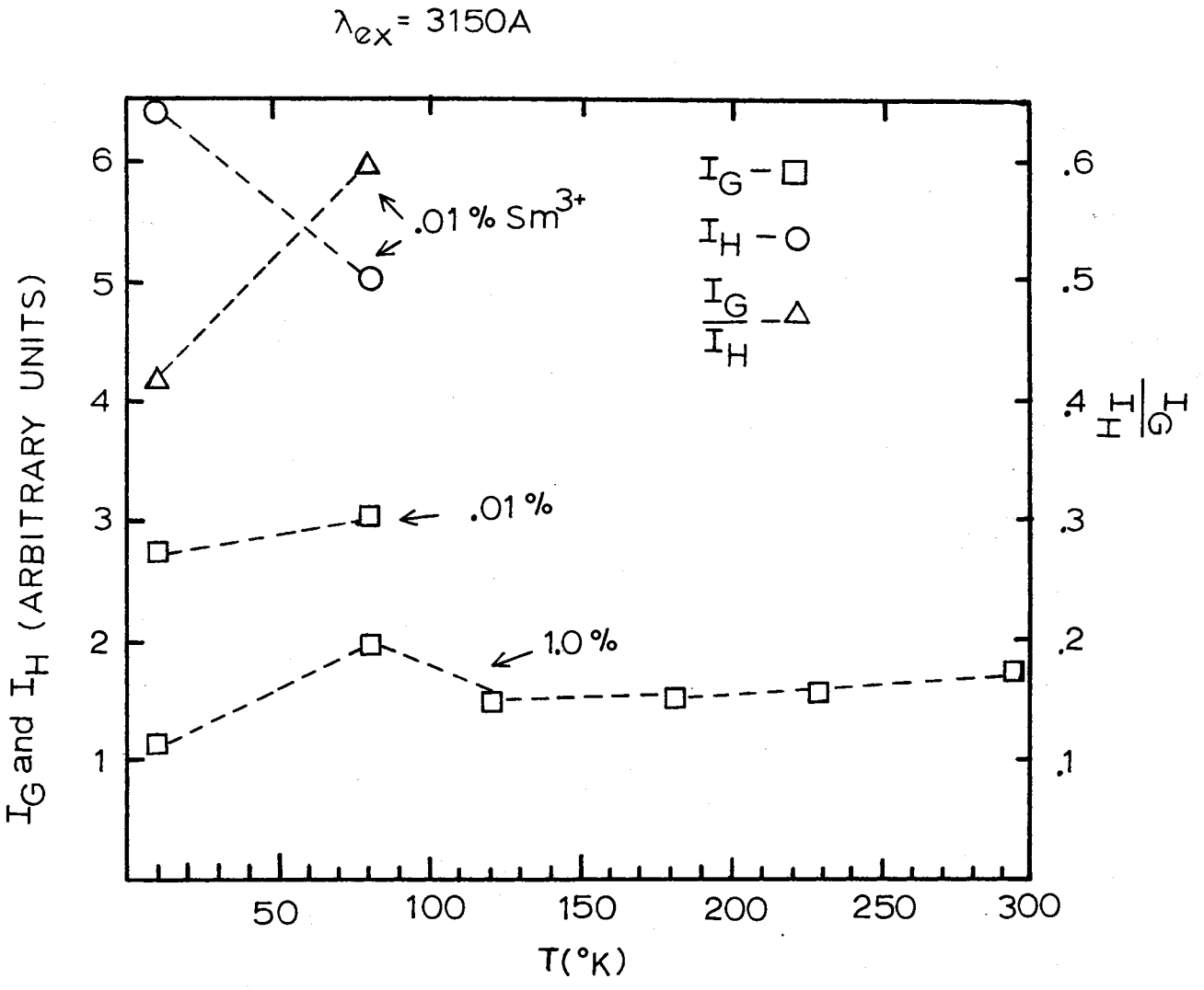

Figure 36. Integrated Fluorescence Intensities Versus Temperature for 3150Å Excitation

TABLE VI

INTEGRATED SAMARIUM AND TUNGSTATE FLUORESCENCE INTENSITIES AND THEIR RATIOS FOR 3150Å EXCITATION

	1% Sm^{3+}		.01% Sm^{3+}		
Temperature °K	I_G	I_H	I_G	I_H	$\frac{I_G}{I_H}$
10	1.164	--	2.711	6.433	.421
81	1.963	--	3.031	5.082	.596
121	1.463	--	-----	-----	----
183	1.570	--	-----	-----	----
228	1.634	--	-----	-----	----
296	1.750	--	-----	-----	----

I_G and I_H in arbitrary units.

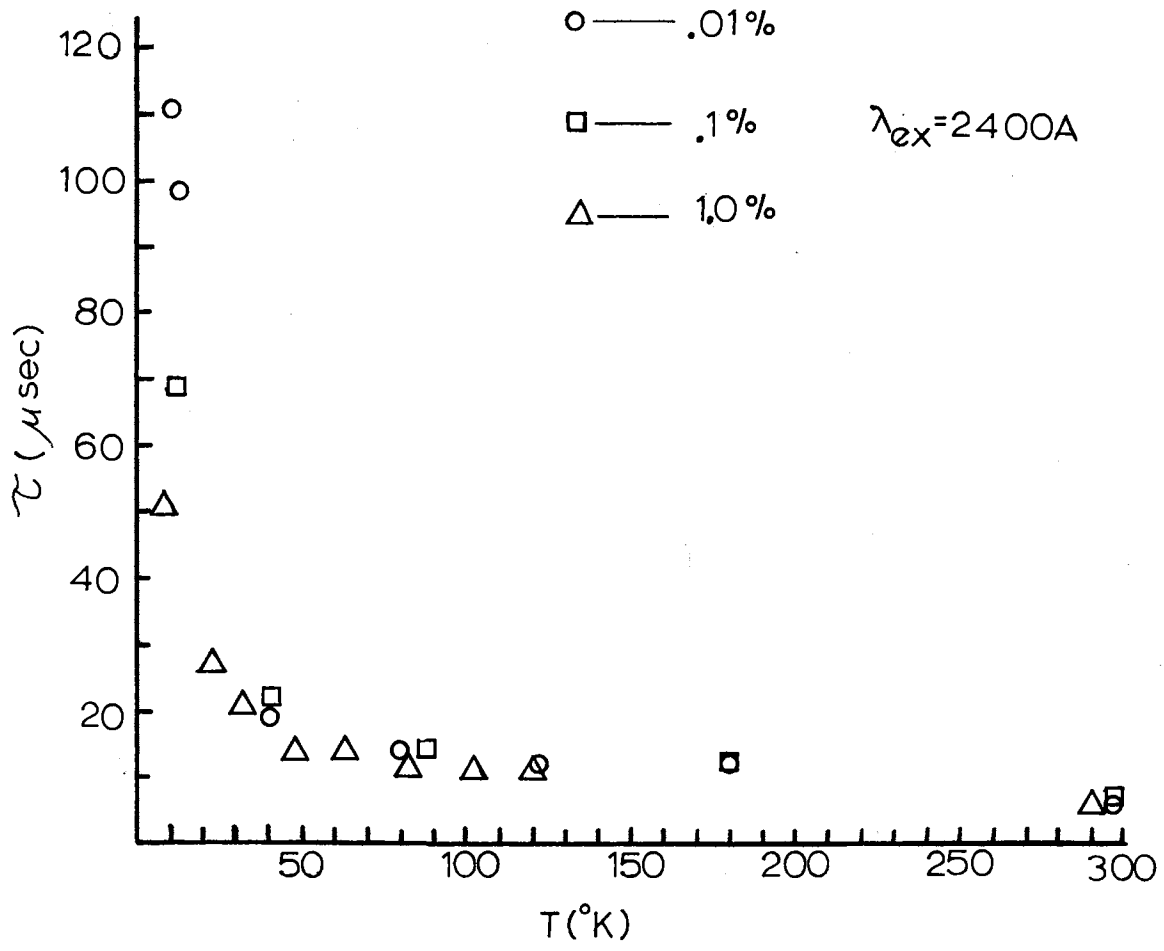

Figure 37. Tungstate Fluorescence Lifetimes Versus Temperature for 2400Å Excitation of Doped Samples

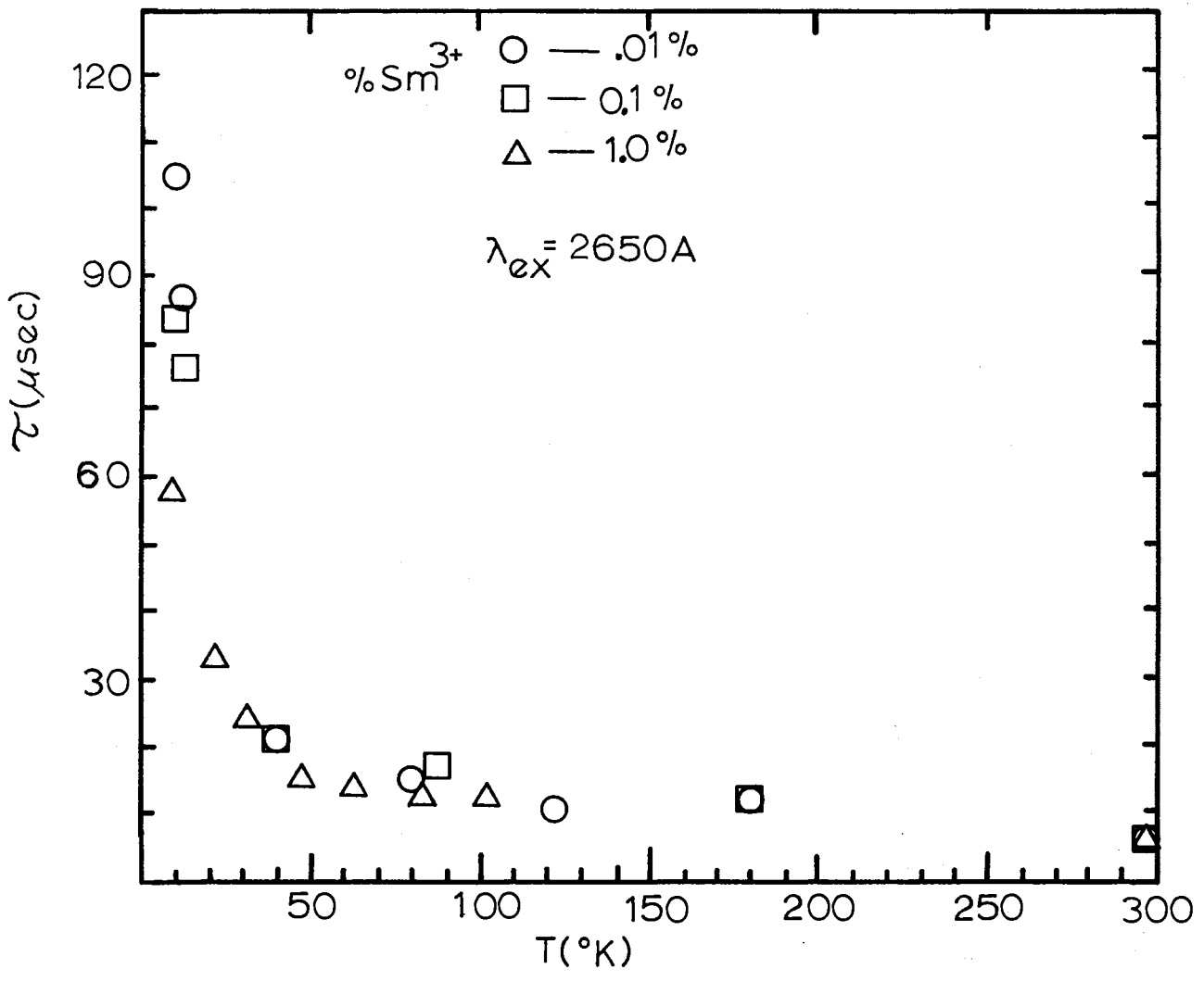

Figure 38. Tungstate Fluorescence Lifetimes Versus Temperature for 2650Å Excitation of Doped Samples

constant to 220°K. This steady value is approximately 12 μsec for 2400 excitation and 13 μsec for 2650 excitation but is relatively independent of the samarium concentration. The tungstate lifetimes are tabulated in Table VII. The measured samarium lifetimes for all concentration for excitation at 2400Å, 2650Å and 3150Å are shown as a function of temperature in Figure 39. The samarium lifetimes are tabulated in Table VIII.

TABLE VII

TUNGSTATE LIFETIMES IN SAMPLES CONTAINING SAMARIUM

	.01% Sm^{3+}		.1% Sm^{3+}			1.0% Sm^{3+}	
Temperature °K	2400Å Excitation	2650Å Excitation	2400Å Excitation	2650Å Excitation	Temperature °K	2400Å Excitation	2650Å Excitation
10	111. (11.5°K)	105. (11.5°K)	-----	83.8	8	52.	54.
11	98.	88.	69.	77.	9.5	-----	58.
40	19.6	21.8	22.5	22.5	22	22.7	33.4
80	13.8	16.6	-----	-----	32	20.1	24.4
88	--------	--------	13.7	17.8	48	14.5	16.4
123	11.8	12.7	-----	-----	63	14.3	13.9
180	11.5	13.0	12.9	13.1	82	12.5	13.5
296	6.84	7.05	7.58	7.39	102	11.2	12.9
					120	11.4	12.5
					290	6.33	6.68
					296	5.85	

All lifetimes in μsec.

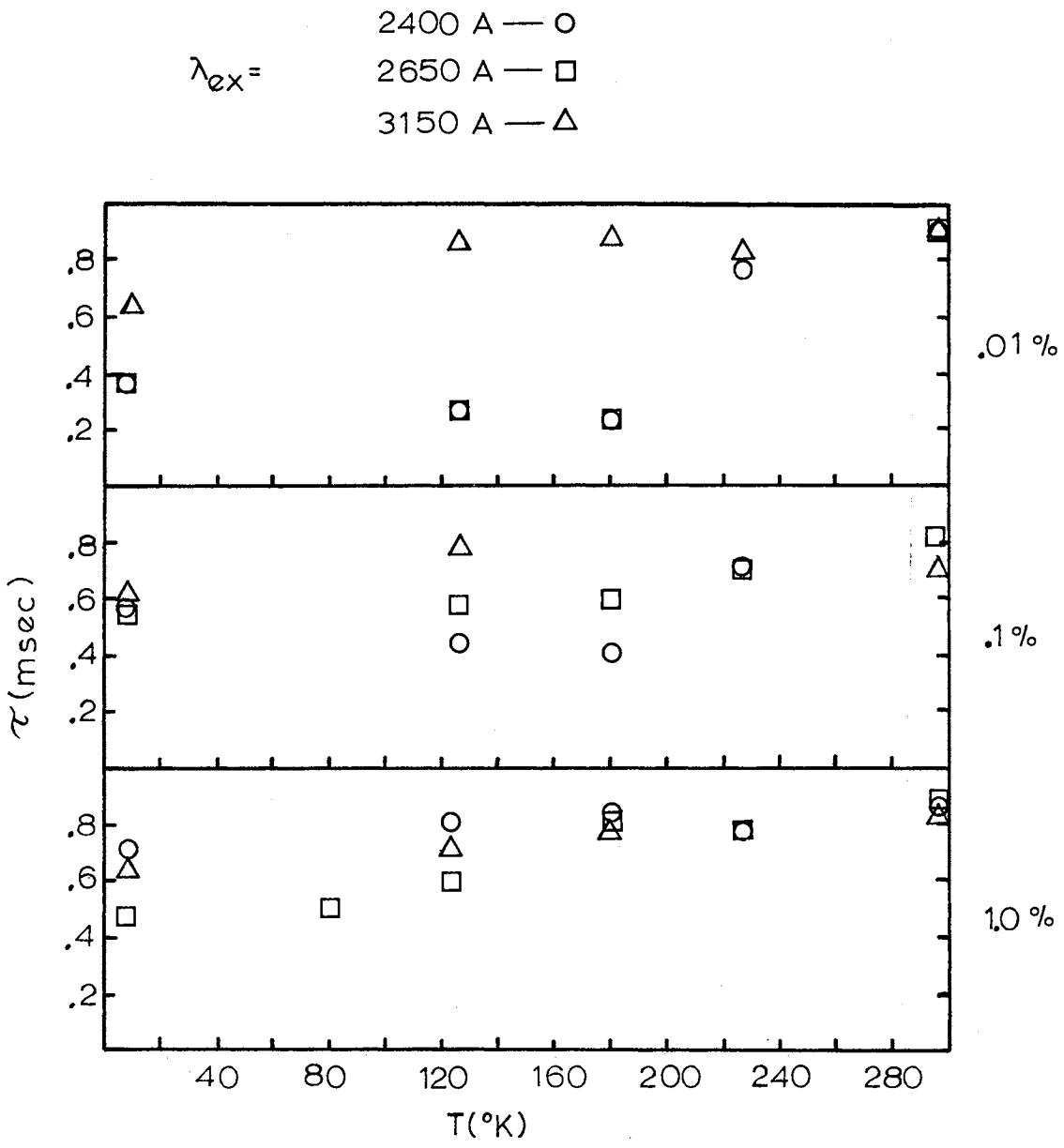

Figure 39. Samarium Fluorescence Lifetimes Versus Temperature for 2400Å, 2650Å and 3150Å Excitation of Doped Samples

TABLE VIII

Sm^{3+} LIFETIMES

Temperature	2400Å Excitation			2650Å Excitation			3150Å Excitation		
°K	.01% Sm	.1% Sm	1.0% Sm	.01% Sm	.1% Sm	1.0% Sm	.01% Sm	.1% Sm	1.0% Sm
8°	.36	.56	.71	.37	.53	.48	.64	.62	.65
80	---	---	.76	---	---	.51	---	---	---
123	.28	---	.81	.30	---	.58	.86	.78	.72
180	.23	.41	.84	.25	.59	.83	.87	---	.79
227	.75	.72	.78	---	.70	.79	.84	---	---
296	.90	---	.86	.92	.82	.88	.85	.70	.84

All lifetimes in msec.

CHAPTER V

ENERGY LEVELS AND ENERGY MIGRATION IN $CaWO_4$

Calcium tungstate crystallizes in the scheelite structure (33). As shown in Figure 40 each Ca^{2+} is surrounded by 8 WO_4^{2-} anions giving a symmetry of S_4. That absorption in calcium tungstate takes place at the WO_4^{2-} ions was demonstrated by Kröeger (6). He showed the absorption band of the tungstates to be relatively invariant with different cations. The absorption transitions have been widely accepted as charge transfer transitions in which an oxygen 2p electron goes into one of the empty tungsten 5d orbitals. Butler (8) has performed molecular orbital calculations for the complex WO_4^{2-} ion. His results are shown in Figure 41 and he qualifies them as being highly speculative. The levels up to and including the t_1 level are completely filled giving rise to a $^1A_1$ ground state. Excitation of a single electron from the t_1 to the 2e level results in a $1a_1^2\ 1t_2^6\ 1e^4\ 2t_2^6\ 2a_1^2\ 3t_2^6\ t_1^5\ 2e^1$ excited state configuration. In the T_d symmetry of the WO_4^{2-} ion this configuration gives rise to four levels which are in turn split by the crystal field of S_4 symmetry and spin orbit interaction as shown in Figure 42. The ordering of the molecular terms and crystal field levels to this point has been arbitrary. It is expected in general that the triplets will have a lower energy than the singlet levels and the molecular orbital splitting is greater than the crystal field splitting which is greater than the spin orbit splitting. In the free ion the only allowed transition is

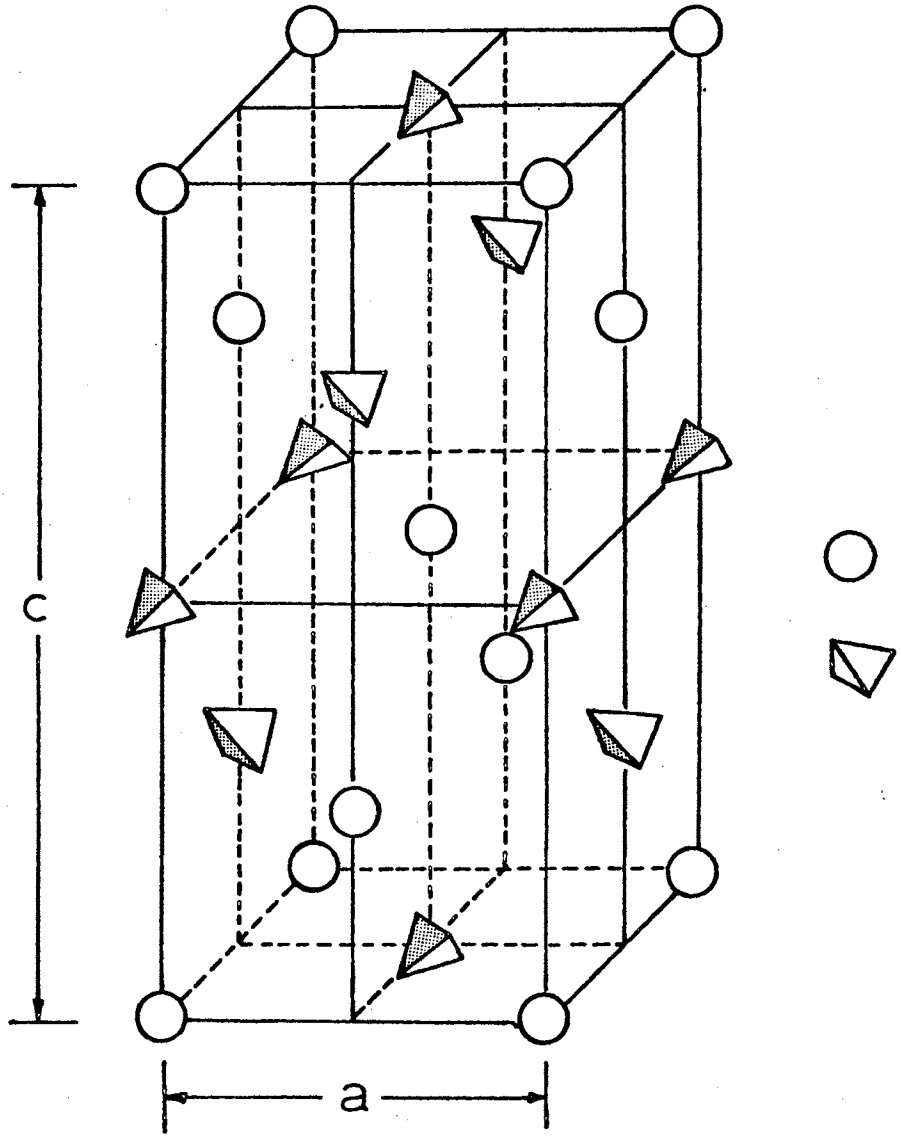

Figure 40. Scheelite Structure of $CaWO_4$

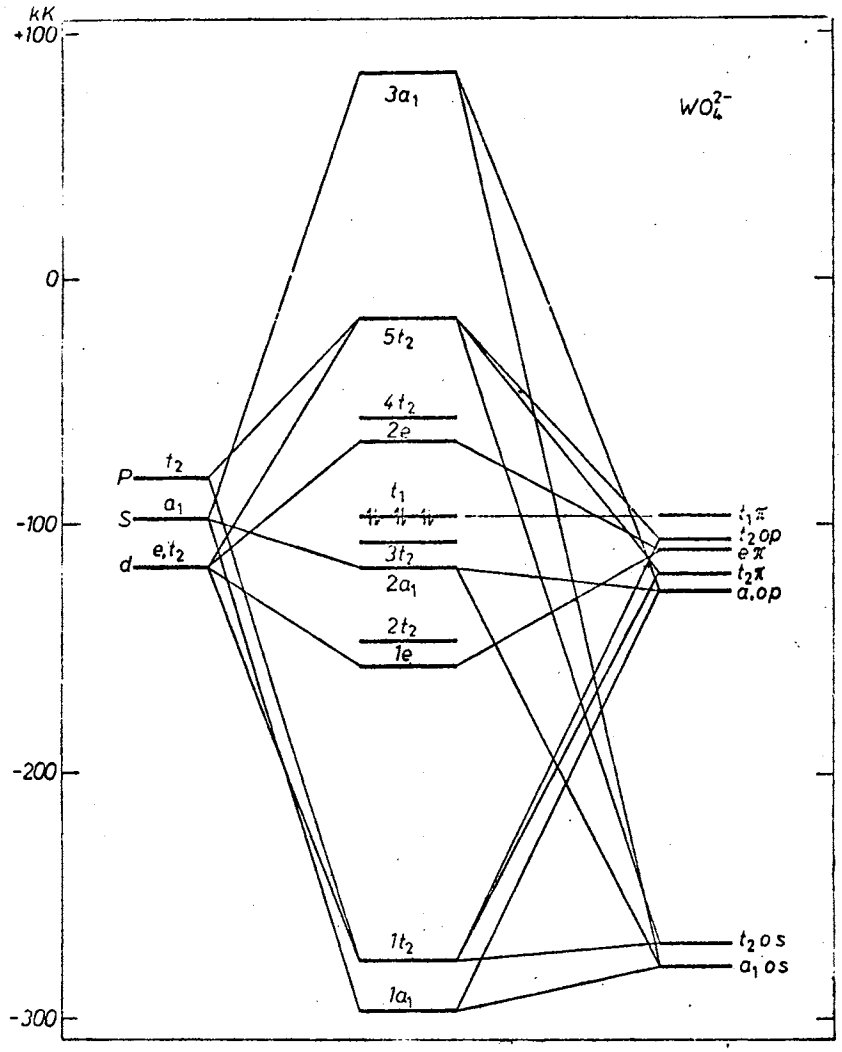

Figure 41. WO_4^{2-} Molecular Orbital Scheme Calculated by Butler

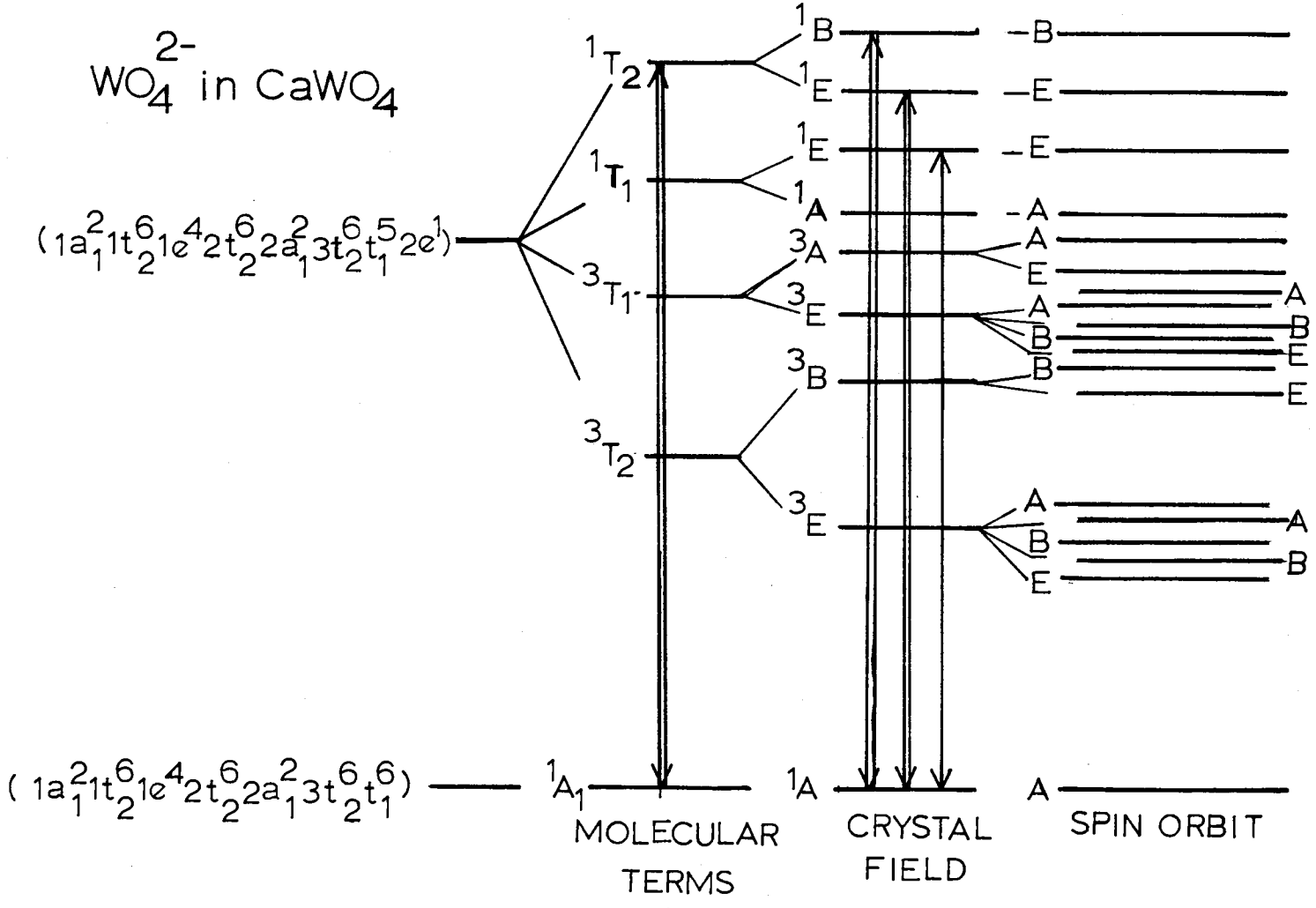

Figure 42. Splitting of WO_4^{2-} Energy Levels in $CaWO_4$

$^1A_1 \rightarrow {}^1T_2$ which in the crystal field gives rise to two allowed transitions from the groundstate to the ^1E ($^1T_2$) and ^1B ($^1T_2$). In the crystal field a third transition becomes allowed ^1A ($^1A_1$) $\rightarrow$ ^1E ($^1T_1$).

Ordering of the crystal field levels is usually made by comparison of the relative intensity of the absorption peaks. Due to the large number of absorbing sites in a crystal of the size used for this investigation it was impossible to obtain any information about the structure of the WO_4^{2-} absorption below 3200Å as shown in Figure 5. However, the excitation spectra shown in Figures 6 and 7 indicate that there is structure in the tungstate absorption band below 3200Å. Ordering of the levels shown in Figure 42 was obtained from the excitation spectra of undoped calcium tungstate. The structure in Figures 6 and 7 can be explained by proposing four bands near 2500Å, 2800Å, 3050Å and 3550Å. The accuracy of the assignment of the position is obviously not high nor is it important in the level ordering. The weakest band near 3550Å was assigned to the forbidden transition $^1A(^1A_1) \rightarrow {}^1A(^1T_1)$. The next most intense band was the 3050Å one which was assigned to the ^1E level since transitions from the ground state to the ^1E level are allowed only in the crystal field. Extension of the band edge to 3100Å has been previously observed but was attributed to impurities (6). The two most intense bands at 2800Å and 2500Å have been arbitrarily assigned to transitions from the ground state to the $^1E(^1T_2)$ and $^1B(^1T_2)$ levels respectively. There is no evidence that the last two assignments cannot be reversed.

Assignment of the emission transitions is not as straightforward. Blassee (34) in his work on YWO_4 pointed out that the oscillator strength of the absorption is about .1 while that of the emission transition is about 10^{-5} as indicated by the lifetime of the emission. This indicates that either the emission transition begins from a state different than

the terminal level of the absorption transition or the lattice near an excited site relaxes before emission takes place and changes the surroundings of the site sufficiently to cause the observed long lifetime of the emission (35).

The first possibility would in light of Figure 42 imply that the emission transition would take place from the triplet states. This would explain the large wavelength shift between the absorption and emission transitions and would predict a long lifetime. Although emission from the triplet states cannot be ruled out, two considerations make it seem unlikely. The first is that for transitions that are spin forbidden one would expect lifetimes longer than those measured in this investigation. The second consideration is the emission from triplet states has not been reported in similar systems.

If then the emission is associated with the Stokes shift of the absorption, the degree of the Stokes shift would be on the order of several thousand wavenumbers. Such a large Stokes shift is not unreasonable, however, it would indicate a great deal of relaxation of the lattice surrounding the excited site which could easily explain the long observed lifetime of the emission.

What must be determined now is the number of levels from which fluorescence is observed. Excitation at 2400 and 2650Å at room temperature produces similar fluorescence bands as shown in Figures 8 and 11 respectively. The measured lifetimes of the fluorescence bands are 7.6 and 7.8 μsec respectively. The similarity of the shape of the bands and the lifetimes indicates that the fluorescence is the result of transitions from the same level.

Excitation at 2650Å and 3150Å at 10°K produces similar broad fluo-

rescence bands as shown in Figures 11 and 10 respectively. Lifetime measurements show that at 10°K the fluorescence produced for 2650Å excitation has a lifetime of 117 μsec while that produced for 3150Å excitation has a lifetime much longer, so long that we could not measure it. Although this is not conclusive proof that the fluorescence is the result of transitions from two different levels, the presence of the zero phonon lines in the fluorescence spectra for 3150Å excitation that are never observed for 2650Å excitation verifies that there are two fluorescing levels responsible for the similar 5200Å fluorescence bands.

The shift in the peak of the tungstate fluorescence band for 2650Å excitation from 4400Å at room temperature to 5200Å at 10°K is the result of thermal crossing between the 4400Å and 5200Å fluorescence levels. The probability of thermal crossing decreases with temperature as the probability of absorption of a phonon decreases. As the probability of thermal crossing decreases the intensity of 4400Å fluorescence observed for 2650Å excitation decreases and at the same time the intensity of the 5200Å fluorescence increases. At 229°K the peak shift is almost complete and below 183°K very little shift is observed with temperature.

The connection between the zero phonon lines and the 5200Å band observed for 3150Å excitation is not clear. The 5200Å band could be the vibronic sideband of the zero phonon lines or the 5200Å band and zero phonon lines could be due to fluorescence from two different levels that are connected via some radiationless process. For the second case the absence of the zero phonon lines at high temperatures could also be explained in terms of radiationless processes. From the results of this investigation neither explanation could be either proved or disproved.

There are then at least three and possibly a fourth level from

which fluorescence is observed in calcium tungstate. Figure 43 shows the latter possibility as a configurational coordinate diagram.

An important point to note about the zero phonon lines is the temperature dependence of their relative intensities as shown in Figure 10. At $10^{o}K$ the high energy line is much more intense than the low energy line while at $121^{o}K$ the intensities are about the same. If the two lines were due to different transitions at similar WO_4^{2-} sites one would expect the low energy line to increase in intensity relative to the high energy line with decreasing temperature which is not the case.

The observed temperature dependence of the relative intensity of the two lines can only be explained if they are assigned to the same transition at two types of sites. The high energy line is due to transitions at normal lattice sites while the low energy line is due to transitions at trap sites. The traps are proposed as tungstate ions next to either chemical or structural defects and thus have a different symmetry than tungstate ions in normal lattice sites. The observed temperature dependence of the relative intensities can then be explained by a model as shown in Figure 44 where B_s and B_x are the decay rates of the normal and trap sites, respectively, kC_x is the rate of energy transfer to traps, C_x is the trap concentration and ΔE is the activation energy that must be overcome for the excitation to become mobile. The trap depth can be approximated from the difference in energy of the zero phonon lines and is about 507 cm^{-1}; therefore, thermal detrapping is considered negligible. At $10^{o}K$ the excitation at normal sites (self trapped excitons) has a small probability of absorbing a phonon and thus overcoming the activation energy ΔE. As a result most all of the observed fluorescence is emission from the absorbing sites. The low energy zero phonon line

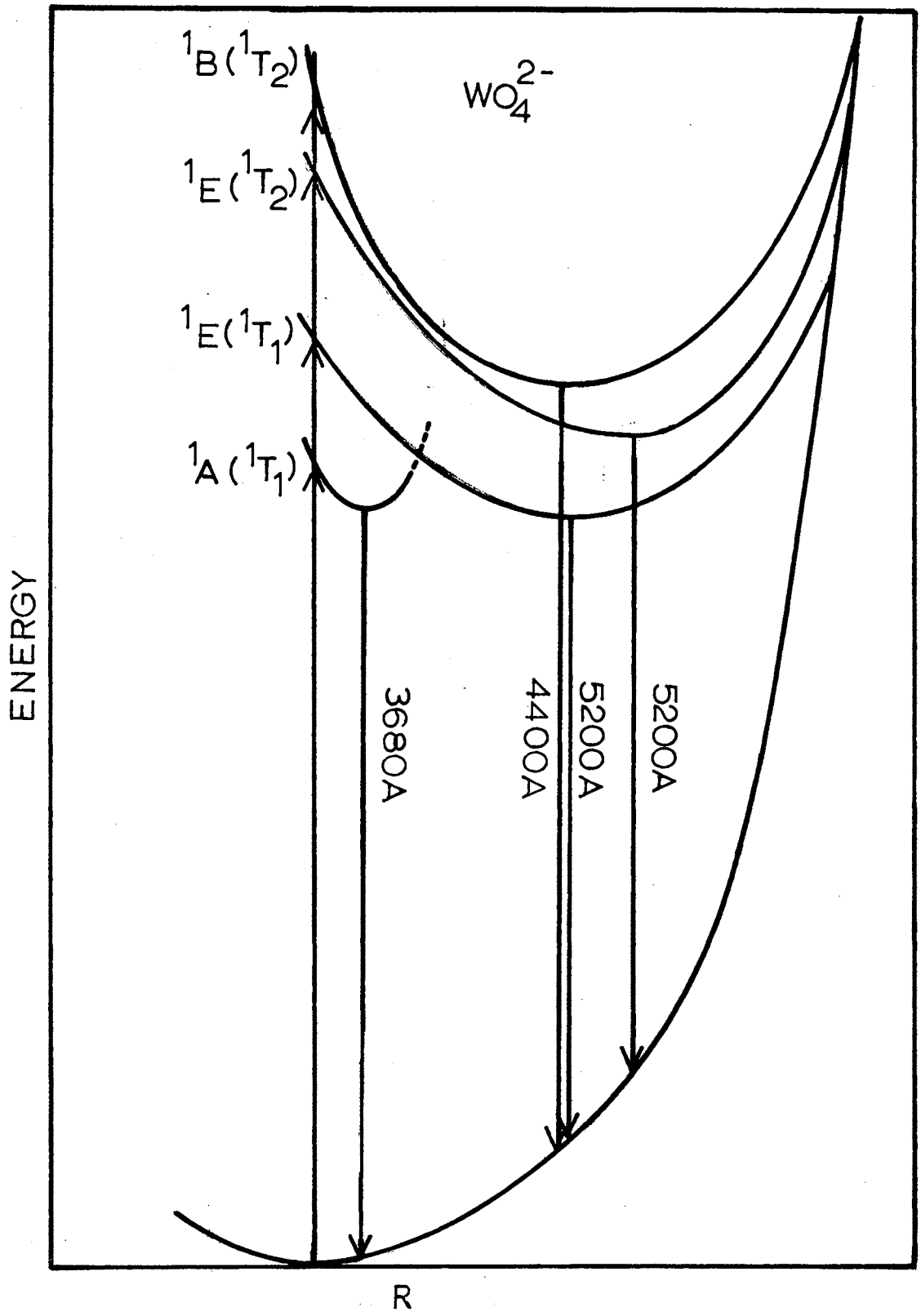

Figure 43. Proposed Configurational Coordinate Diagram of Tungstate Ions in $CaWO_4$

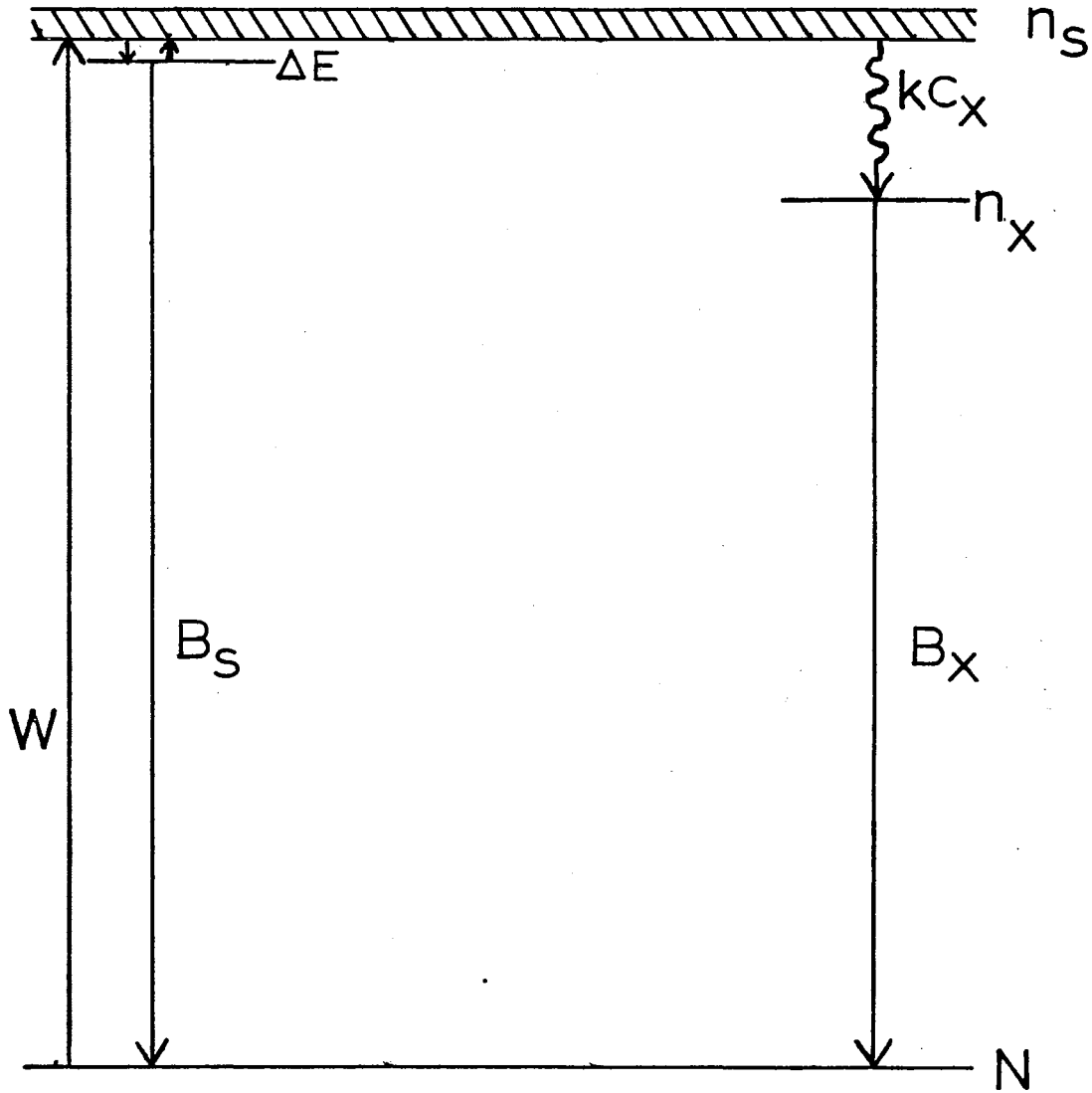

Figure 44. Proposed Energy Migration Model of Undoped $CaWO_4$

at $10^{o}K$ is mostly due to direct excitation of the traps and since there are many more normal sites the high energy line is much more intense. As the temperature is increased the self trapped excitons have a higher probability of thermally overcoming the activation energy and energy migration to traps increases. As the energy migration to traps increases the high energy zero phonon line decreases in intensity and the low energy zero phonon line increases.

This model also explains the temperature dependence of the tungstate lifetimes. Writing the differential equations for the time rate of change of the normal site and trap site excited state populations as

$$\dot{n}_s(t) = -(B_s + kC_x)n_s(t) \qquad [40]$$

$$\dot{n}_x(t) = -B_x n_x(t) + kC_x n_s(t) \qquad [41]$$

where it has been assumed that the excitation pulse can be approximated by a delta function and the number of directly excited traps is negligible. Due to the length of the excitation pulse (< 15 nsec) the first assumption is reasonable. If the concentration of normal sites is much greater than the concentration of traps then the second assumption is valid. Also the decay rate of the mobile and self trapped excitons have been assumed to be the same to make the problem tractable. Equation [40] and [41] can be integrated to yield

$$n_s(t) = n_s(o)\, e^{-(B_s + kC_x)t} \qquad [42]$$

and

$$n_x(t) = \frac{n_s(o)kC_x}{(B_x - B_s - kC_x)} \left(e^{-(B_s + kC_x)t} - e^{-B_x t}\right) \qquad [43]$$

which are the populations of the normal and trap sites, respectively.

The energy transfer rate from normal sites to traps, kC_x, is a function of temperature. After each hop the mobile exciton has the probability of hopping again or relaxing radiationlessly by the emission of a phonon; however, after relaxing the exciton also has the probability of absorbing a phonon. The temperature dependence of kC_x will then be contained in the diffusion coefficient, Equation [42]. kC_x will then be dependent upon temperature as the ratio of the probability of absorption to emission of a phonon which is $e^{\frac{-\Delta E}{kT}}$.

The observed fluorescence will be a combination of normal site and trap site fluorescence. The intensity (photon flux) from each type of site will be the population of the excited state times the radiative decay rate. Therefore, the observed tungstate fluorescence for pulsed excitation will be

$$I_H(t) = n_s(o)\left[\left(B_s' + \frac{B_x' kC_x}{(B_x - B_s - kC_x)}\right) e^{-(B_s + kC_x)t} - \frac{B_x' kC_x}{(B_x - B_s - kC_x)} e^{-B_x t}\right] \qquad [44]$$

where the primes indicate radiative decay rates. The first coefficient, B_s', arises due to the contribution normal host site fluorescence makes to the total observed fluorescence, and the second and third coefficients represents the fluorescence from traps. What will be shown in the following development is that due to the temperature dependence of kC_x, Equation [44] can be considered in the low and high temperature limit and predicts a lifetime at low temperatures of $(B_s + kC_x)^{-1}$ which is temperature dependent and a high temperature limit $(B_x)^{-1}$ which is tem-

perature independent.

Consider the low temperature limit of Equation [44]. At $10^{o}K$ kC_x is very small and the second and third coefficients approach zero, then only the first coefficient remains and Equation [44] becomes

$$I_H(t) = n_s(o)B'_s e^{-(B_s + kC_x)t} \qquad [45a]$$

at low temperatures and predicts a lifetime of

$$\tau_s^o = (B_s + kC_x)^{-1} \qquad [45b]$$

where the superscript zero indicates lifetimes of undoped samples. Since kC_x increases with increasing temperature the lifetime will decrease with increasing temperature.

In the high temperature limit if kC_x increases to a limit such that $B_s + kC_x \geq B_x$ then Equation [44] becomes

$$I_H(t) \approx n_s(o)\ B'_s e^{-(B_s + kC_x)t} \approx n_s(o)\ B'_s e^{-B_x t} \qquad [46a]$$

and the measured lifetime becomes

$$\tau_s^o = (B_x)^{-1} \qquad [46b]$$

which is the lifetime of the traps and is independent of temperature. The accuracy of the assumption $B_s + kC_x \approx B_x$ at high temperatures will be discussed at the end of this development.

Thus it can be seen from Equations [45b] and [46b] that the proposed model predicts a lifetime near $10^{o}K$ which decreases with increasing temperature and approaches at high temperature a temperature independent limit of $(B_x)^{-1}$. Comparison of these predictions with Figure

12 shows very good qualitative agreement and shows that the transition to the high temperature limit occurs near 100°K.

As mentioned earlier the energy transfer rate to traps, kC_x, varies with temperature as $\exp(\frac{-\Delta E}{kT})$. The measured lifetime at low temperature as given by Equation [45b] can be written (36) as

$$\tau_s^o = (B_s + kC_x)^{-1} = (B_s + k'C_x e^{\frac{-\Delta E}{kT}})^{-1} \quad [47]$$

where k' is the temperature independent value of the energy transfer rate and at high temperatures $k'C_x \approx kC_x$. The values of B_s, $k'C_x$ and ΔE can be obtained plotting the logarithm of the lifetimes measured at low temperatures versus the inverse of the temperature. The values obtained for 2400Å excitation are $B_s = 1.5 \times 10^4$ sec^{-1}, $k'C_x = 4.3 \times 10^4$ sec^{-1} and $\Delta E = 33.9$ cm^{-1}. For 2650Å excitation the values are $B_s = 8.2 \times 10^3$ sec^{-1} $k'C_x = 4.6 \times 10^4$ sec^{-1} and $\Delta E = 55.6$ cm^{-1}. In the transition from Equation [44] to Equation [45a] it was assumed that at high temperatures $B_s + kC_x \approx B_x$. The validity of this assumption can now be considered in light of the values of kC_x and B_s just determined. For 2400Å above 100 °K $B_s + kC_x = 5.8 \times 10^4$ sec^{-1} which can be compared to the value of B_x obtained from Equation [46b] and the data from Table I of 4.5×10^4 sec^{-1}. Likewise for 2650Å $B_s + kC_x = 5.42$ sec^{-1} and $B_x = 4.0 \times 10^4$ sec^{-1}. This less than ideal agreement necessitates further discussion. The assumption that $B_s + kC_x \approx B_x$ at high temperatures was made so that Equation [44] could be written approximately as Equation [46a] and thus predict no initial rise of the fluorescence intensity in order to be consistent with the experimental fact that no initial rise was observed. However, based upon the results just presented this approximation is not within experimental error and Equation [44] does

predict an initial rise on the order of 19 μsec. This is not surprising due to the very simple nature of the model. By expanding the model to allow for direct excitation of the traps and energy transfer to the traps before relaxation of the absorbing site the predicted rise can be easily reduced by more than an order of magnitude. That an initial rise was not observed in any of the time resolved spectra is due to the limitations of the time resolved apparatus. Although the ultimate resolution of the apparatus is on the order of a few nanoseconds, measurement of rise times less than 1 μsec becomes difficult when the fluorescence decay time is several orders of magnitude larger. This is a result of the low intensities measured and the statistical limitations which are incurred when the signals produced by fluorescence striking the photomultiplier and noise signals produced internally by the measuring electronics are of the same order of magnitude.

It would be of interest to be able to experimentally obtain a value of k, the concentration independent energy transfer rate to traps. However, in all equations the trap concentration and k appear together and it is not possible to derive a value of k from measurements made only on the undoped sample, since the trap concentration is unknown.

Also of great interest is the activation energy ΔE which must be overcome in order for self trapped excitons to become mobile. That energy migration to traps quenches the fluorescence lifetime of the normal host sites indicates that the migration takes place from the fluorescing level and therefore after relaxation of the lattice surrounding the absorbing site. It is hard to understand how such a small amount of energy ΔE on the order of tens of wavenumbers can bring the fluorescence which peaks near 23×10^3 cm^{-1} into resonance with the absorption which

occurs near 40 x 10^3 cm^{-1}. Consider the diagram shown in Figure 45. The broad band fluorescence of the WO_4^{2-} complex ion indicates that the electronic potential energy curve of the ground state has a steep slope as shown in Figure 45. The relatively sharp absorption bands as indicated by the excitation spectra indicates that the slope of the excited state curves is not as steep. At low temperatures the fluorescence transition originates from the lowest vibrational level of the excited state and the fluorescence has only a small overlap with the absorption transitions. By excitation to the first excited vibrational level of the excited electronic state the energy available in a fluorescence transition can be brought into much closer resonance with the absorption transition. So by the absorption of a phonon the self overlap between the emission and absorption transitions of neighboring WO_4^{2-} sites can be greatly increased and as pointed out in the theoretical development the degree of self overlap determines to what extent the excitons are mobile.

Consideration must be given now to what this model predicts for the case of continuous excitation of the samples. Equations [40] and [41] can be solved for the steady state case and easily yield

$$n_s = \frac{WN_s}{(B_s + kC_x)} \qquad [48a]$$

and

$$n_x = \frac{WN_s}{(B_s + kC_x)} \frac{C_x k}{B_x} \qquad [48b]$$

where W is the rate of excitation of normal host sites and N_s is the total number of normal host sites. Direct excitation of the traps is assumed to be negligible. The population of the excited levels are re-

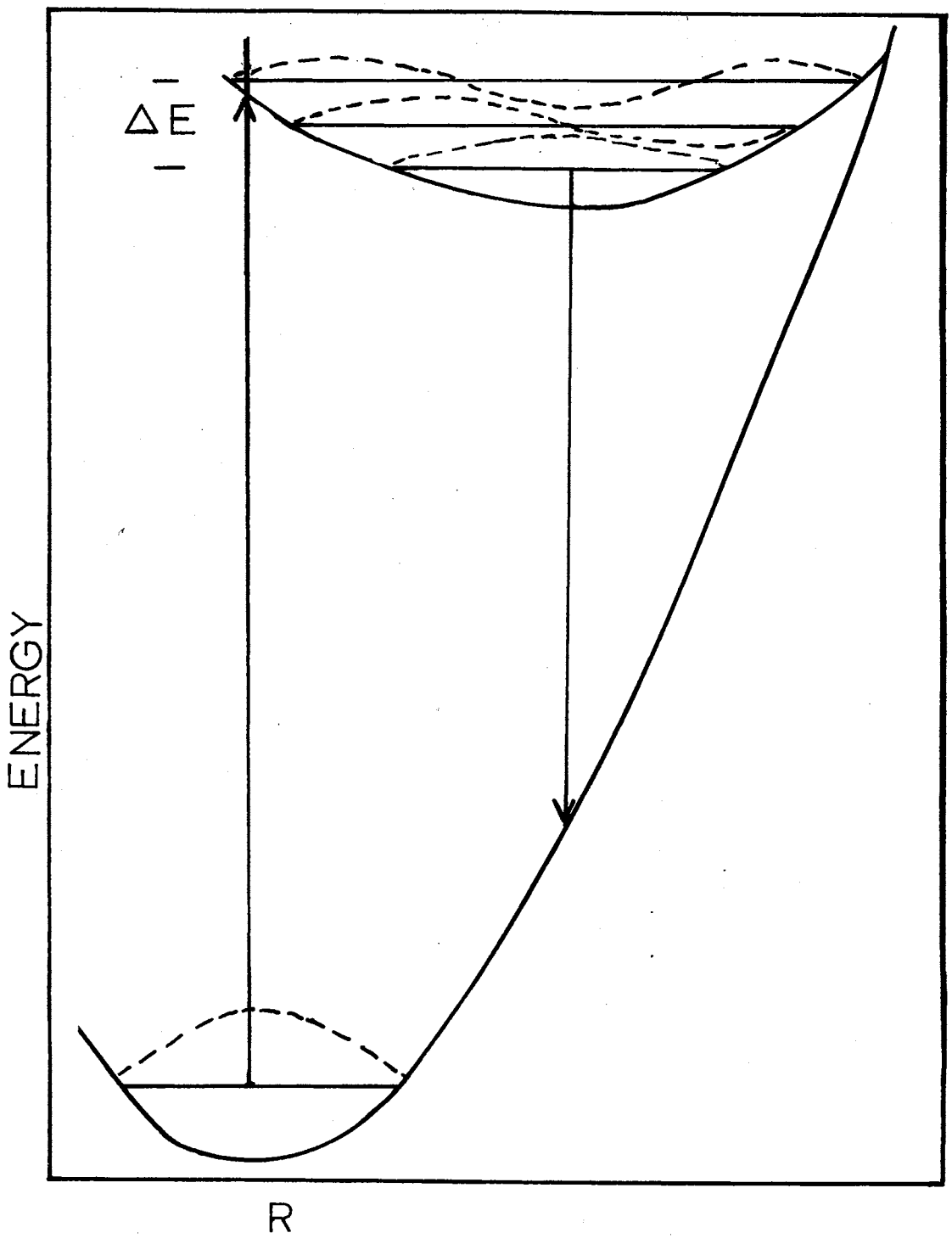

Figure 45. Activation Energy Model

lated to the fluorescence intensities by the radiative decay rates. The host fluorescence is again a combination of normal site and trap fluorescence and the intensity is

$$I_H = B'_s n_s + B'_x n_x = \frac{WN_s}{(B_s + kC_x)} \left[B'_s + B'_x \frac{kC_x}{B_x}\right] \qquad [49]$$

where the primes indicate radiative lifetimes. At temperatures below 220 ^{o}K the radiative and fluorescence lifetimes are approximately equal, due to the absence of radiationless processes. The total host intensity is then

$$I_H = WN_s$$

which is independent of temperature. Comparison of this prediction of the model to the integrated fluorescence intensity for 2400Å excitation as shown in Figure 9 shows good qualitative agreement. For 2650Å excitation the shift in the peak of the fluorescence band with temperature must be considered. As discussed previously the shift in the fluorescence emission is the result of thermal crossing between two levels. Below 120 ^{o}K the shift in the emission is complete and the integrated fluorescence intensity is indeed independent of temperature as for 2400Å and as predicted by Equation [49]. The increase in the integrated fluorescence intensity above 120 ^{o}K is probably due to the state associated with the 4400Å fluorescence having a slightly greater quantum efficiency than the state which gives rise to the 5200Å fluorescence. The decrease in the integrated fluorescence intensity above 220 ^{o}K is the result of increasing radiationless quenching of the fluorescence intensity. The change with temperature of the intensity of the 5200Å fluorescence for 3150Å excitation is probably due to thermal crossing to the $^{1}E(^{1}T_2)$ level.

Empirical Energy Level Scheme for Sm^{3+} in $CaWO_4$

The observed optical spectra of Sm^{3+} in calcium tungstate is due to transitions between energy levels of the samarium $4f^5$ configuration. Several attempts have been made to calculate the free ion energy levels of Sm^{3+}. (13-15) The most recent results (15) indicate that the lowest lying fluorescent state is $^4F_{5/2}$. The terminal levels for the fluorescent transitions are the various multiplets of the ^6H term with the ground state being $^6H_{5/2}$.

When Sm^{3+} is placed in $CaWO_4$ it substitutes for Ca^{2+} since it has an ionic radius of .946 Å which is approximately the same as that of Ca^{2+} (.99 Å) and is much greater than the ionic radius of W^{6+} (.62 Å). This site is surrounded by 8 WO_4^{2-} ions giving a symmetry of S_4 which splits the multiplets into their Stark components. Crystal field splittings for multiplets with various J values in S_4 symmetry have been previously worked out (37) and are shown in Table IX. The two possible crystal field levels are both Kramers degenerate.

In the free ion electric dipole transitions are Laport forbidden. Odd crystal field terms can cause electric dipole transitions to become allowed for the ion in the crystal but their intensity will be of the same order of magnitude as magnetic dipole transitions. Thus selection rules for both types of transitions in the crystal must be examined. These can be found from group theory considerations of the site symmetry. Table X summarizes these selection rules where E stands for electric dipole, M for magnetic dipole, π for light polarized parallel to the C axis and σ for light polarized perpendicular to the C axis of the crystal.

Tables IX and X are useful in deriving an empirical energy level

TABLE IX

CRYSTAL FIELD LEVELS FOR UNGARAD MULTIPLETS IN S_4 SYMMETRY

J	1/2	3/2	5/2	7/2	9/2	11/2
Γ_i						
Γ_{56}	1	1	1	2	3	3
Γ_{78}		1	2	2	2	3

TABLE X

SELECTION RULES FOR S_4 SYMMETRY

Γ_i \ Γ_f	Γ_{56}	Γ_{78}
Γ_{56}	E,σ	E,σπ
	M,σπ	M,σ
Γ_{78}	E,σπ	E,σ
	M,σ	M,σπ

scheme and identifying transitions that give rise to the observed spectral lines. The multiplets of the ^6H term should split into $J + \frac{1}{2}$ crystal field levels and if all the fluorescence originates from the same metastable level, a line should appear in the spectrum for a transition to each of these levels. Figure 22 shows the correct number of lines for each multiplet group in the three high energy regions of the samarium fluorescence and this leads to the proposed energy level diagram shown in Figure 46. The $^6H_{11/2}$ energy levels were derived from Figure 21 since spectra were extended to the wavelength region beyond6700Å only for the calcium tungstate sample with 1.0% samarium. The designations for the crystal field states were obtained by noting that within each set of lines the number of intense transitions equaled the number of Γ_{56} levels predicted by Table IX. The $^4F_{5/2}$ metastable level is arbitrarily assigned to Γ_{78} since this makes electric dipole transitions to the Γ_{56} levels allowed in both polarizations. However, the selection rules in Table X predict that the π spectrum should contain fewer lines than the σ spectrum. The fact that this is not observed indicates that both electric and magnetic dipole transitions are taking place with about the same probability.

The number of weak intensity lines observed in the fluorescence spectra of calcium tungstate with 1.0% samarium as shown in Figure 21 could arise from several sources. One is the presence of non-equivalent sites for the samarium ions. This can be especially important due to the problem of charge compensation. The samples used in this investigation have an amount of Na^{1+} equal to the concentration of Sm^{3+} added to give charge neutrality. Published electron spin resonance measurements on this system (38) imply that for the concentrations of interest the

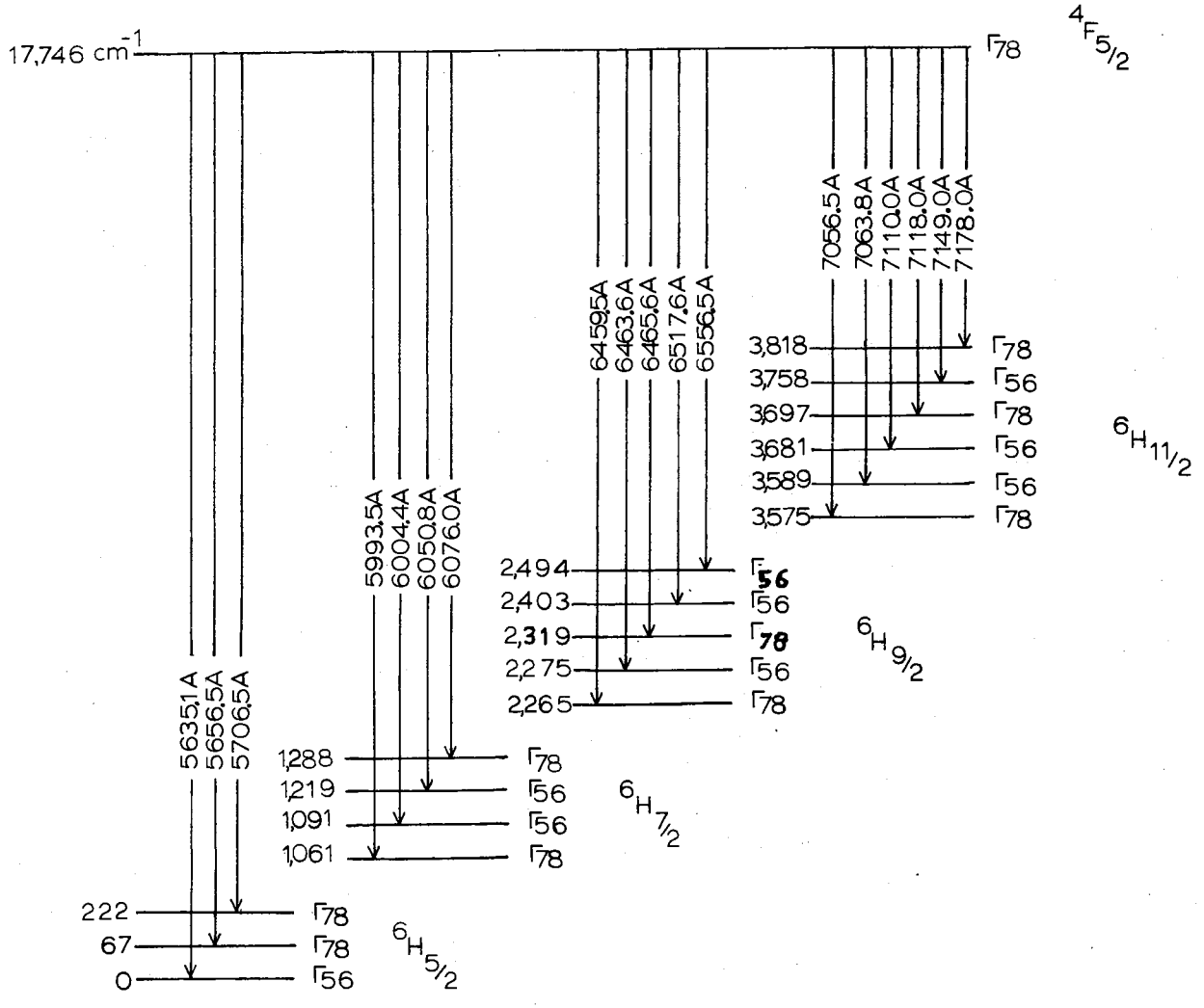

Figure 46. Emperical Energy Level Diagram of Sm^{3+} in Calcium Tungstate

charge compensation will be non-local for the majority of sites but some local compensation does exist. In the latter case the samarium site symmetry will be C_1, instead of S_4. For this symmetry there is only one type of crystal field state and all transitions are allowed for both electric and magnetic dipole radiation. The different crystal field cannot lift the Kramer's degeneracy but can cause a shift of the samarium levels.

Emission from higher excited metastable states can also result in minor spectral lines. Such emission has been observed from two levels in other systems (39,40). This mechanism would predict minor lines with spacings similar to those in the proposed energy level diagram Figure 46. Examination of Table II shows several sets of lines which suggests fluorescence from levels at 17,796 cm^{-1} and 18,292 cm^{-1}.

Another possible source for the weak lines in the spectra is vibronic transitions. These vibrational-electronic bands may appear on the low energy side of the strong electronic transitions at low temperatures with peaks occurring at distances from the electronic line equal to phonon frequencies. Phonon frequencies for calcium tungstate (41,42) lie between 100 cm^{-1} and 450 cm^{-1}.

A final possible source of the extraneous lines is the interaction of neighboring Sm^{3+} ions at high concentrations. It has been shown (16) that such interaction leads to quenching of the fluorescence intensity above about 1.0%. Results of this effect should be observable as a concentration dependence of the spectrum. It is not clear if the weak lines cannot be observed in the .01% sample is attributable to some physical effect or simply to a decrease in the fluorescence intensity beyond the sensitivity of our apparatus.

Energy Transfer Model

Before attempting to establish an energy transfer model for $CaWO_4$: Sm^{3+} it is useful to replot the data in a more instructive manner. The presence of energy transfer in general quenches the lifetime of host fluorescence for the case of host sensitization. Figure 47 and 48 show a plot of the ratio of the lifetimes as measured in the doped and undoped samples as a function of samarium concentration at several temperatures for 2400Å and 2650Å excitation respectively. That the ratio is greater than 1 for 2400Å excitation at $10^{o}K$ for .01 and .1% Sm^{3+} tends to indicate that the undoped lifetime at $10^{o}K$ is questionable.

Similarly the presence of energy transfer usually tends to decrease the intensity of the host fluorescence with a corresponding increase in the activator fluorescence intensity. This effect usually increases with increasing activator concentration and is reflected in an increase of the ratio of activator to host fluorescence intensity. Figures 49 and 50 show a ratio of the samarium to tungstate integrated fluorescence intensities as a function of samarium concentration for 2400Å and 2650Å excitation respectively.

In attempting to establish a model for the host sensitized energy transfer in $CaWO_4$:Sm^{3+} several experimentally observed facts were considered of primary importance: 1) below $100^{o}K$ the lifetime ratio of the tungstate fluorescence as shown in Figure 47 and 48 in the samarium doped samples decreased with increasing samarium concentration, 2) above $100^{o}K$ the tungstate lifetimes were relatively independent of the samarium concentration, and 3) at all temperatures the ratio of the samarium to tungstate integrated fluorescence intensities increased with increasing samarium concentration as shown in Figures 49 and 50. Any proposed model must explain these effects. In addition it is important that the model be compatable with the model proposed for undoped calcium tungstate.

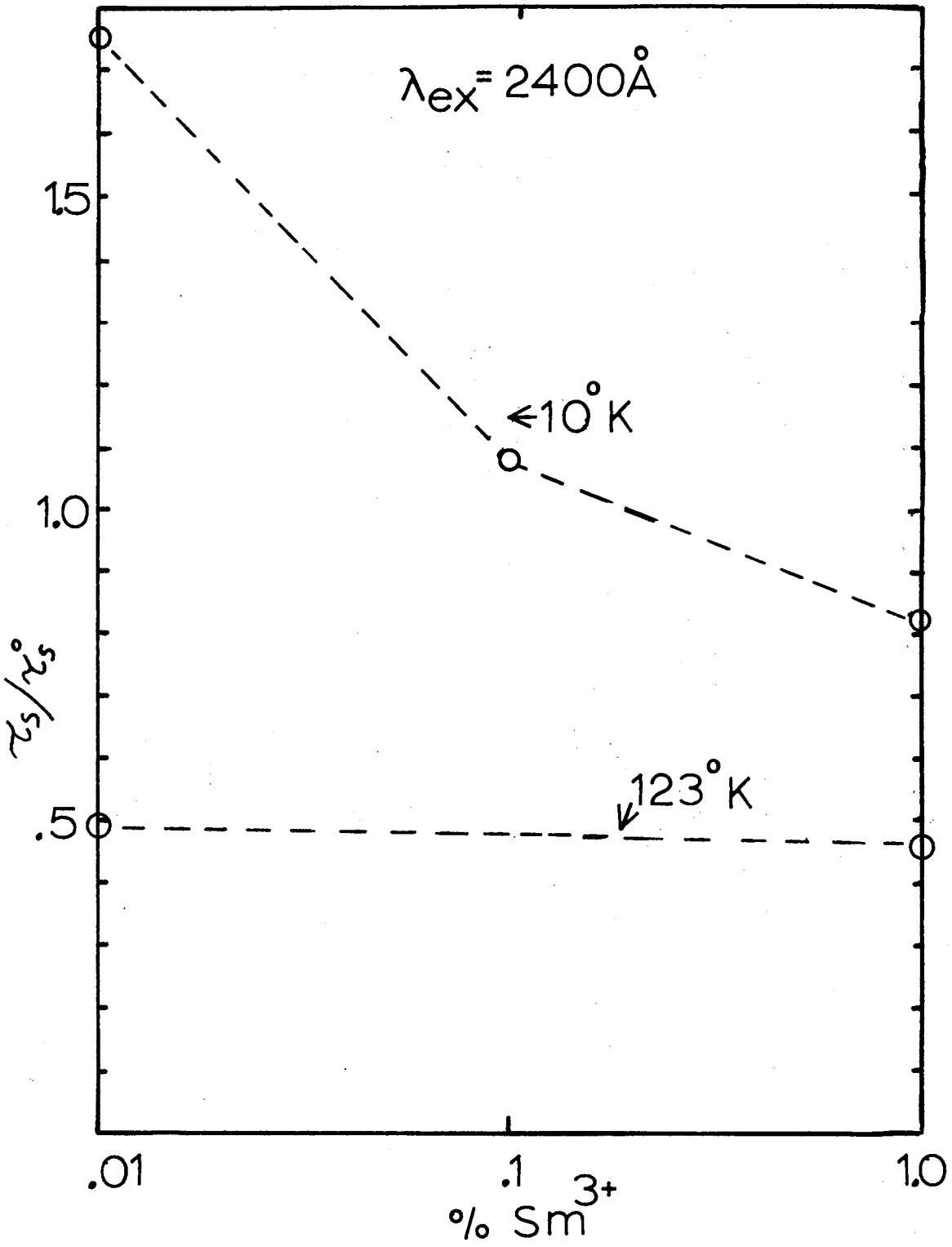

Figure 47. Ratio of Tungstate Lifetimes in Doped and Undoped Samples Versus Samarium Concentration for 2400Å Excitation

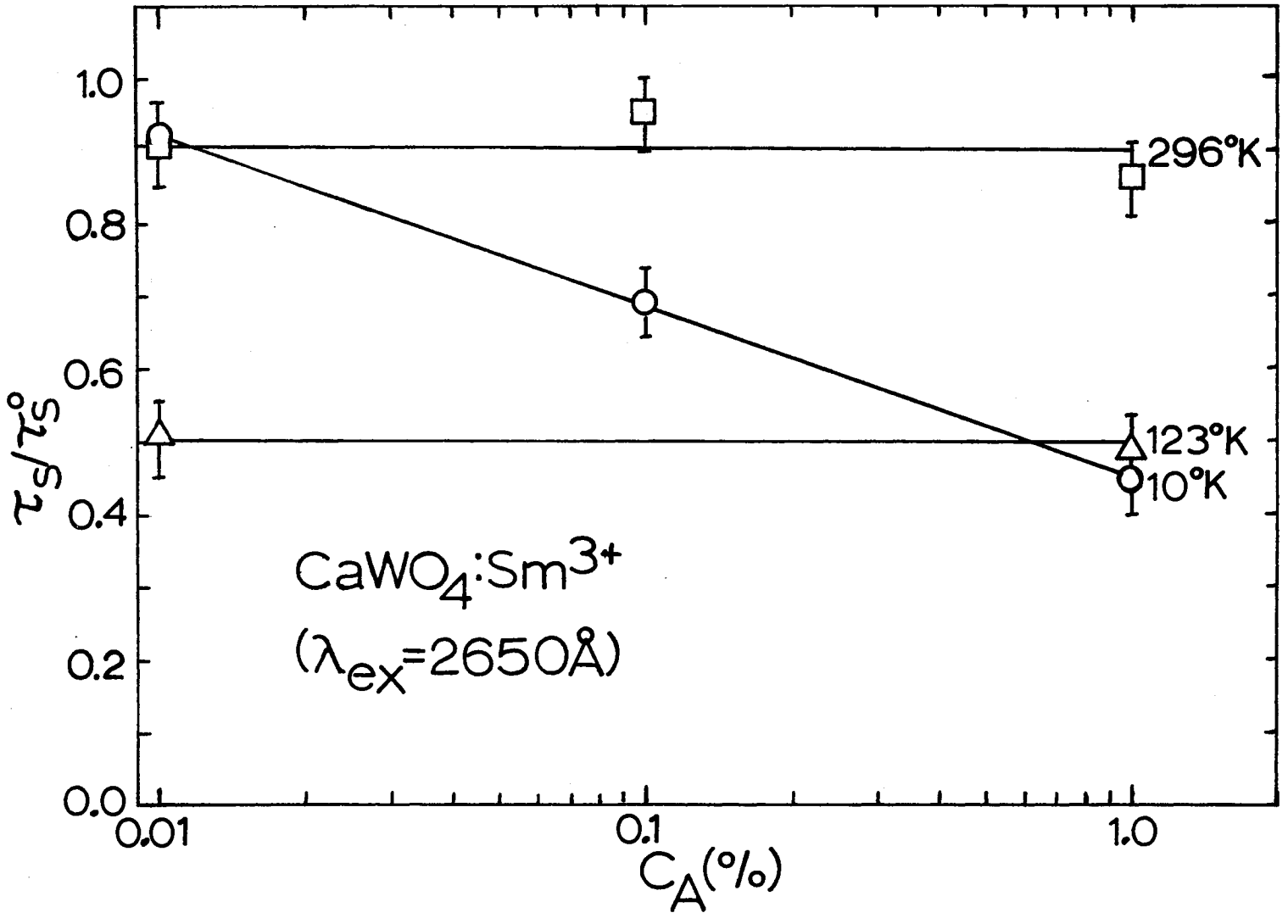

Figure 48. Ratio of Tungstate Lifetimes in Doped and Undoped Samples Versus Samarium Concentration for 2650Å Excitation

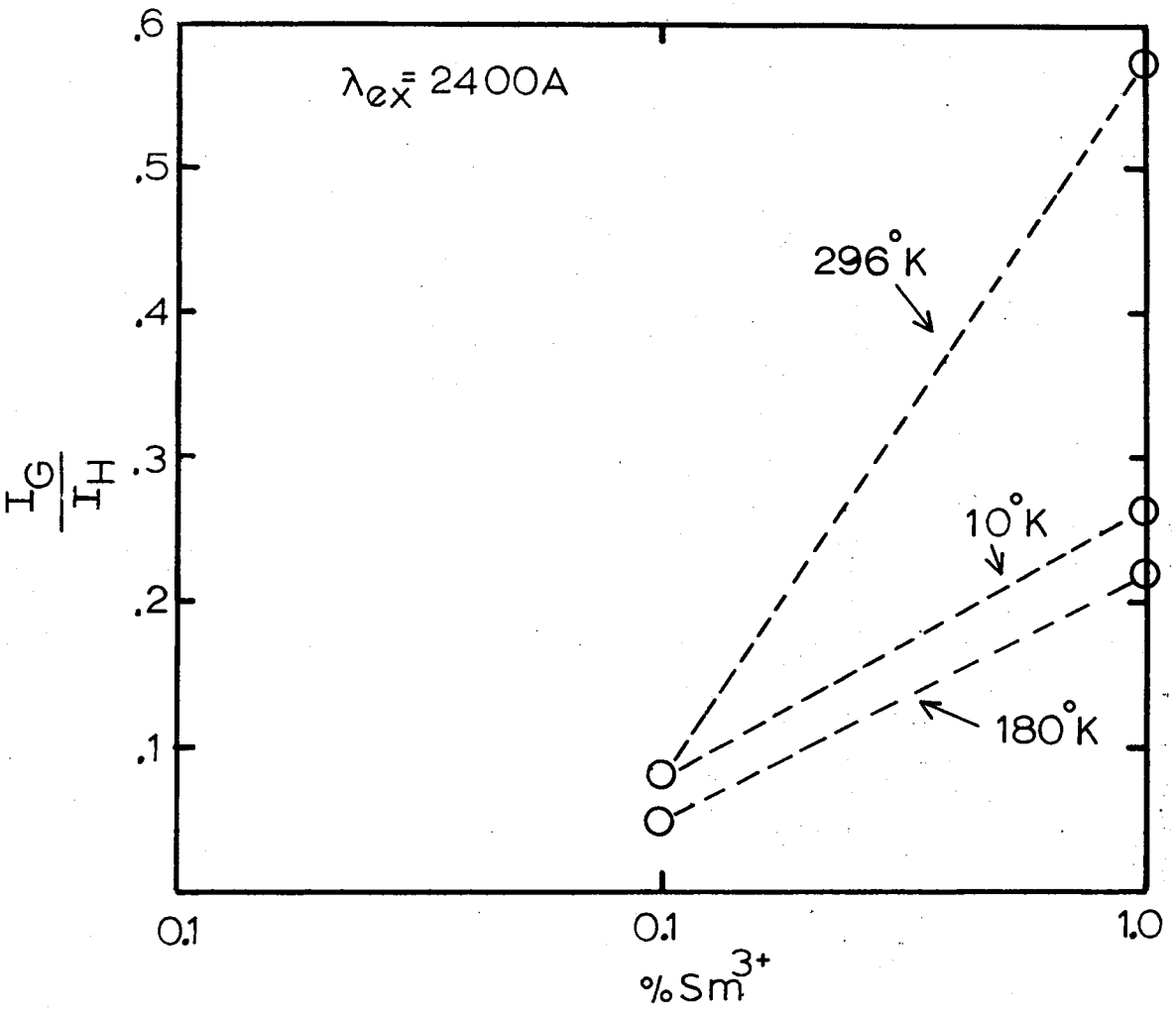

Figure 49. Ratio of Samarium to Tungstate Integrated Fluorescence Intensities Versus Samarium Concentration for 2400Å Excitation

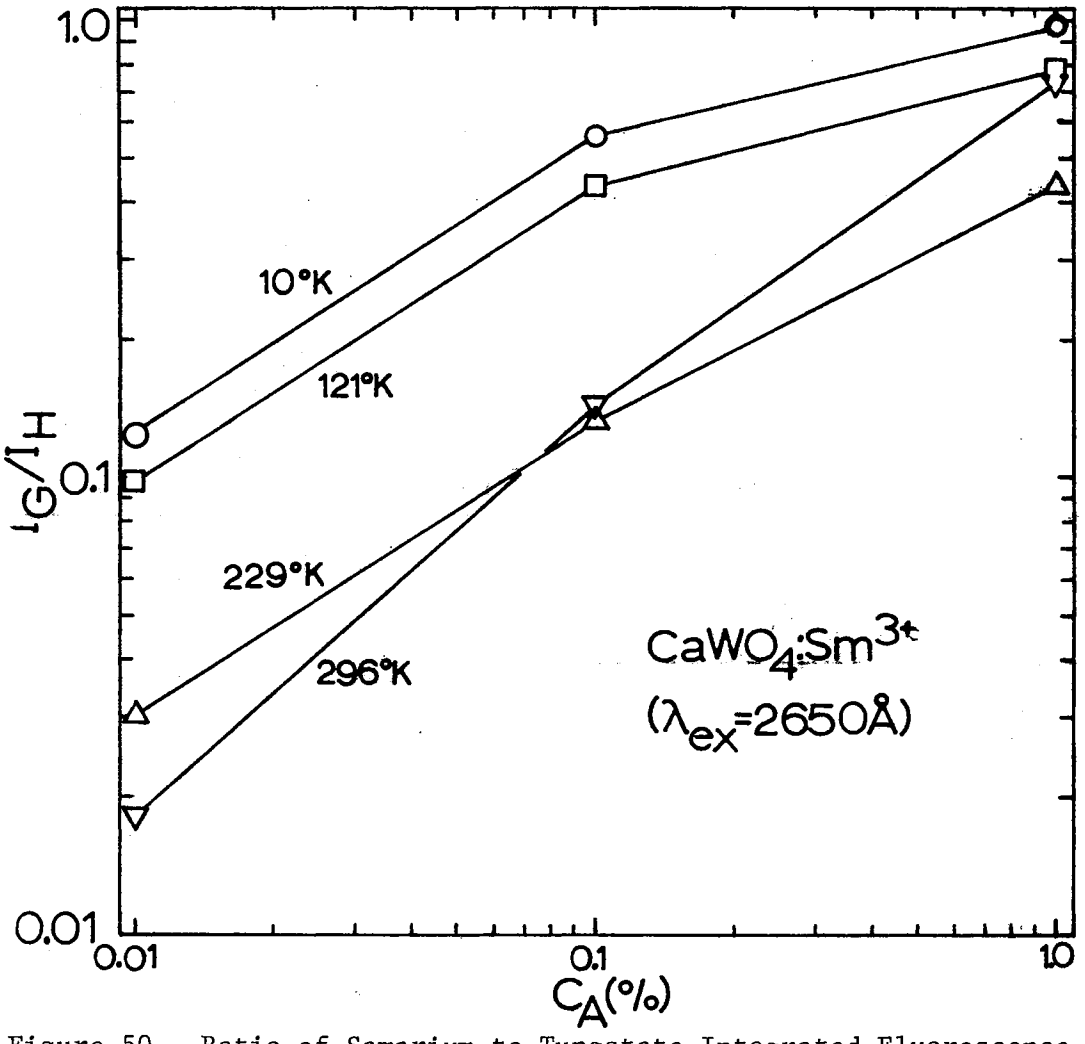

Figure 50. Ratio of Samarium to Tungstate Integrated Fluorescence Intensities Versus Samarium Concentration for 2650Å Excitation

The proposed model is shown in Figure 51. This is essentially the same model proposed for undoped calcium tungstate except that it has been assumed that the presence of a samarium ion sufficiently perturbes the surrounding tungstate ions to induce a trap site similar to the in trinsic host traps proposed for the undoped calcium tungstate model, this is reasonable in light of the complicated nature of the Sm^{3+} spectra. C_x is the concentration of intrinsic traps, C_A is the concentration of samarium ions and also the concentration of induced traps. B_s, B_x and B_A are the intrinsic decay rates of the normal tungstate sites, traps and samarium ions respectively. k_AC_A, kC_A and kC_x are the energy transfer rates from normal lattice sites to samarium ions, induced traps and intrinsic traps, respectively. $F(C_A)$ is the Förster-Dexter energy transfer rate for transfer directly from self trapped excitons to samarium ions, which is a function of the samarium concentration. q_A is the energy transfer rate from induced traps to samarium, which is independent of the samarium concentration since the induced traps are all nearest neighbor to the samarium ions. n_s, n_x, n_{xA} and n_A are the excited state populations of the normal lattice sites, intrinsic traps, induced traps and samarium ions respectively. Again ΔE is the activation energy that a self trapped exciton must overcome in order to become mobile.

From the model in Figure 51 the differential equations for the time rate of change of the excited tungstate ions can be written assuming delta function excitation as

$$\dot{n}_s(t) = -(F(C_A) + kC_x + kC_A + k_AC_A + B_s)\, n_s(t) \qquad [50]$$

$$\dot{n}_x(t) = -B_x n_x(t) + kC_x\, n_s(t) \qquad [51]$$

$$\dot{n}_{xA}(t) = -(B_x + q_A)\, n_{xA}(t) + kC_A\, n_s(t) \qquad [52]$$

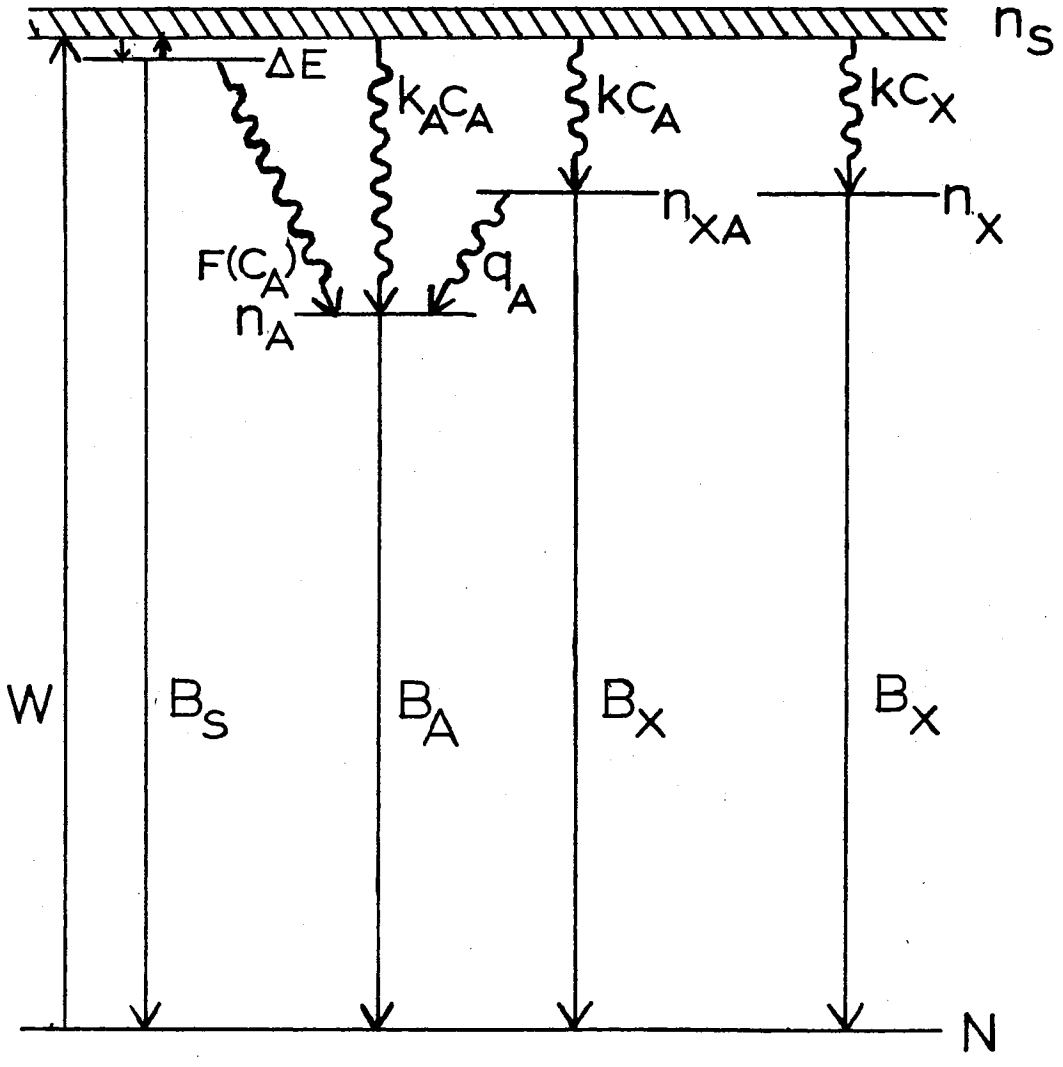

Figure 51. Propose Model of Energy Transfer in $CaWO_4:Sm^{3+}$

which can be integrated easily to yield

$$n_s(t) = n_s(o)\, e^{-(F(C_A) + kC_x + kC_A + k_AC_A + B_s)t} \qquad [53]$$

$$n_x(t) = n_s(o)\, \frac{C_x\, k}{(B_x - B_s - kC_x - kC_A - k_AC_A - F(C_A))}$$

$$[e^{-(B_s + kC_x + k\,C_A + k_AC_A + F(C_A))t} - e^{-B_x t}] \qquad [54]$$

$$n_{xA}(t) = n_s(o)\, \frac{C_A k}{(B_x + q_A - B_s - kC_x - kC_A - k_AC_A - F(C_A)}$$

$$[e^{-(B_s + kC_x + kC_A + k_AC_A + F(C_A)t} - e^{-(B_x+q_A)t}] \qquad [55]$$

The observed tungstate fluorescence is a combination of fluorescence from the normal sites, intrinsic traps and activator induced traps. The intensity that each contributes to the observed fluorescence intensity is the excited state population times the radiative decay time of the excited state. Thus the observed tungstate fluorescence becomes

$$I_H(t) = n_s(o)\, [(B'_s + \frac{B'_x\, C_x\, k}{(B_x - B_s - kC_x - kC_A - k_AC_A - F(C_A)}$$

$$+ \frac{B'_x\, C_A\, k}{(B_x+q_A-B_s-kC_x-kC_A-k_AC_A-F(C_A)}) e^{-(B_s+kC_x+kC_A+k_AC_A+F(C_A))t}$$

$$- \frac{B'_x\, C_x\, k}{(B_x-B_s-kC_x-kC_A-k_AC_A-F(C_A)} e^{-B_x t}$$

$$- \frac{B'_x\, C_A\, k}{(B_x+q_A-B_s-kC_x-kC_A-k_AC_A-F(C_A))} e^{-(B_x + q_A)t}] \qquad [56]$$

the B''s are radiative decay rates.

At $10^{o}K$ the self trapped excitons cannot gain enough thermal energy to overcome the activation energy to become mobile. As a result k and k_A are about zero and Equation [56] becomes

$$I_H(t) = B_s' n_s(o) e^{-(B_s + F(C_A))t} \quad [57a]$$

therefore at $10^{o}K$

$$\tau_s = (B_s + F(C_A))^{-1} \quad [57b]$$

as the temperature is increased slightly the self trapped excitons become somewhat more mobile. This increased mobility means that k and k_A are somewhat larger than their value at $10^{o}K$ but they are still small enough that the majority of the observed fluorescence is from the normal host sites. Therefore, the first coefficient in the first term of Equation [56] still dominates and the lifetime becomes approximately

$$\tau_s = (B_s + kC_x + kC_A + k_AC_A + F(C_A))^{-1} \quad [58]$$

for temperatures slightly above $10^{o}K$. As a result as temperature is increased from $10^{o}K$ the model predicts that the lifetime will decrease. As shown in Figures 37 and 38 this is what was observed experimentally.

If as the temperature is increased the energy migration rate to traps becomes very fast so that $kC_A + kC_x >> B_x + q_A$ and $kC_A + kC_x >> B_s$ then the first exponent in Equation [56] will be negligible after short times. Ignoring terms of B_s, B_x and q_A with respect to $kC_x + kC_A$ the coefficients of the terms can be rewritten and Equation [56] can be written in the high temperature limit as

$$I_H(t) = n_s(o)\left[(B'_s - B'_x)\, e^{-(kC_x + kC_A)t} + \frac{B'_x\, C_x\, k}{kC_x + kC_A}\, e^{-B_x t} + \frac{B'_x\, C_A\, k}{kC_x + kC_A}\, e^{-(B_x + q_A)t}\right] \qquad [59]$$

which if $C_A >> C_x$ and temporarily ignoring the first exponential becomes

$$I_H(t) = B'_x\, n_s(o)\, e^{-(B_x + q_A)t} \qquad [60a]$$

and the lifetime becomes

$$\tau_s = (B_x + q_A)^{-1} \qquad [60b]$$

Equation [60b] predicts that at high temperatures the temperature dependence of the lifetime is contained in the temperature dependence of B_x and q_A. The most important point to note about Equation [60b] is that it predicts a lifetime which is independent of the samarium concentration since B_x^{-1} is the fluorescence lifetime of the traps and q_A is the one step Förster-Dexter energy transfer rate to nearest neighbor samarium ions which is independent of the samarium concentration, see Equations [13] and [26].

The first exponential in Equation [59] predicts that the fluorescence intensity should exhibit an initial rise. At high temperatures, above 120°K, $kC_A + kC_x$ will be large and the initial rise will be very fast and thus the first exponential was not included in Equation [60a]. That an initial rise was not observed was discussed in Part A of this chapter.

For the measured fluorescence lifetimes the model then predicts that at $10^{o}K$ the lifetime is given by Equation [57b] and is dependent upon the samarium concentration. As the temperature is increased slightly the lifetime will decrease as predicted by Equation [58] and will still be a function of the samarium concentration. Further increase in the temperature results in a lifetime which is independent of temperature and samarium concentration as predicted by Equation [60b]. Comparison of these predictions to Figures 37 and 38 shows very good qualitative agreement.

What then does the proposed model predict for measurements of the fluorescence intensities for the case of continuous excitation of the sample? What does it predict for the ratio of the samarium to tungstate fluorescence intensities? The time rate of change of the excited samarium population can be written as

$$\dot{n}_A(t) = - B_A n_A(t) + q_A n_{xA}(t) + (k_A C_A + F(C_A)) n_s \ . \qquad [61]$$

for excitation of the samarium via energy transfer from the tungstate ions. Equations [50] - [53] and [61] can be solved for the case of continuous excitation of the tungstate ions to yield the steady state populations as

$$n_s = \frac{WN_s}{(B_s + kC_x + kC_A + k_A C_A + F(C_A)} \qquad [62]$$

$$n_x = \frac{kC_x}{B_x} n_s \qquad [63]$$

$$n_{xA} = \frac{kC_A}{(B_x + q_A)} n_s \qquad [64]$$

$$n_A = \frac{1}{B_A} [q_A n_{xA} + (k_A C_A + F(C_A)) n_s] \qquad [65a]$$

which by making use of Equation [64] becomes

$$n_A = \frac{n_s}{B_A}\left[\frac{q_A\, kC_A}{(B_x + q_A)} + k_A C_A + F(C_A)\right] \qquad [65b]$$

Equations [62], [63] and [64] can be related to the observed tungstate fluorescence intensity by the radiative lifetimes of the normal sites and traps. The tungstate fluorescence intensity becomes

$$\begin{aligned} I_H &= B'_s\, n_s + B'_x\, n_x + B'_x\, n_{xA} \\ &= n_s\left[B'_s + \frac{B'_s}{B_x} kC_x + \frac{B'_x}{(B_x + q_A)} kC_A\right] \end{aligned} \qquad [66]$$

Similarly the samarium fluorescence intensity becomes

$$I_G = n_s \frac{B'_A}{B_A}\left[\frac{q_A\, kC_A}{(B_x + q_A)} + k_A C_A + F(C_A)\right] \qquad [67]$$

The ratio of the samarium to tungstate fluorescence intensity becomes

$$\frac{I_G}{I_H} = \frac{\left[\frac{q_A\, kC_A}{(B_x + q_A)} + k_A\, C_A + F(C_A)\right]}{\left[B'_s + \phi^o_H\, kC_x + \phi_H\, kC_A\right]} \qquad [68]$$

where ϕ^o_H and ϕ_H are the quantum efficiencies of calcium tungstate in the undoped and doped samples respectively and the quantum efficiency of samarium has been assumed to be 1. Quantum efficiency is defined as the ratio of the rate of radiative decay to the rate of all possible decay.

Again looking at the high and low temperature limits predicted by the proposed model. At 10^oK k and k_A are very small and Equation [68] becomes

$$\frac{I_G}{I_H} \approx \frac{F(C_A)}{B'_s} = \frac{F(C_A)}{\phi^o_H B_s} = \frac{F(C_A)}{\phi^o_H} \tau^o_s \qquad [69]$$

where use has been made of Equation [45b]. At high temperatures (above 100^oK) kC_A becomes large relative to $F(C_A)$ and Equation [68] becomes

$$\frac{I_G}{I_H} = \frac{\frac{q_A\, kC_A}{(B_x + q_A)}}{\phi^o_H\, kC_x + \phi_H\, kC_A}$$

$$= \frac{q_A\, \tau_s\, C_A}{\phi^o_H\, C_x + \phi_H\, C_A} \qquad [70]$$

where use has been made of Equation [60b]. Equations [69] and [70] predict that at all temperatures the ratio of the samarium to tungstate fluorescence will be a function of the samarium concentration which is what was observed experimentally as shown in Figures 49 and 50.

Equations [45b], [57b] and [60b] predict that

$$\left(\frac{\tau^o_s}{\tau_s} - 1\right) \frac{1}{\tau^o_s} = F(C_A) \text{ at } 10^oK \qquad [71]$$

$$= q_A \text{ above } 100^oK \qquad [72]$$

From the expressions for the intensity ratio Equations [69] and [70] predict

$$\frac{I_G}{I_H} \frac{1}{\tau^o_s} = \phi^o_H\, F(C_A) \quad \text{at } 10^oK \qquad [73]$$

$$= \frac{q_A \frac{\tau_s}{\tau_s^o} C_A}{\phi_H^o C_x + \phi_H C_A} \quad \text{above } 100^oK \qquad [74]$$

So from the intensity and lifetime measurements a value for the Förester-Dexter energy transfer rate at 10^oK from self trapped excitons directly to samarium ions can be obtained. Above 100^oK the energy transfer rate from traps to samarium ions can be obtained from the lifetime data. The values of the energy transfer rates obtained by plotting the lifetime and intensity data as the left hand side of Equations [71] and [72] are tabulated in Table XI. As a check of the internal consistency of the model the temperature dependence of the energy transfer rates obtained from lifetime measurements and those obtained from intensity measurements is shown in Figure 52 and indicates a high degree of correlation. The energy transfer rates increase with temperature from 10^oK to 100^oK as thermally activated migration to the traps increases. The decrease above 220^oK in the energy transfer rate as determined from lifetime measurements is not indicative of a real decrease in the energy transfer rate but instead is the result of radiationless processes. In this temperature range the tungstate lifetime in the undoped sample is the lifetime of the intrinsic host traps and in the doped samples is the lifetime of the induced traps as quenched by energy transfer to the samarium ions. Since the origin of the traps is different it seems reasonable that they would be affected slightly different by radiationless processes. The apparent decrease in the energy transfer rate is then the result of the lifetime of the undoped sample being quenched more than the lifetime of the doped samples by radiationless processes. The apparent disagreement above 220^oK between the energy transfer rates predicted by

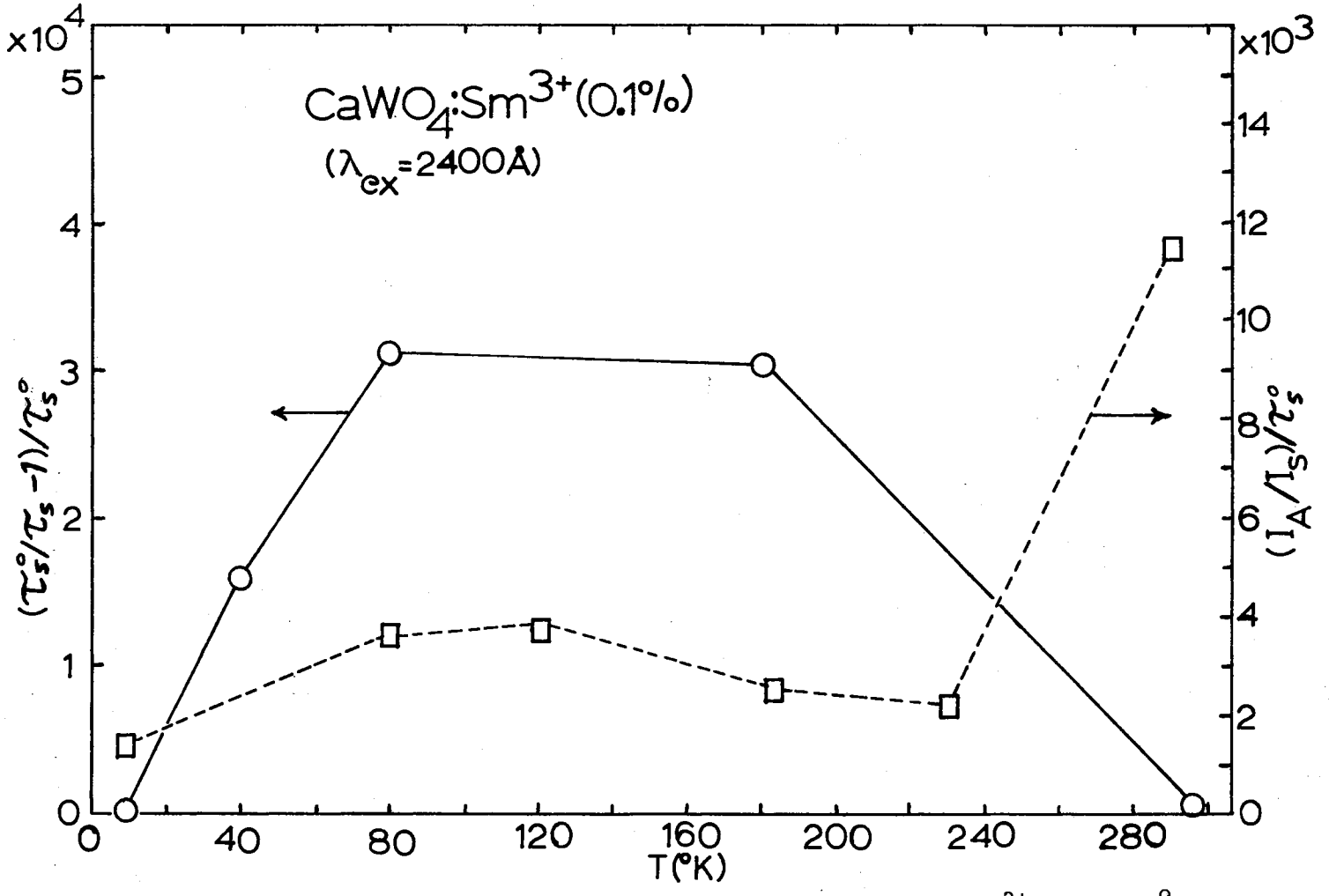

Figure 52. Energy Transfer Rate Versus Temperature for $CaWO_4:Sm^{3+}$ .1% 2400Å Excitation

TABLE XI

ENERGY TRANSFER RATES

	2400Å					
	$(\frac{\tau_s^o}{\tau_s} - 1)\frac{1}{\tau_s^o} \times 10^{-4}$ sec^{-1}			$\frac{I_G}{I_H}\frac{1}{\tau_s^o} \times 10^{-4}$ sec^{-1}		
T °K \ %Sm^{3+}	.01%	.1%	1.0%	.01%	.1%	1.0%
10	----	----	----	----	.14	.42
40	2.3	1.7	3.5	----	----	---
80	3.3	----	4.1	----	.35	.82
88	----	3.4	----	----	----	---
123	4.2	----	4.5	----	.37	1.2
180	4.0	3.1	----	----	.25	1.1
229	----	----	----	----	.28	1.4
296	1.5	.069	4.0	----	1.1	7.6
	2650Å					
11	.098	.34	.81	.11	.47	.83
40	3.3	.31	3.6	----	----	---
80	3.6	----	5.0	.29	1.3	1.8
123	3.9	----	4.0	.39	1.7	3.1
180	3.7	3.7	----	.19	.95	2.1
229	----	----	----	.14	.61	2.0
296	1.3	.66	2.0	.23	1.8	9.4

lifetime and intensity measurements is the result of these same radiationless processes which quench not only the lifetime but also the intensity of the tungstate fluorescence. As a result the ratio $\frac{I_G}{I_H}\frac{1}{\tau_s^o}$ increases due to a decrease in both I_H and τ_s^o rather than due to an increase in the energy transfer rate which would appear as an increase in I_G. Also due to ion-ion (16) interaction the energy transfer rates determined from intensity, data at high concentrations are questionable.

As a further comparison the data in Table XI plotted as a function of the samarium concentration for 2400Å excitation and 2650Å excitation is shown in Figures 53 and 54 respectively. Note that at low temperatures both the intensity and lifetime data predict an energy transfer rate which increases with increasing samarium concentration. At high temperatures the lifetime results indicate that the energy transfer rate is independent of the samarium concentration, while the intensity results are still a function of the samarium concentration as is predicted by Equation [74]. Special consideration must be given to the intensity data for 2650Å excitation. As shown in Figure 11 for 2650Å excitation the undoped calcium tungstate fluorescence shifts to longer wavelengths with decreasing temperature. Comparison with Figure 28 shows that the longer wavelength fluorescence is not observed in samples containing samarium. As shown in Figure 31 the tungstate fluorescence intensity for 2650Å excitation of samples containing samarium decreases with decreasing temperature, however, the samarium intensity does not display a corresponding increase. It appears then that the longer wavelength tungstate fluorescence is quenched by the presence of the samarium and is quenched radiationlessly. This is also indicated by the decrease in the intensity of the 2650Å band with decreasing temperature in the excitation spectra shown in Figures 18, 19 and 20. Therefore, the increase in the intensity ratio with decreasing temperature for 2650Å excitation does not indicate an increase in the energy transfer rates considered in the

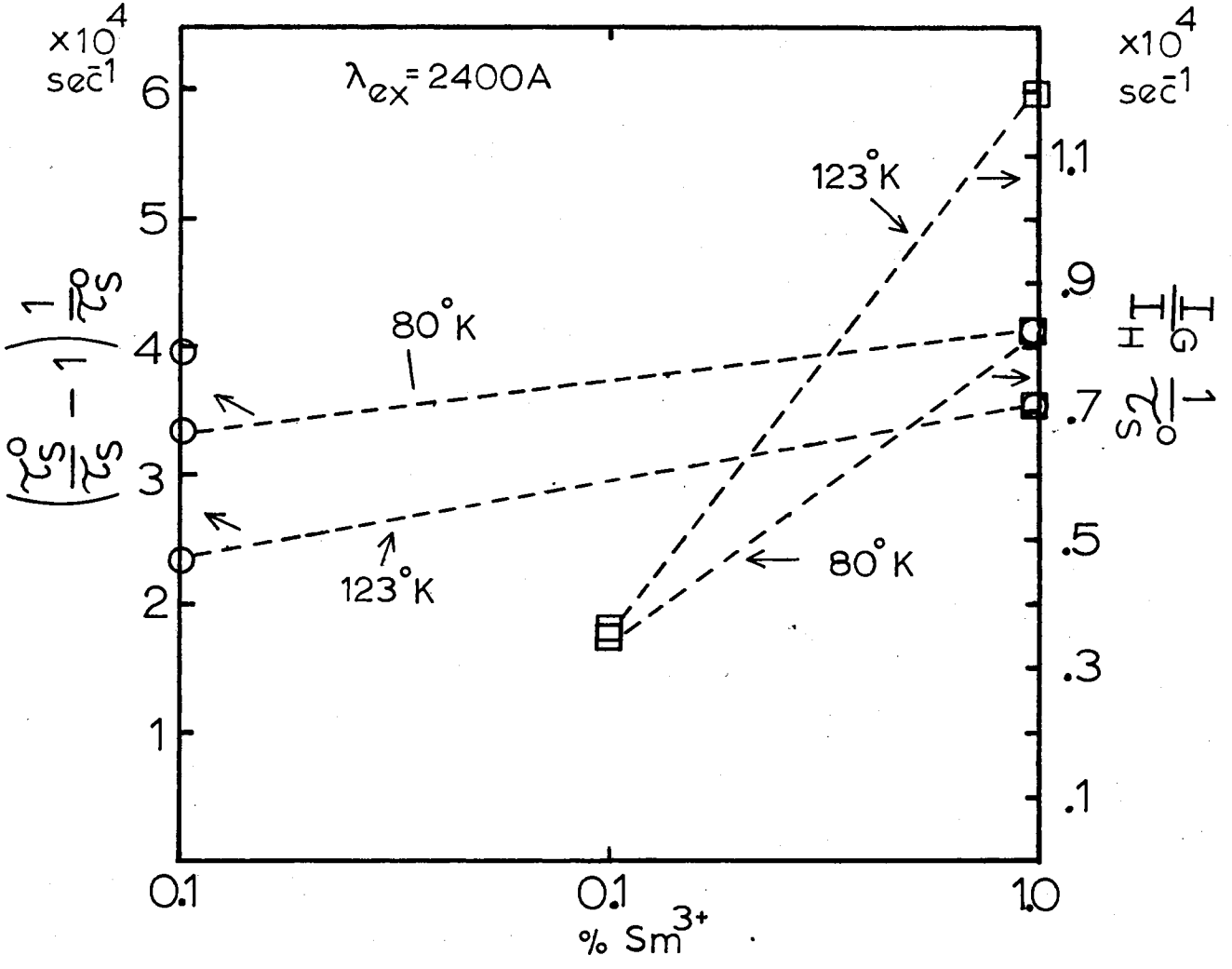

Figure 53. Energy Transfer Rates Versus Samarium Concentration for 2400Å Excitation

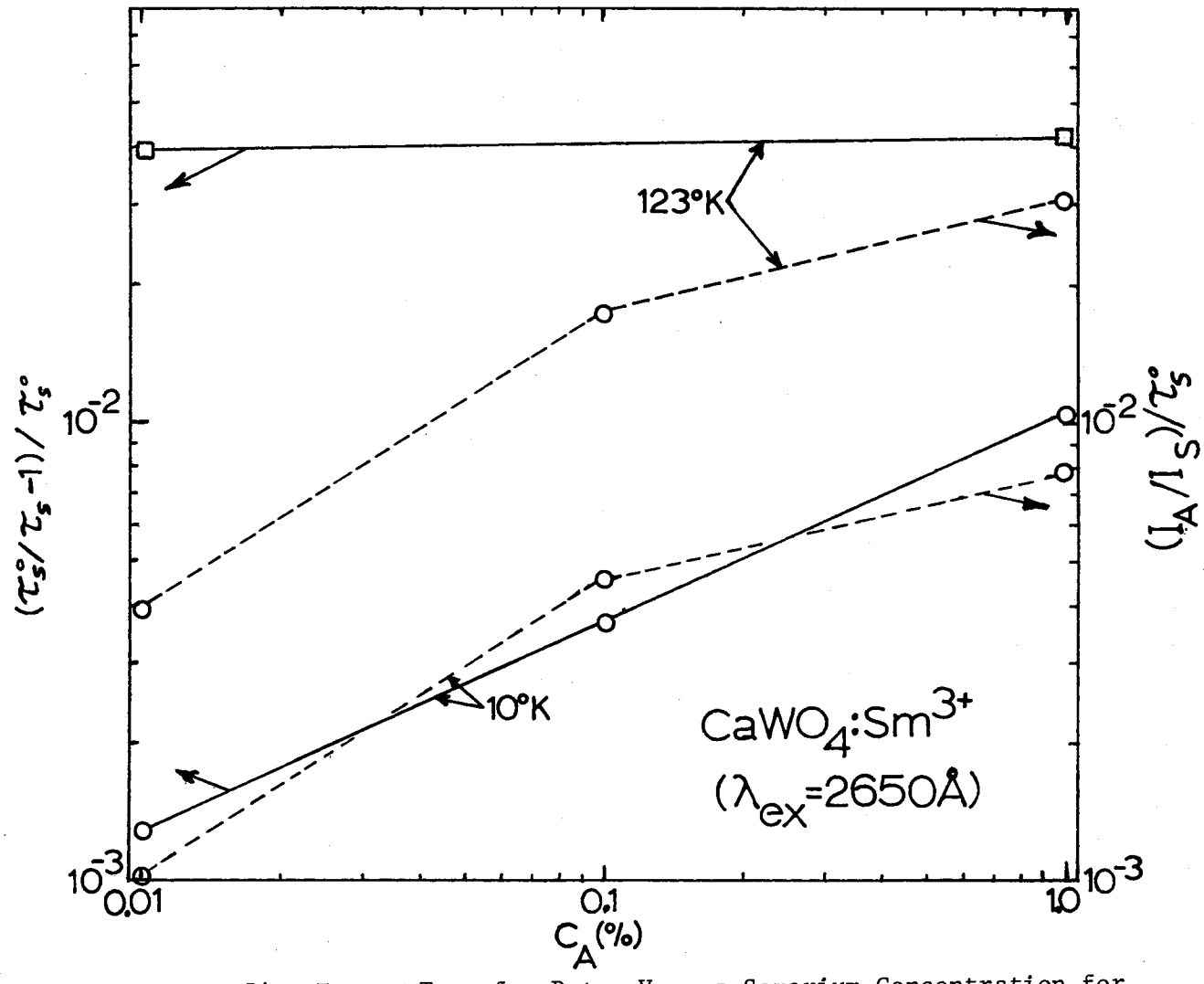

Figure 54. Energy Transfer Rates Versus Samarium Concentration for 2650Å Excitation

model. Note also that the 5200Å fluorescence band produced for 3150Å excitation of the undoped calcium tungstate sample is not observed in samples containing samarium.

How do the values of the energy transfer rate determined empirically compare to the theoretically calculated and what is the mechanism by which energy is transferred from traps to nearest neighbor samarium ions. From Equation [13a] value for R_o can be calculated using the index of refraction n = 1.92, the mean overlap energy E = 2.48×10^4 cm^{-1}, $\phi_s = 1$ and a calculated value of the spectral overlap integral of 3.35×10^{-2} $mole^{-1}$ cm^{-1} $liter^{-1}$. R_o is found to be 3.95Å. Using a trap-activator separation of 3.68Å which is the nearest neighbor WO_4^{2-} - Ca^{2+} separation the energy transfer rate for dipole-dipole interaction can be calculated using Equation [13]. At 180°K this yields 7.2×10^4 sec^{-1} for 2400Å excitation and 6.0×10^4 sec^{-1} for 2650Å excitation. The energy transfer rate for exchange interaction can be calculated from Equation [27] using an effective Bohr radius, L, of .9Å which is half the W-O separation. The calculated values for the energy transfer rates due to exchange interaction are 8.6×10^4 sec^{-1} and 7.2×10^4 sec^{-1} at 180°K for 2400Å and 2650Å excitation respectively. The experimentally determined values at 180°K are 3.5×10^4 sec^{-1} and 3.7×10^4 sec^{-1} for 2400Å and 2650Å excitation as determined from Equation [72]. By comparison of these theoretically and experimentally calculated values of the energy transfer rate it is impossible to isolate either dipole-dipole or exchange as the interaction mechanism. However, the good agreement between the theoretical and empirical values indicates that at high temperatures the energy transfer to samarium ions does take place mainly from nearest neighbor trap sites and thus further substantiates the proposed model.

From Equations [71] and [73] the Förster-Dexter energy transfer rate for transfer from self-trapped excitons to the samarium ions at 10 ^{o}K can be determined, and the values are tabulated in Table XI. What is the energy transfer mechanism? From Equation [23] the quenching of the tungstate lifetime can be calculated for the case of dipole-dipole interaction. Using the value of R_o previously calculated Equation [23] predicts a ratio of $\frac{\tau_s}{\tau_s^o}$ of .95 for 1% Sm^{3+} which can be compared to the measured value of .5. This indicates that if the transfer mechanism were dipole-dipole a much smaller quenching of the lifetime would be expected, and therefore the interaction mechanism is probably not dipole-dipole interaction. As mentioned earlier calculation of lifetime quenching due to exchange is very complex and must be performed by computer. However, comparison of the experimentally determined lifetime quenching to the results given by Inokuti and Hirayama for exchange indicates that simple exchange also predicts a much smaller quenching of the lifetime than is observed. Inokuti and Hirayama's calculations were performed using Dexter's simple model for exchange. It has been shown (43,44) that by consideration of the relative orientation of the ions the predicted energy transfer rate due to exchange can be increased by several orders of magnitude. Since the development of the dipole-dipole energy transfer rate is relatively straightforward and predicts a much lower energy transfer rate than is observed, the interaction mechanism is probably an exchange interaction.

The energy migration rate to traps (k) can be characterized by the diffusion coefficient (D), the hopping time (t_H) and the diffusion length (ℓ). Using the method described for the undoped sample, the energy migration rate can be determined from the temperature dependence of the tungstate lifetimes in the doped samples. For the $CaWO_4:Sm^{3+}$ .01% sample kC_A is found to be 7×10^4 sec^{-1} and knowing C_A to be 1.27×10^{18} cm^{-3} k was calculated and is 5.5×10^{-14} cm^3 sec^{-1}. Using Equation [33] the diffusion coefficient can be calculated and is 1.27×10^{-7} cm^2 sec^{-1} where R has been taken to be 3.68Å, a tungstate-tungstate lattice spacing. This is a smaller diffusion coefficient than has been found for excitons in organic crystals (45) but larger than those reported for migration among rare earth sensitizers in other host crystals and glasses (46). The diffusion length can be determined from the diffusion coefficient by the relationship $\ell = (D\tau)^{\frac{1}{2}}$ and using the measured lifetime of 12 μsec at 100°K for 2400 excitation this yields a value for ℓ of 2.82×10^{-6} cm. Comparison of this value to the average tungstate-samarium separation for a sample containing .01% Sm^{3+} of 5.7×10^{-7} cm shows that after an exciton becomes mobile it has a high probability of being trapped next to a samarium ion which is consistent with the proposed model.

If a hopping model is considered, then the hopping time can be determined from the diffusion coefficient from the relationship $D = a^2/3t_H$ where a is the average hopping distance. Considering only nearest neighbor hops t_H is found to be 4.14×10^{-9} sec where a is taken to be the tungstate-tungstate separation. A theoretical estimate of t_H can be made by calculating the probability of tungstate-tungstate transfer, $p_H = t_H^{-1}$. Using the value measured in this investigation for the tung-

state spectral self overlap integral of 1.72×10^{-3} liter $mole^{-1}$ cm^{-1} and a mean overlap energy of 2.95×10^{4} cm^{-1}, R_o can be calculated using Equation [13] to be 2.16Å. Taking L to be 0.9Å and $\gamma = 4.8$ then from Equation [26] $p_H^{-1}(ex) = .14$ msec and from Equation [13] $p_H^{-1}(dd) = .18$ m sec for 2400Å excitation which is much longer than the experimentally determined value of 4.14×10^{-9} sec. This indicates that the activation energy (ΔE) is important in increasing the resonance of the absorbing site and the surrounding tungstate ions. This increase in resonance can be expressed as an increase in R_o. It is not unreasonable to expect R_o to be on the order of 16Å which gives $t_H(dd) = 3.3 \times 10^{-9}$ sec or on the order of 8Å which gives $t_H(ex) = 1.7 \times 10^{9}$ sec, which gives a hopping time that is in good agreement with the experimentally determined hopping time.

Finally a comparison of kC_A obtained for $CaWO_4:Sm^{3+}$ .01% and the values of q_A given in Table XI shows that even at the lowest samarium concentration, $kC_A > q_A$. This indicates that the limiting step in the energy transfer process is the transfer from traps to the samarium ions.

CHAPTER VI

SUMMARY AND CONCLUSIONS

The results of this investigation indicate: 1) the presence of intrinsic host traps even in undoped calcium tungstate, 2) at low temperatures the excitons are self trapped and must overcome an activation energy in order to become mobile, 3) the presence of a trivalent samarium ion sufficiently perturbs the surrounding lattice so as to produce a host trap nearest neighbor to the samarium ion, 4) above $100^{o}K$ energy transfer to the samarium ions takes place by diffusion to the host traps from the absorbing site followed by transfer from the traps to the samarium ions in a one step process, 5) the mechanism for the energy transfer from traps to samarium ions is either dipole-dipole or exchange interaction, 6) at low temperatures energy transfer takes place from self trapped excitons to samarium ions by a one step Förster-Dexter process and 7) the mechanism by which this transfer takes place is probably exchange.

I would like to propose that this investigation be extended in several areas. By obtaining the proper photomultiplier base single shot measurements of the fluorescence lifetimes not measureable by the methods used in this investigation could be obtained. Also single shot measurements would make it possible to measure the risetimes predicted by the model which was discussed in Chapter V.

A second very interesting extension would be to use a highly mono-

chromatic light source such as a tuneable dye laser to examine the extraneous structure of the samarium spectra in calcium tungstate. By selective excitation of specific samarium absorption bands the resulting fluorescence spectra could be examined to determine if the extraneous structure is the result of excitation of samarium ions near defects and/or samarium-samarium ion interaction. Also with an intense monochromatic source a high resolution monochrometer could be used to obtaine the time resolved spectra of very narrow wavelength regions of the samarium spectra such as the low intensity lines. This would provide a means of determining to what extent transitions from higher excited metastable states contribute to the extraneous structure.

Since one area in which inorganic phosphors is of great commercial value is C.R.T. displays, this investigation should definitely be extended to include a study of cathodoluminescence of powdered samples of $CaWO_4:Sm^{3+}$. The usefulness of a phosphor in C.R.T. displays depends not only upon the spectral distribution of the fluorescence but also depends greatly on the efficiency of the phosphor when excited by low energy electrons.

Finally I think an investigation of host sensitized energy transfer in similar systems would be of great interest. One such system is $YVO_4:Eu^{3+}$. Although exciton migration has been studied extensively in organic systems, very little work has been done in inorganic systems. The results of this investigation have shown that exciton migration can play an important role in the energy transfer process in inorganic systems; however, the complexity of the $CaWO_4:Sm^{3+}$ system made it virtually impossible to characterize the exciton migration in terms of the parameters used to describe the exciton motion. By studying a system that

is not as complicated as $CaWO_4:Sm^{3+}$ it is hoped that more knowledge about the dynamics of exciton migration in inorganic phosphors could be obtained. The commerical and academic value of inorganic phosphors as sources of artificial lighting, C.R.T. displays and as laser host materials warrants further investigation of these systems.

BIBLIOGRAPHY

(1) Klick, C. C. and J. H. Schulman, in Solid State Physics, Vol. 5, edited by F. Seitz and D. Turnbull (Academic Press, New York, 1957), p. 57.

(2) Dexter, D. L., J. Chem. Phys. 21, 836 (1953).

(3) Thayer, R. N. and B. T. Barnes, J. O. S. A. 29, 131 (1939).

(4) Besse, N. C., J. O. S. A. 29, 278 (1939).

(5) Johnson, R. P. and W. L. Davis, J. O. S. A. 29, 283 (1939).

(6) Kröger, F. A., Some Aspects of the Luminescence of Solids (Elsevier Publishing Company, New York, 1948).

(7) Botden, Th. P. J., Philips Res. Rep. 6, 425 (1951).

(8) Butler, K. H., Proc. Inter. Conf. on Luminescence 1313, (1966).

(9) Day, P., Czech. J. Phys., B20, 641 (1970).

(10) Wolfsburg, M. and L. Helmholz, J. Chem. Phys. 20, 837 (1952).

(11) Jones, G. R., J. Chem. Phys., 47, 4347 (1967); 45, 4348 (1966).

(12) Gualtierri, J. G. and T. R. AuCoin, J. Chem. Phys.

(13) Wybourne, B. G., J. Chem. Phys. 36, 2301 (1962).

(14) Rast, H. E., J. L. Fry and H. H. Caspers, J. Chem. Phys. 46, 1460 (1967).

(15) Babkina, T. V., V. F. Zolin and E. N. Muravev, Optics and Spect. (USSR) 32, 613 (1972).

(16) Van Uitert, L. G. and L. F. Johnson, J. Chem. Phys. 44, 3514 (1966).

(17) Randall, J. T. and M. H. F. Willkins, Proc. Roy. Soc. 184, 347 (1945).

(18) Klick, C. C. and J. H. Schulman, Appl. Phys. Let., 25, 347 (1954).

(19) Cook, J. R., Proc. Phys. Soc. B68, 148 (1954).

(20) Sayer, M. and A. Souder, Physics Letters 24A, 246 (1967).

(21) Hahn, D. and K. Lertes, Zeit. für Physik 169, 331 (1962).

(22) Förster, Th., Ann. Physik 2, 55 (1948).

(23) Förster, Th., Z. Naturforschg. 4a, 321 (1949).

(24) Dexter, D. L., J. Chem. Phys. 21, 836 (1953).

(25) Eisenthal, K. B. and S. Siegel, J. Chem. Phys. 41, 652 (1964).

(26) Miyakawa, Toru and D. L. Dexter, Phys. Rev. B1, 2961 (1970).

(27) Inokuti, Mitio and Fumio Hirayama, J. Chem. Phys. 15, 1978 (1965).

(28) Wannier, G. H., Phys. Rev. 52, 191 (1937).

(29) Mott, N. F., Trans. Faraday Soc. 34, 500 (1938).

(30) Frenkel, J., Phys. Rev. 37, 1276 (1931).

(31) Chandrasekar, S., Rev. Mod. Phys. 15, 1 (1943).

(32) Application note, The Single Photon Technique for Measuring Light Intensity and Decay Characteristics, Ortec, Inc., AN 35.

(33) Harmer, Alan Lewis, Massachusetts Institute of Technology Crystal Physics Laboratory, Technical Report #10, August, 1967.

(34) Blasse, G., Philips Res. Repts. 24, 131 (1969).

(35) Fowler, W. B. and D. L. Dexter, Phys. Rev. 128, 2154 (1962).

(36) Agranovich, V. M. and Yu. V. Konobev, Phys. Status Solidi 27, 435 (1968).

(37) Prather, J. L., Atomic Energy Levels in Crystals, NBS Monograph (1961).

(38) Nassau, K., J. Chem. Solids 24, 1511 (1963).

(39) Magno, M. S. and G. H. Dieke, J. Chem. Phys. 37, 2354 (1962).

(40) Prener, J. S. and J. D. Kingsley, J. Chem. Phys. 38, 667 (1963).

(41) Russel, J. P. and R. Loudon, Proc. Phys. Soc. (London) 85, 1029 (1965).

(42) Barker, A. S., Phys. Rev. 135, A742 (1964).

(43) Soules, T. F., R. L. Bateman, R. A. Hewes and E. R. Kreidler, Phys. Rev. B7, 1657 (1973).

(44) Anderson, P. W., in Magnetism, Vol. 1, edited by G. T. Rado and H. Sukl (Academic Press, New York, 1963), p. 25.

(45) Wolf, H. C., in Advances in Atomic and Molecular Physics, Vol. 3, edited by D. R. Bates and I. Easterman (Academic Press, New York, 1967), p. 119.

(46) Weber, M. J., Phys. Rev. B4, 2932 (1971).

APPENDIX

SIMPLIFICATION OF THE INTERACTION HAMILTONIAN

Classically the interaction Hamiltonian can be written as the electrostatic interaction of all the electrons of the sensitizer with all the electrons of the activator, plus the electrostatic interaction of all the electrons of the sensitizer with the nucleus of the activator, plus the electrostatic interaction of all the electrons of the activator with the nucleus of the sensitizer. This can be written as

$$H = \frac{e^2}{2K} \sum_i^n \sum_j^m \left[\frac{1}{|\bar{R} + \bar{r}_{Aj} - \bar{r}_{Si}|} - \frac{Z_S}{|\bar{R} + \bar{r}_{Aj}} - \frac{Z_A}{|\bar{R} - \bar{r}_{Si}|}\right] \qquad [75]$$

where n and m are the number of electrons on the sensitizer and activator, respectively and Z_S and Z_A are the nuclear charge of the sensitizer and activator respectively.

If only one electron on the sensitizer and one electron on the activator make a transition in the energy transfer process then the initial and final electronic states can be written as a product of one electron states as

$$|\Psi_I\rangle = |\Psi_{S1}\rangle|\Psi_{S2}\rangle\ldots|\psi'_{Si}\rangle\ldots|\psi_{Sn}\rangle|\psi_{A_1}\rangle|\psi_{A_2}\rangle\ldots|\psi_{A_j}\rangle\ldots|\psi_{A_m}\rangle$$

and [76]

$$|\Psi_F\rangle = |\psi_{S1}\rangle|\psi_{S2}\rangle\ldots|\psi_{Si}\rangle\ldots|\psi_{Sn}\rangle|\psi_{A_1}\rangle|\psi_{A_2}\rangle\ldots|\psi'_{A_j}\rangle\ldots|\psi_{A_m}\rangle$$

the only elements of the transition matrix which will be non zero is

$$\langle\psi_{Si}|\langle\psi'_{Aj}|\frac{1}{|\bar{R} + \bar{r}_{Aj} - \bar{r}_{Si}|}|\psi_{Aj}\rangle|\psi'_{Si}\rangle \ . \qquad [77]$$

Therefore, the only term in the Hamiltonian which needs to be considered is the term

$$\frac{e^2}{K}\left[\frac{1}{|\bar{R} + \bar{r}_{Aj} - \bar{r}_{Si}|}\right] \qquad [78]$$

and the interaction Hamiltonian is written then as

$$H = \frac{e^2}{K}\left[\frac{1}{|\bar{R} + \bar{r}_A - \bar{r}_S|}\right] \qquad [79]$$

where the subscripts i and j have been dropped.

To avoid confusion when considering exchange effects the subscripts S and A are replaced by the subscripts 1 and 2 respectively whenever a state is written as a function of both $\bar{r}$ and ω, therefore $\psi(\bar{r}_S,\omega_S)$ is written $\psi(\bar{r}_1,\omega_S)$.

VITA

Michael Joseph Treadaway

Candidate for the Degree of

Doctor of Philosophy

Thesis: HOST SENSITIZED ENERGY TRANSFER IN $CaWO_4:Sm^{3+}$

Major Field: Physics

Biographical:

Personal Data: Born at New Orleans, Louisiana, February 28, 1948 the son of Merrill L. and Marion D. Treadaway.

Education: Graduated from Holy Cross High School in 1966; received Bachelor of Science degree from Tulane University, New Orleans, Louisiana in May, 1970; completed the requirements for the degree of Doctor of Philosophy at Oklahoma State University, Stillwater, Oklahoma in May, 1974.

Other: Member American Physical Society; presented paper, "Energy Transfer in $CaWO_4:Sm^{3+}$", at American Physical Society Meeting, San Diego, California (March 1973); presented paper "Temperature Dependence of Energy Transfer in $CaWO_4:Sm^{3+}$," American Physical Society Meeting, Philadelphia, Penn. (March 1974).